CHAPTER 2

Spacecraft Instrument Calibration and Stability

Panel Members

J. Gille, Chair NH 31570a
P. Feldman TRW D(55G, Red, Bldg
R. Hudson — NC999967
J. Lean
R. Madden
L. McMaster
G. Mount
G. Rottman
P. C. Simon

Chapter 2

Spacecraft Instrument Calibration and Stability

Contents

2.1 INTRODUCTION

The advent of artificial Earth satellites has created great possibilities for remotely sounding the atmosphere on a global basis. Ozone was one of the first gases to be proposed for measurement in this way. Its strong and distinct spectral features in the ultraviolet (UV), visible, and infrared (IR) portions of the spectrum, combined with its abundance and distribution, make it a relatively easy gas to detect, and offer the hope of accurate quantitative measurements. Since then, a large number of ozone-measuring experiments has been flown.

The great advantage of regular global observations from satellites is that they provide good information on spatial and short-term temporal variations, and thus allow entirely new types of problems to be addressed. However, soon after the first sounders flew, concern began to be expressed that human activities or natural causes might result in long-term changes in the amount of ozone in the stratosphere. Consequently, attempts have been made to use these sounders to measure long-term changes.

The purpose of this chapter is to review the instruments and techniques that provide the most information on ozone trends, to assess the evidence on the stability of the instrumental calibration, and to reach conclusions on the uncertainties to be associated with any reported trends. Although the Working Group relied heavily on the various experimenters, and could not have done its work without their cooperation, it has attempted to reach independent conclusions and estimates of the errors in the trend determinations.

The trend measurement problem is fraught with great difficulty. In general, when one is interested in trends, it is not the absolute accuracy but the stability of the instrument that is important. However, the measurements must be made over long periods of time in a hostile environment, with no chance to check the instrument in detail or to readjust it. Two strategies for making long-term measurements immediately suggest themselves: making the results insensitive to instrument change, by, for instance, using a ratio technique, or incorporating an in-orbit calibration procedure. Various experiments have used one or both of these approaches.

Different instruments, especially those employing different techniques, generally have different systematic errors. Therefore, it is usually not possible to use measurements by two instruments operating at different times to derive a reliable trend. (It may be possible, however, if the two instruments are very similar and individually reliable.) A discussion of trends, then, must concentrate on those instruments having data records long enough to provide an indication that stands out above seasonal and natural fluctuations. These records must be considered along with others that are simultaneous with them, thereby providing a check on them, or insight into their features.

Figure 2.1 plots the time of operation of several ozone sounders that meet these criteria. They begin with the launch of the Solar Backscatter Ultraviolet/Total Ozone Mapping Spectrometer (SBUV/TOMS) and Limb Infrared Monitor of the Stratosphere Spectrometer (LIMS) on Nimbus–7 late in 1978, and continue to 1987. SBUV measured ozone profiles, while SBUV and TOMS determined total ozone amounts, over virtually the entire period, and thus are central to this discussion. Stratospheric Aerosol and Gas Experiment (SAGE)–I and –II are two very similar instruments, each with an appreciable data record. The two instruments on the Solar Mesospheric Explorer (SME) also have appreciable data records, although their altitude coverage does not greatly overlap that of the others. LIMS has the shortest data record, but has high vertical resolution coupled with temporal and spatial detail. All of these use different measurement

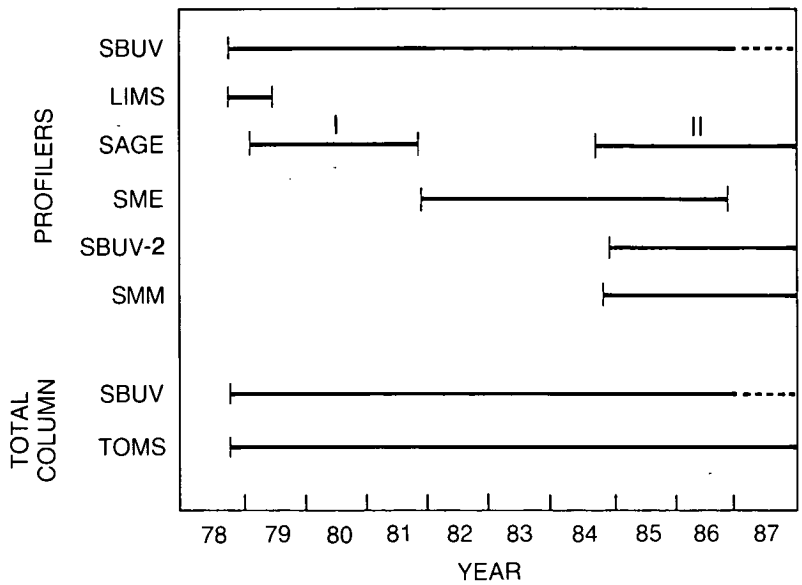

Figure 2.1 Periods of available data for satellite ozone-measuring systems.

techniques than do SBUV/TOMS. SBUV–2 is a National Oceanic and Atmospheric Agency (NOAA) operational version of the SBUV that began collecting data in 1985. However, even with the urgency of this assessment, NOAA has not yet reduced any of the data in a way that would allow comparison with the SBUV results. The SBUV–2 data could have provided an extremely important check on the degradation of the SBUV/TOMS diffuser plate, and indicated ozone trends.

The focus here has been entirely on the internal evidence from the instrument and its test procedures. Ground-based measurements could also serve as a check on calibration changes; this will be discussed in Chapters 4 and 5.

This assessment was greatly assisted by the considerable efforts of several experiment groups to study and reprocess their data to enhance their applicability to trend studies. The SAGE data were reprocessed to take advantage of improvements developed for SAGE–II processing. Similarly, the SME–UVS (ultraviolet spectrometer) and near infrared (NIR) instruments did extensive reanalysis of errors and data reprocessing. Additionally, the TOMS data were reprocessed using new absorption coefficients.

Because of the length of the data record, amount of data, and visibility of the results, more attention was focused on the SBUV experiment than on the others. Additionally, it lent itself to further analysis. However, all experiments were examined critically.

This chapter begins with a general outline of the mechanisms that can cause the performance of a satellite instrument to change with time. Subsequently, Sections 2.3–2.7 discuss each of the relevant techniques and instruments, followed by a review of the evidence for any change of response in orbit, an assessment of its magnitude, and a summary of conclusions about the capabilities of the various instruments. Four instruments that were briefly considered are reviewed in Section 2.8. The last section (2.9) summarizes the conclusions about the ability of the various instruments to determine trends.

2.2 INSTRUMENT DEGRADATION

The fact that the performance of optical instruments changes with time is a well-known phenomenon, both in the laboratory and in space. Overwhelmingly, these changes lead to reduced performance. The causes for the degradation are many, and are discussed in greater detail below:

- Contamination of optical surfaces by thin films.
- Aging of the optical surface of mirrors, diffraction gratings, etc.
- Changes in the transmission of lenses, plates, etc.
- Detector changes.
- Movement or separation of optical elements.

2.2.1 Contaminant Film Formation

The formation of thin films on optical surfaces that are irradiated with ultraviolet radiation is well known in the laboratory, particularly in vacuum systems that use oil pumps and oil diffusion pumps. Much research has been carried out on the nature of the films, and the consensus is that the films arise from the dissociation of oil molecules on the surface of the optical component when it is irradiated (see, e.g., Osantowski, 1983). Figure 2.2 shows the result of exposing an uncoated aluminum surface to 123.6 nm radiation in a vacuum system pumped with

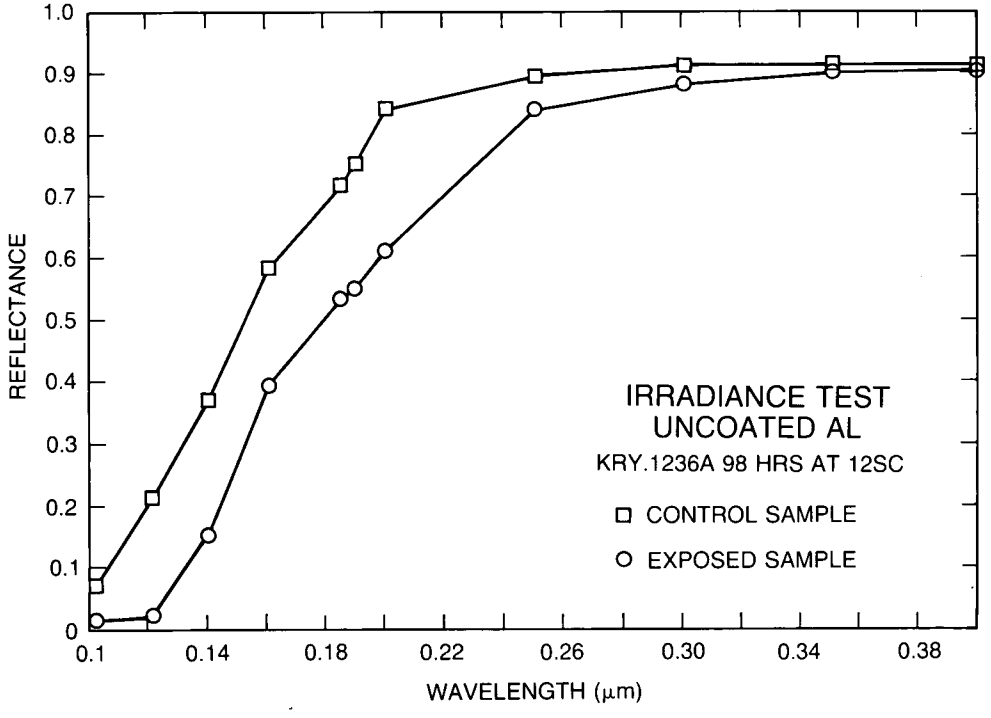

Figure 2.2 Reflectivity as a function of wavelength for uncoated aluminum surfaces, one of which was exposed to an oil-pumped vacuum system, and the other (control sample) not.

oil pumps. There is a considerable change in the reflectivity of the surface even at the longer wavelengths. In some cases, the oil is deposited on the surface in the form of droplets, and then broken down by solar radiation (Figure 2.3). However, the work of Hunter (1977) indicates that the original droplets evaporate quickly if not irradiated. Thus, it is unlikely that an oil film will retain its integrity on a surface in a hard vacuum for longer than a few days.

Figure 2.4 shows results from the SCATHA spacecraft, which carried two quartz microbalances. One of the balances was exposed to the solar irradiance, while the other was not. One can see from this figure that the sunlit sensor shows a steady increase of mass accumulation with

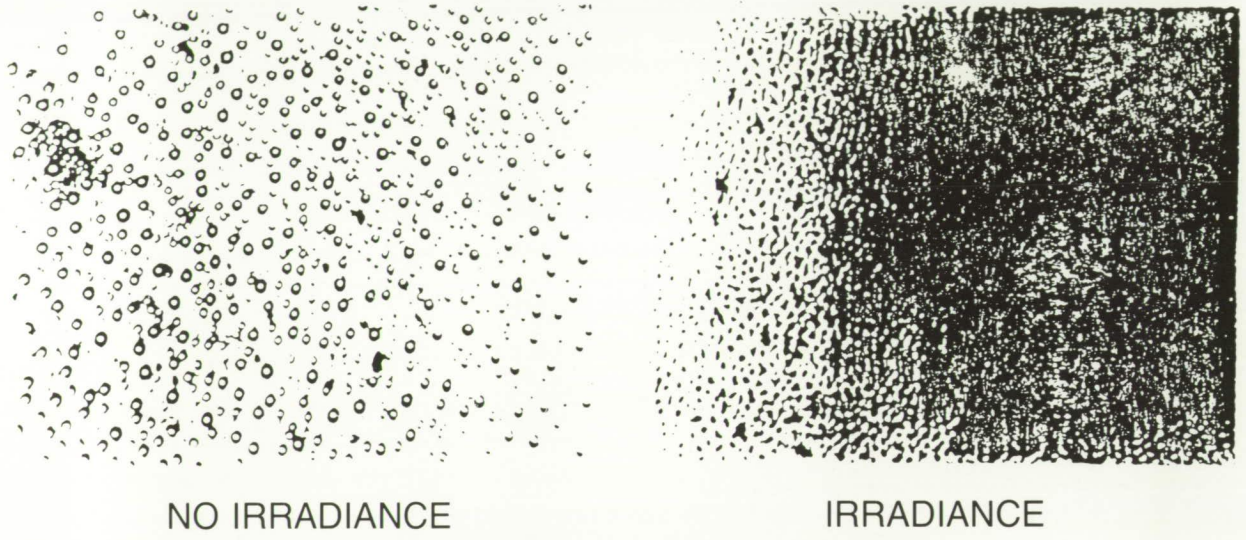

Figure 2.3 Effect of UV irradiation on evaporated DC 705 oil. The effective layer thickness is ≅200Å, evaporated onto an aluminum surface coated with MgF_2 (enlarged 700 times).

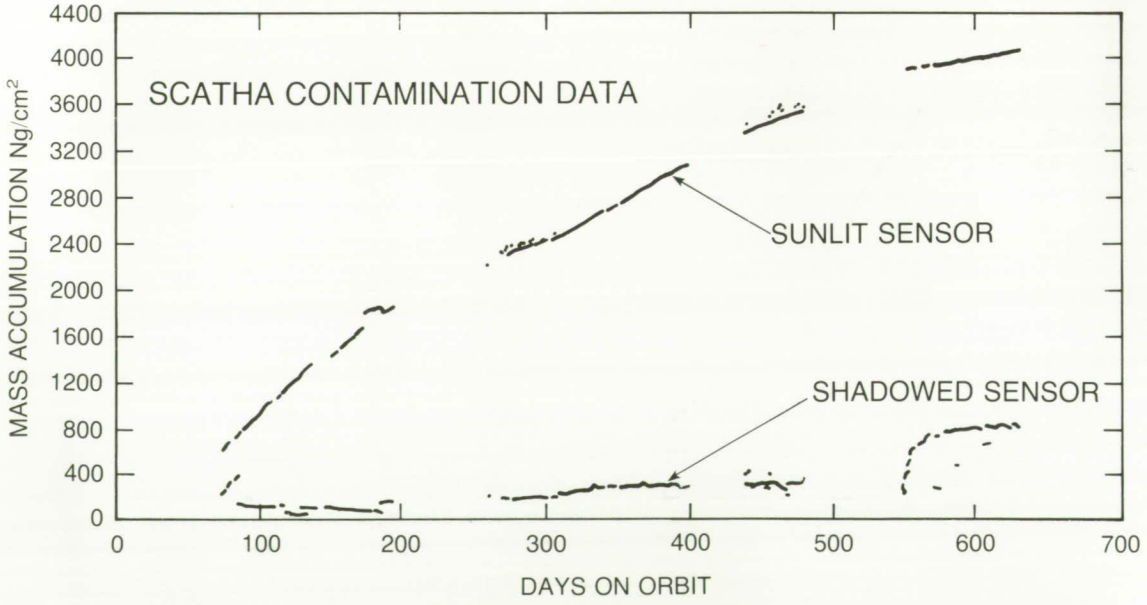

Figure 2.4 Mass accumulation as a function of time in orbit for illuminated and shadowed quartz microbalances on the SCATHA spacecraft.

time while the shadowed balance shows much less of an increase. It is significant, however, that it does show a slight increase, although this could be due to scattered sunlight. The solar wavelengths that can produce the film need not be at the high energies. Figure 2.5 shows the likely points at which the bonds could be broken in the methyl phenyl siloxane (silicon rubber) molecule. The energies correspond to wavelengths in the near ultraviolet.

In the laboratory, the deposited film has many of the characteristics of a carbon film. Figure 2.6 shows the change in the reflectivity at 270 nm for an uncoated oxidized aluminum surface versus the thickness of a carbon film deposited on the surface. It is unlikely, however, that any

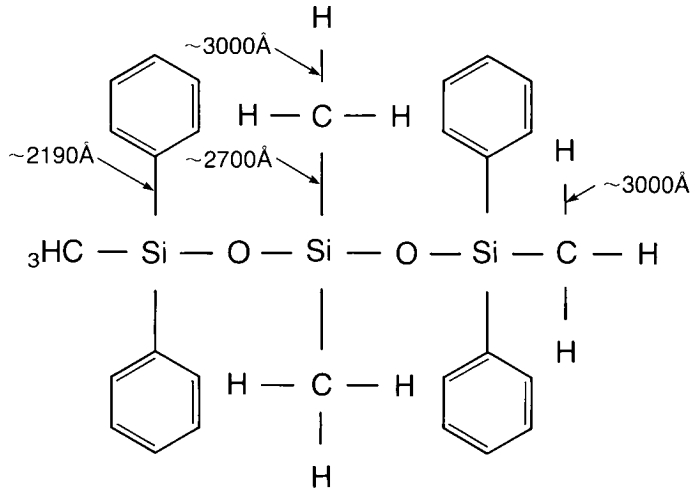

Figure 2.5 Bond energy of likely breaks of methyl phenyl siloxane (silicone rubber).

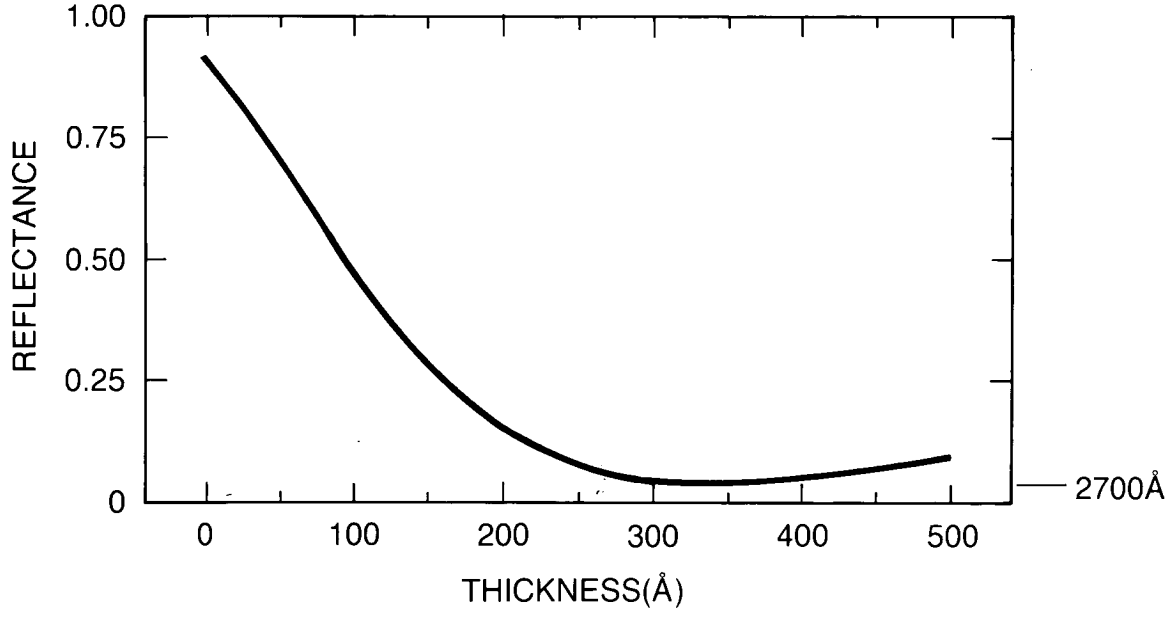

Figure 2.6 Reflectance at 270 nm of an uncoated oxidized aluminum plate as a function of the thickness of a carbon film deposited on its surface.

film deposited in space would be only carbon. The exact nature of the contaminant film will depend on the parent molecule or, in the case of a spacecraft environment, on several parent molecules.

Flight instruments and spacecraft contain many sources of contamination. Potting compounds, conformal coatings, insulation blankets, and attitude control gases are only a few of the possibilities. For most satellite launches, including Nimbus–7, the spacecraft is allowed to outgas for a few days after launch before the instruments are turned on; this should eliminate some of the surface contaminants. However, those sources of contaminants that are deeply rooted in the instruments or spacecraft will take much longer to outgas, and the traditional view that the outgassing will fall off exponentially with time may not hold (or the time constant may be very long).

2.2.2 Aging of Optical Surfaces

Most optical surfaces when incorporated into flight instruments have had a short history of exposure to radiation. There is considerable evidence that uncoated aluminum surfaces continue to lay down a protective layer of aluminum oxide, thus changing the optical properties of the surface. There is some evidence that the surface of replica diffraction gratings flows and changes the reflective properties of the grating. In general, it is usually incorrect to assume that optical surfaces will retain their original properties.

2.2.3 Changes in the Optical Transmission of Lenses, Filters, Etc.

The optical properties of transparent lenses, filters, windows, etc., can change as a result of exposure to radiation. These changes have many causes. Lithium fluoride and magnesium fluoride, for example, form color centers when exposed to ultraviolet radiation.

2.2.4 Detector Changes

Changes in detector response are one of the most common causes of changes in overall instrument responsivity. For this reason, most instruments have some method of monitoring the detector response. For the photomultipliers used in the experiments critiqued, one might expect to encounter:

- Changes in the window transmission.
- Changes in the cathode response.
- Changes in the dynode response. This is coupled with changes in the bleeder voltages to produce changes in the overall gain of the photomultiplier.
- Changes in the electronics.

2.2.5 Movement or Separation of Optical Components

Wearing of the surfaces of grating drive cams, dimension changes due to temperature fluctuations, and relaxation of stressed components are but a few of the mechanical instrument changes that could lead to changes in the optical response of instruments. For example, the SBUV instrument uses a quartz depolarizer at the entrance slit. This consists of a set of thin plates under tension in a holder, with the interfaces filled with an adhesive. During recent tests on one

of the SBUV–2 instruments, the plates were observed to move with respect to one another under thermal stress.

2.3 THE SOLAR BACKSCATTER ULTRAVIOLET (SBUV) EXPERIMENT

2.3.1 Physical Principles

Absorption of sunlight in the Hartley bands and continuum of ozone produces a complete attenuation at Earth's surface of solar radiation between 200 and almost 300 nm. (For a discussion of the spectroscopy of this spectral region, see Brasseur and Solomon, 1984, or Craig, 1965.) Thus, it is not possible to use ground-based absorption spectroscopy of this band system. Absorption spectroscopy is possible in the longer wavelength Huggins and Chappuis bands, but this technique does not provide any information about the vertical distribution of the ozone in the atmosphere. However, since ozone is a minor atmospheric constituent, unit optical depth for absorption in the Hartley continuum occurs at altitudes (wavelength dependent) where significant Rayleigh backscattering of sunlight occurs (despite the seven-order-of-magnitude difference in cross-section). Singer and Wentworth (1957) suggested that observations from above the atmosphere, in which the fraction of sunlight reflected back to space (the planetary albedo) is measured as a function of wavelength, could be used to deduce the concentration of ozone as a function of altitude. This is the principle of the SBUV experiment that flew on Nimbus–7. Other experiments utilizing the same principle have flown on Kosmos–65, OGO–4, Nimbus–4, Atmosphere Explorer–D, and, most recently, TIROS–9 and the Japanese Exos–C. Mathematically, the expression for the backscattered signal can be written as

$$I(\lambda) = F_o(\lambda)A[X(p),\alpha(\lambda),\beta(\lambda),\psi(\mu_o), R(\lambda)] \quad (1)$$

where $I(\lambda)$ is the observed backscattered radiance at wavelength λ, F_0 is the solar irradiance, and A is the albedo of the atmosphere and surface. This latter depends, as indicated, on $X(p)$, the total amount of ozone above a level where the pressure is p, the ozone absorption coefficient α, the Rayleigh scattering coefficient β, the Rayleigh phase function ψ for the solar zenith angle whose cosine is μ_0, and the surface reflectivity R. The full expression is given in Chapter 3 (Algorithms).

It was recognized from the outset that this technique was intrinsically capable of very high accuracy and stability, since the requirement was for a relative measurement of the ratio of Earth's backscattered UV radiance $I(\lambda)$ to the solar UV irradiance $F_0(\lambda)$ at the same wavelength. Because both measurements could be made with the same instrument, the determination of albedo as a function of wavelength over the range 250–340 nm should not depend on either the absolute calibration of the instrument nor on long-term variations in the sensitivity of the instrument.

However, for the SBUV, a major uncertainty is introduced by the use of an optical component not common to both measurements—the diffuser plate—which is used to transform the solar flux (irradiance) into a radiance that is comparable in magnitude to the backscattered Earth radiance, and can be measured instrumentally in exactly the same manner.

The extraction of the ozone profile, depends, then, on two factors: the precision and accuracy of the relative measurement, and the algorithm used to retrieve the information from the measured albedo. The second factor is treated in Chapter 3; the first is our principal concern in this chapter.

The SBUV experimenters recognized the need to achieve as high a measurement precision as possible with the spectrometer, and have devoted much effort to controlling sources of systematic error (e.g., polarization, scattered light, short-term gain changes, etc.). They have also taken care with the absolute calibration procedures, in part to properly address a secondary goal of the SBUV experiment, the long-term monitoring of variability of the solar UV irradiance at the top of Earth's atmosphere. The long-term behavior of the diffuser plate in the Nimbus–7 SBUV instrument remains a crucial area of concern for the evaluation of long-term trends of both ozone and solar irradiance.

The diffuser plate on the earlier Nimbus–4 Backscatter Ultraviolet (BUV) experiment was continually exposed to space, and its reflectivity decreased rapidly. In order to prevent this, the SBUV diffuser was designed to be stored inside the instrument, in a protected position, and deployed only when a measurement of the solar irradiance was made, which was usually once per day.

The plan for maintaining long-term stability was not stated explicitly, but appears to have been based on a belief that the degradation would be slow enough to be negligible. There is no provision for measuring any change of diffuser reflectivity in orbit.

The more recent operational version of SBUV, SBUV–2 (Frederick et al., 1986) has included a reference mercury lamp for evaluating the behavior of the diffuser plate with time. However, to provide a useful calibration, the lamp or other elements that direct its output to the diffuser and spectrometer must be positioned very repeatably, frequently over a long period of time. In addition, the lamp output must be stable over the time period when it illuminates successively the instrument and the diffuser. These conditions were not met for the first SBUV–2 instrument, and the inflight calibration has not been useful. Design changes have been made in an attempt to obtain reliable inflight calibrations on future versions of the SBUV–2 (see also Section 2.8.2).

2.3.2 Instrument

Descriptions of the instrument, together with diagrams, are given in Heath et al. (1975 and 1978, referred to below as User's Guide UG). For ease in following this discussion, a schematic is presented in Figure 2.7. The basic optical system consists of two Ebert–Fastie monochromators used in a double monochromator arrangement to provide twice the dispersion of a single instrument. The use of two monochromators in series, together with a holographically produced diffraction grating, ensures a very low level of instrumental scattering ($<10^{-9}$) in order to eliminate the possibility of contamination of radiance measurements near 250 nm by more intense long-wavelength (400 nm and longer) scattered light in the instrument. The wavelengths used for ozone measurements are, in nm, 255.5, 273.5, 283.0, 287.6, 292.2, 297.5, 301.9, 305.8, 312.5, 317.5, 331.2 and 339.8. The channel at 255.5 nm was measured, but not used because of fluorescence by NO. The next seven are used for extracting profile information, while the latter four are for determining total ozone. The methods by which the ozone profiles and column amounts are retrieved are described in the next chapter.

Another important feature is the use of a depolarizer at the entrance slit to remove the polarization sensitivity of the monochromator to the Rayleigh backscattered radiation. The diffuser plate, used to view the Sun (the field of view FOV of the instrument is normally directed toward the nadir for Earth radiance measurements) is a ground aluminum plate that is rotated into the FOV for the solar measurements.

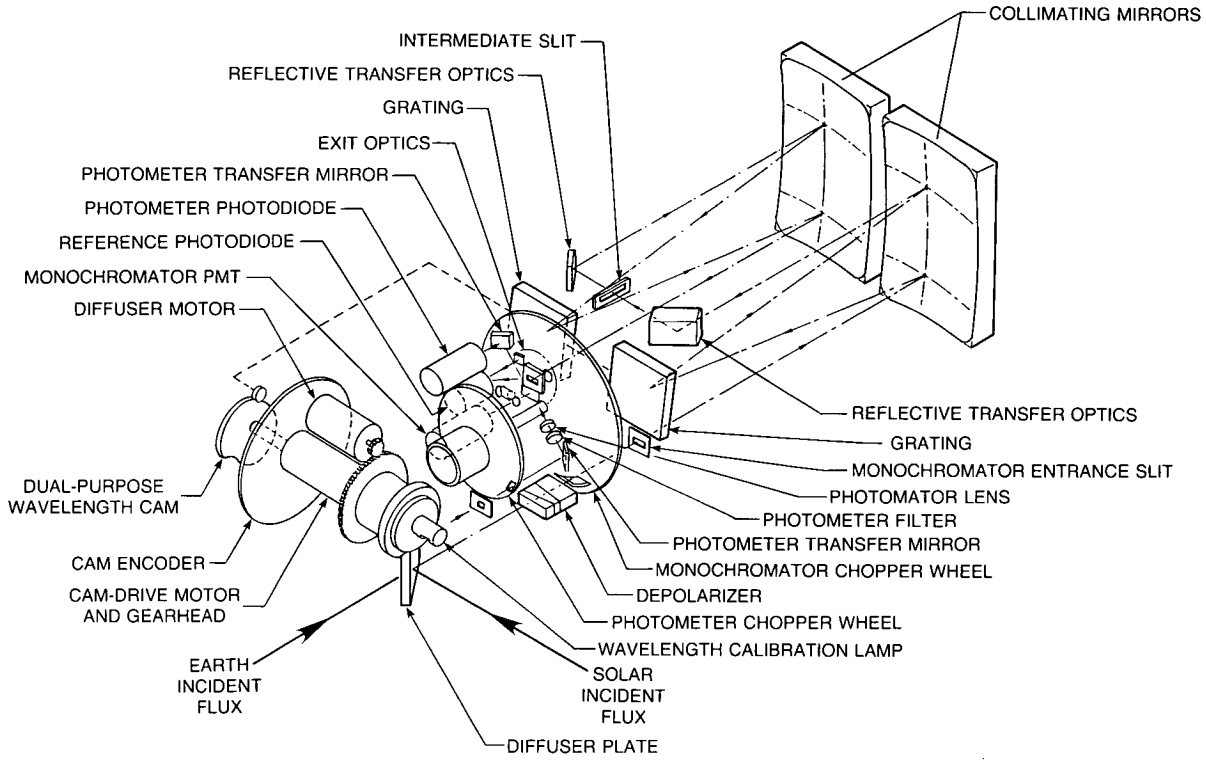

Figure 2.7 Schematic diagram of the SBUV instrument (from Heath et al., 1975).

The various operating modes of the instrument are also described in UG. Unfortunately, much of the material in UG and other reports is not available in the refereed literature, and in any case is difficult to obtain. This lack of available documentation was a serious problem in this investigation.

2.3.3 Prelaunch Calibration

The plan for prelaunch calibration is outlined in UG. Basically, various spectral irradiance sources, traceable to the National Bureau of Standards (NBS), were used, together with several diffusing screens, to produce a source of known radiance as a function of wavelength. The different diffusing screens were both intercompared and measured independently at NBS. The solar irradiance mode is similarly calibrated using the flight diffuser, except that for the spectral region <200 nm, the tests require a clean vacuum system (this region is of no interest for evaluating ozone trends). It should be noted that the quoted uncertainty in the absolute calibration, which is ~3–11 percent using NBS-traceable sources (Heath, private communication, 1987) is considerably larger than the measurement precision (<1 percent) achieved by the instrument itself, which is a measurement only of the reproducibility of a given measurement. In addition, there are two other critical calibration requirements: wavelength knowledge and reproducibility (the grating is coupled to the motor drive through a stepped cam), and electronics system linearity. The prelaunch tests for these parameters are also given in UG. Provisions for inflight calibration checks of the wavelength drive, detector, and the electronics are also described there.

All of the calibrations were performed at Beckman Instruments prior to the thermal–vacuum (T/V) testing that was done at General Electric. One of the goals of the T/V test was to determine

the stability of the instrument after repeated temperature cycles that simulate the expected environment in space. Following these tests, the absolute calibration of the spectrometer was checked at the T/V test site and was found to have changed by ~11 percent in the wavelength band 270–290 nm, 6 percent at 294 nm, 10 percent at 306 nm, and 7 percent at 315 nm and longer. The diffuser plus spectrometer calibration varied similarly with wavelength, so that the albedo change was ~3.5 percent at all wavelengths. This effect introduces an uncertainty of up to 8 percent in the solar output in the 270–290 nm band.

The launch schedule precluded any further measurements to determine possible sources of the change or even a recalibration using the same equipment that was used for the detailed prelaunch calibration. The post-T/V data were used for the initial flight calibration. While the change in absolute calibration does not affect the retrieval of trends in ozone profiles or column amounts, it does lay open the possibility of an undetected change of a similar nature occurring between the post-T/V test and operations in space. During the 7 years of operation of the instrument in orbit, a sudden change of 2 percent would probably be detected. A slow change would be treated as discussed below.

2.3.4 Results in Orbit

The SBUV was launched on Nimbus–7 on October 24, 1978, into a Sun-synchronous polar orbit. The instrument initially operated 3 out of 4 days, beginning on October 31, 1978, and provided an average of 1,200 sets of measurements per day. The observations cover the daylight portion of the globe, and are made close to local noon, except in polar regions. Solar measurements were initially made on one orbit per day, for a period of about 4 minutes.

The most crucial in-orbit observations for the present discussion are those of the time history of the results of the solar observations, shown in Figure 2.8a,b. At all wavelengths, they show a decrease in instrument response with time, with four episodes of rapid decrease interspersed with longer periods of slower decrease. The effect is larger at the shorter wavelengths, reaching a total decrease of about 50 percent after 8 years. There does not appear to be any possibility that more than a small part of this at the shorter wavelengths can be due to changes of the solar output. The response of the spectrometer–diffuser to solar radiation seems to have degraded over the life of the experiment.

The second observation of interest to the question of instrument change is that the response of the photomultiplier tube (PMT) detector changed by about 9 percent relative to a photodiode placed to serve as a check on any PMT changes over the period 1978–1983.

2.3.5 Possible Mechanisms Leading to Change in SBUV Instrument Response During the Mission

In general, instrument response change during orbit will be due to changes in the detection systems (electronics and detector) or in the optical system—including the optical elements, their alignment, and proper deployment (see Section 2.2). This section will point out the large number of mechanisms that are likely sources of change in the SBUV response; it should also discourage us from believing simplistic models of instrument degradation in the absence of independent data. Here we consider how these potential sources of change may affect the response of SBUV.

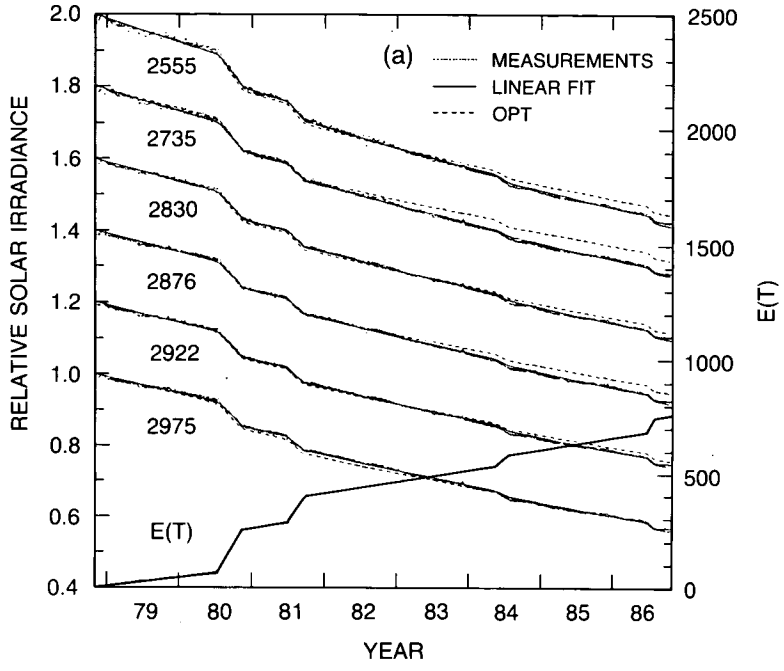

Figure 2.8a The measured degradation of the SBUV instrument, Fm(t)/Fm(0), for 1978–1987. The data, Fm(t), are the solar irradiance viewed by the spectrometer after reflection off the diffuser plate. The data consist of 2,303 measurements taken during one orbit per day. The abrupt inflection regions in 1980, 1981, 1984, and 1986 are for times when the diffuser plate was deployed on each of 14 orbits per day. Also shown are the exponential fit obtained by Cebula et al. (1988) (CPH) and adopted by the OPT (labeled OPT) and the 4-term quasi-linear fit (solid line) passing through the center of the data. The curve labeled E(t) is the accumulated exposure time in hours. The numbers on the left side correspond to the shortest six observing wavelengths. Each wavelength curve is normalized to 1 and displaced by 0.2 units.

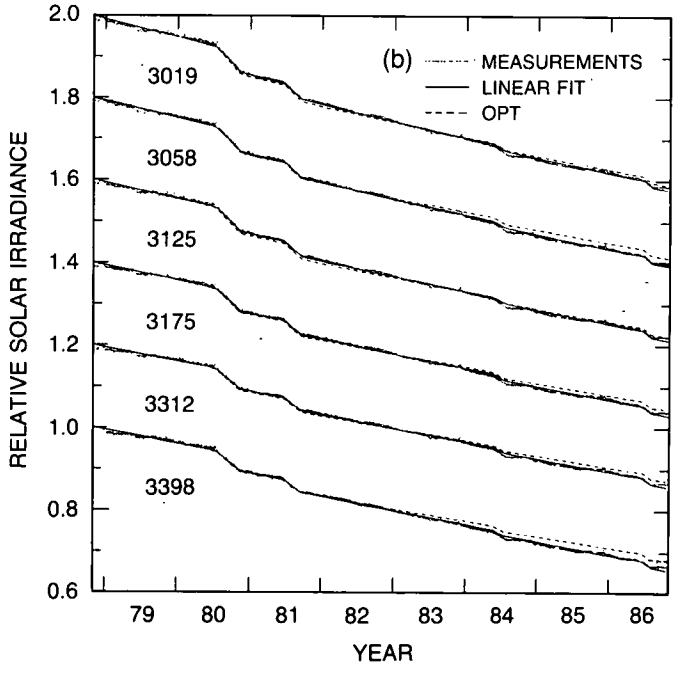

Figure 2.8b The same as for Figure 2.8a, except for the six longest wavelengths.

Detection System

SBUV did not have on board a constant current source often provided (as on TOMS) to check the performance and gain of the amplifier electronics, nor did it have the capability to look at the current from the first dynode of the PMT, which would allow monitoring the gain of the PMT. Rather, SBUV relied on monitoring a "constant" fraction of the light leaving the spectrometer exit slit with a reference vacuum photodiode. On the plus side, this method has the advantage of a "systems" approach, testing the stability of the PMT photocathode response, as well as, simultaneously, the gain of the PMT and the amplifier. On the negative side, it relies on the stability of the optical systems used as well as the diode for its interpretation. The elements involved are a mirror used to select about 10 percent of the light exiting the slit, a second mirror to redirect the selected light to a vacuum diode, and the window and cathode of the diode. In addition there is also a focusing mirror system used to relay the remaining light from the exit slit to the PMT. Changes in the reflectance of any of these mirrors or in the transmission of the diode window or the photoyield of the diode cathode could be misinterpreted as a change in gain of the PMT/amplifier system.

A final factor in evaluating this monitor system is that the light sampled apparently comes from a small portion of the exit slit. Since astigmatism in the spectrometer optical system is reasonably small, the intensity distribution of light along the exit slit would be expected to be proportional to the light distribution along the entrance slit. Any change in this distribution would affect the monitor-to-signal ratio.

In the SBUV data reduction, a change in this monitor signal was interpreted as a gain change. Clearly, this change could also have been due to changes in the relevant optics or the diode, or the intensity distribution along the slit. In their analysis of the observed degradation effects, the Ozone Processing Team (OPT), which is responsible for the operational reduction of SBUV and TOMS data, concluded that a significant degradation of the spectrometer optics has taken place. Thus, it would be logical to assume that some degradation in the detector optics has also taken place, even if the diode is assumed to be completely stable. At least the assignment of the change in monitor signal during the mission as a gain change of the PMT appears to be open to reinterpretation. The effect of a change like this on the ozone trend cannot be quantified without a model of the time history of the change, and of the instrument degradation. For the models described in Section 2.3.6, the effects would probably be small.

Optical Systems

The optical system may be divided into the prespectrometer, spectrometer, and detector (postspectrometer) optics. The prespectrometer optics consist of the reflective scatter (diffuser) plate used in the irradiance measurement (but not in the backscatter radiance measurement), and the depolarizer (used in both). The spectrometer optics consist of six mirror and two grating reflectances in a double Ebert–Fastie mounting. The detector optics consist of a reflector focusing field optic to image the second grating on a field stop in front of the PMT using one or two reflecting surfaces. It should be reiterated at the outset that changes in the spectrometer will affect both solar and ozone measurements, while changes in the diffuser will affect only the solar measurements. However, unless there is a way to unambiguously separate a diffuser change from a spectrometer change in orbit, one kind of change will almost certainly be misidentified, leading to errors in ozone trends.

- Diffuser and Depolarizer—The diffuser is a ground aluminum plate overcoated with evaporated aluminum positioned as the first optical element of the SBUV instrument. The second optical element, the depolarizer, consists of four appropriately oriented and tapered layers of quartz. Since both elements are outside the spectrometer entrance slit, they can receive more UV radiation and higher exposure levels to any contaminants in the vicinity of the spacecraft. The diffuser is the only optical element exposed to the full solar irradiance when deployed. To the extent that the solar radiation contributes to the degradation of the instrument response, it is likely that the diffuser plate is responsible for most of this form of decreased response. On the other hand, the depolarizer is exposed to reflected solar radiation, especially at long wavelengths, for the Earth-viewing period, which is 25 times longer. Even if the reflected solar radiation on the diffuser is only 1 percent of that on the diffuser, its degradation is not negligible.

  In the absence of solar exposure, the optical surfaces should have contamination layers that are at equilibrium with the local low-pressure atmosphere surrounding the spacecraft. Hydrocarbons deposited on a surface exposed to solar UV radiation tend to form strong bonds with the surface and adjacent carbon atoms. The resulting film has a much lower vapor pressure than the original hydrocarbons and so can gradually build up to a considerable thickness at a rate that seems to be proportional to the UV exposure time (for SBUV conditions). The buildup of a permanent film may or may not be proportional to the deposition rate depending on how quickly equilibrium is established during the periods of no solar exposure.

  The presence of a film on the optical surfaces is likely to reduce the reflectance of the scatter plate and, to a lesser extent, the transmission of the depolarizer. If the overall instrumental response can be considered to be a product of the independent degradation of the spectrometer and diffuser plate, then the effect of a film forming on the depolarizer is eliminated when the instrument is used to determine ozone from the measured UV albedo. That is, the effect of spectrometer degradation cancels when calculating the ratio of backscattered radiance to solar irradiance (albedo). The problem is to be able to separate the effects of the diffuser plate and spectrometer degradation when analyzing the measured albedo.

  If a thin film model of the SBUV diffuser plate degradation is correct, then certain characteristics of the film (thickness, real and imaginary parts of the refractive index) must be specified in addition to identifying its bulk characteristics. For example, it can be shown that a nonuniform film thickness across the surface of the optical elements can have an additional effect on the calculated degradation that is comparable to degradation from uniform films of the same average thickness. The radiance–irradiance ratio may be a complex function of the growth rate of a contaminating film of unknown bulk properties, the known rate of solar exposure and total elapsed time since the spacecraft launch, the known number and frequency of diffuser plate deployments, the unknown film geometry, and possible unknown exposure-dependent effects on the depolarizer and other internal spectrometer components. To some extent, the properties contributing to the degradation can be characterized from a series of four experiments performed during 1980 to 1986 (so-called "frequent deployment" experiments), and from the long-wavelength measurements of the radiance and irradiance.

- Spectrometer and Detector Optics—The spectrometer optical system is a double monochromator (Ebert–Fastie), which is a very good design for the reduction of scattered light.

This feature is further enhanced by the field stop in the exit optics to confine radiation reaching the detector to that coming from the second diffraction grating. Thus, only scattering coming from the optical elements themselves can be seen by the detector. In addition, holographic diffraction gratings that are known for low scattered light were employed. The excellence of this overall design in reducing the dangers of scattered light in UV solar measurements was demonstrated by preflight testing. There remains the hazard, however, that the growth of contamination on the spectrometer optics over many years in orbit can increase the scattering from the optical elements and contribute to spectral impurity of the exiting radiation. Also, aging (deterioration of evaporated films) after this long service and UV exposure is a possibility. Regardless of the scattering introduced by contamination and aging of the optics of the spectrometer and detector systems, there is little question that some reduction in specular reflectivity due to contaminants can be expected. Since there are 9 or 10 reflections, a 1 percent average loss per element would result in about a 10 percent overall transmission loss of the system. This "leverage" offsets somewhat the lower level of short-wavelength irradiance existing on the optical elements within the spectrometer. Thus, this is a serious probable change in instrumental response for which there is no method of separate evaluation.

- Other Deleterious Effects—Two other possible sources of change in instrumental response should at least be mentioned. The first is the possible fluorescence of the contaminating layers developing on the optical elements, excited by the UV component of the incident radiation but fluorescing at longer wavelengths. A fluorescence signal from the diffuser or polarizer would add to the intensity arriving at the entrance slit of the spectrometer at the fluorescent wavelengths. Fluorescence from optical elements within the spectrometer would appear similar to scattered light.

  The second possibility relates to the unfortunate change in calibration that was discovered after a thermal vacuum (T/V) test of the SBUV prior to launch. This significant change (radiance 6–11 percent; irradiance 4–8 percent) was most likely due to some contamination during the thermal vacuum test. Credit is due the determined Principal Investigator (PI) who insisted on a post-T/V calibration, which unfortunately was a hurried in-the-field evaluation of the instrument response. This final calibration necessarily was taken to be the initial response of the SBUV in orbit. It is conceivable that some of the contamination that occurred at this time was subject to "cleanup" during the initial flight exposure to high vacuum before exposure to solar UV.

In conclusion, there are many possible sources of change of instrument response during inflight life, with various effects on the solar irradiance and backscatter radiance measurements and the albedo determination. It is not possible to determine which of these effects may be operative to a significant degree in causing the overall instrument degradation observed.

2.3.6 Diffuser Plate Degradation

General Discussion

The problems arising from the SBUV instrument degradation can be understood more easily if $F_{o\lambda}$ and I_λ denote, respectively, the solar irradiance and backscattered radiance determined by applying the values from the prelaunch calibration for diffuser reflectivity and spectrometer sensitivity. Then, denoting the measured quantities, which vary with time t, by subscript M, for each wavelength

$$F_{M\lambda}(t) = F_{o\lambda}(t)D_{\lambda}(t)S_{\lambda}(t) \tag{2}$$

and

$$I_{M\lambda}(t) = I_{\lambda}(t)S_{\lambda}(t) \tag{3}$$

where $F_{o\lambda}(t)$, $D(t)$, and $S(t)$, the solar flux, the diffuser reflectance normalized to its initial (preflight) value and the spectrometer sensitivity normalized to its initial value, are unknown. The quantity related to the atmospheric ozone content is the albedo (radiance–irradiance ratio).

$$A(\lambda,t) = \frac{I_{\lambda}(t)}{F_{o\lambda(t)}} = \frac{I_{M\lambda}(t)}{F_{M\lambda}(t)} D_{\lambda}(t). \tag{4}$$

If $A(\lambda, t)$ increases, it could be due to an increase in I_{λ}, resulting from a decrease in ozone, or an overestimate of $D_{\lambda}(t)$—i.e., an overestimate of diffuser reflectivity, or equivalently an underestimate of its degradation.

From Equation 4, it is clear that a knowledge of $D_{\lambda}(t)$ is critical to deriving the correct albedos, and thus the correct ozone distributions and trends, from the measurements. The SBUV did not include any means to carry out an inflight calibration for evaluating the long-term behavior of either the spectrometer or the diffuser plate, admittedly a difficult task.

The estimation of $D_{\lambda}(t)$ therefore requires the use of other information. Possibilities include making special measurements in orbit to determine $D_{\lambda}(t)$, deriving $D_{\lambda}(t)$ from a comparison with other ozone measurements, or deriving $D_{\lambda}(t)$ from measurements of F_M and I_M. Unfortunately, all of these have problems. There are not enough reliable measurements of the vertical ozone profile to allow $D_{\lambda}(t)$ to be determined at the eight short wavelengths. (Perhaps Dobson measurements could be used for the four long wavelengths, but apparently this was not investigated before the ozone trend studies.) Some inflight measurements will be described below, but they were infrequent, and used only for comparison with other results.

The remaining possibility, which was employed by the OPT, is to use the measurements of I_M and F_M to estimate $D_{\lambda}(t)$. Equations 2 and 3 have four unknowns, since $I_{\lambda}(t)$ may be changing due to a changing ozone distribution. If other information can be used to provide an estimate of the temporal variation of $F_{o\lambda}(t)$, the number of unknowns is reduced to three.

For wavelengths at which the ozone absorption is imperceptible, it is plausible (but not necessarily correct) to assume that the true underlying albedo over a large geographical area (like the Tropics) shows no long-term change. This can be used in Equation 3 to determine $S_{\lambda}(t)$, and thus unambiguously separate the effects of the diffuser from those of the spectrometer.

For wavelengths at which there is measurable ozone absorption, this procedure cannot be followed, because assuming a trend in albedo effectively specifies the ozone trend that is being sought. There is no information that allows one to make this separation with certainty in Equation 3.

Therefore, the approach is to use measurements of $F_{M\lambda}(t)$, expressed by Equation 2, with information on $F_{o\lambda}(t)$ from other data, to estimate the product $D_{\lambda}(t)S_{\lambda}(t)$, and hypothesize the way the product is factored.

The solar irradiance $F_{M\lambda}(t)$ was measured by deploying the diffuser in the direct solar beam for about 4 minutes on at least one orbit per day ("standard" observations) throughout the life of the SBUV instrument. In addition, there were four periods of "frequent" observation, when the diffuser was deployed on each orbit (about 14 per day) for an extended length of time. Figure 2.8a,b shows the measured degradation of the SBUV instrument, $F_{M\lambda}(t)/F_{o\lambda}(=D_\lambda(t)S_\lambda(t))$, for November 1978–November 1986, for the 12 observed wavelengths.

Figure 2.8a also shows the cumulative exposure time E(t) of the diffuser plate to the Sun. From the coincidence between periods of frequent diffuser deployment and rapid decrease of solar signal, it is clear that part of the signal degradation is due to diffuser deployment into the solar beam.

Historically, these are the data on which everything is based. From these, one must first determine how the product DS depends on various factors and, second, separate D from S. Clearly, the solution is not unique. Criteria for assessing the solution are its plausibility and its consistency with the few constraints discussed below. The only physical limits are D = 1 (no degradation on the diffuser) and S = 1 (all degradation on the diffuser).

The Exponential Model (Cebula, Park, and Heath)

Based on the first 6 years of data shown in Figure 2.8, Cebula et al. (1988, referred to as CPH below; see also Park and Heath, 1985) proposed a model of the degradation in which the percentage rate of change of one component was proportional to the total diffuser exposure time E, and the percentage change of the other component was proportional to the total time in orbit, t. Then, after correction for the Sun–Earth distance to 1 AU,

$$\frac{F_{M\lambda}(t)}{F_{o\lambda}} = P(t)e^{-\gamma(\lambda)G(t)}e^{-s(\lambda)t}e^{-r(\lambda)E(t)}. \tag{5}$$

The photomultiplier gain, P(t), is determined from a comparison with the onboard reference diode (which was not stable).

The second term contains the variations in the solar flux, based on the model of Heath and Schlesinger (1984, 1986):

$$\frac{F_{o,\lambda}(t)}{F_{o,\lambda}(0)} = \exp[-\gamma(\lambda)G(t)], \tag{6}$$

where G is the ratio of core to wing radiance of the MgII doublet, and γ are coefficients relating the solar output at λ to G. The γ's were derived from observations of the 27-day rotation period; their use here implicitly assumes that the change in the solar spectrum over the 11-year solar cycle has the same wavelength dependence as the change over a 27-day rotation period. While this is plausible, it neglects the possibility that there could be another component of variation over the longer period (see Lean, 1987). Thus, there is uncertainty in the values used for $F_{o,\lambda}(t)$.

With these assumptions, we have

$$D(t)S(t) = e^{-r(\lambda)E(t)}e^{-s(\lambda)(t)} \tag{7}$$

where the assumptions that $r(\lambda)$ and $s(\lambda)$ do not change with time are included. Thus, to determine the two components, one need only compare time periods in which the ratio E/t

varied substantially. CPH did this by using time spans containing equal periods of nominal and frequent solar observation. Periods of frequent exposure occurred in 1980 and 1981, which were the basis for the original analysis, and again in 1984 and 1986. For those periods, CPH argued that the solar change was small (although they were of several months' duration) and so would not contribute to the variation.

The derived values of $r(\lambda)$ and $s(\lambda)$ are presented for the first two frequent deployment periods in Table 2.1. The values of $r(\lambda)$ were subsequently smoothed in wavelength for use in the OPT processing. The smoothed values are the last column of Table 2.1. The individual values for

Table 2.1 SBUV *r* and *s* Values

Wavelength	*r* (SBUV)	*s* (SBUV)	*r* (smooth)
(nm)	(hr-1)	(dy-1)	(hr-1)
255.5	5.720E–04	1.266E–04	5.8113E–04
273.5	5.090E–04	9.777E–05	4.9232E–04
283.0	4.400E–04	1.096E–04	4.4813E–04
287.6	4.330E–04	9.487E–05	4.2734E–04
292.2	4.090E–04	9.501E–05	4.0737E–04
297.5	3.760E–04	9.708E–05	3.8543E–04
301.9	3.660E–04	8.558E–05	3.6914E–04
305.8	3.620E–04	7.506E–05	3.5619E–04
312.5	3.320E–04	7.554E–05	3.3520E–04
317.5	3.220E–04	6.662E–05	3.2150E–04
331.2	2.880E–04	6.066E–05	2.8983E–04
339.8	2.750E–04	6.181E–05	2.7236E–04

F/F_o = exp (-*r*E(*t*) - *st*) fit to the first two "rapid deployment" periods (1980, 1981). The *r*(smooth) data are the most recent numbers used in SBUV processing.

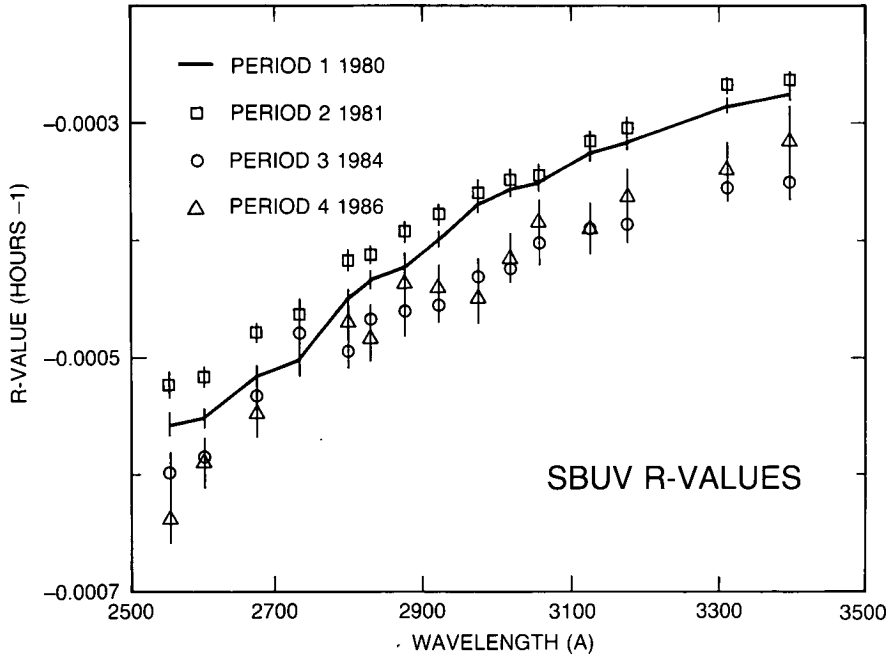

Figure 2.9 Values of $r(\lambda)$ determined during the four frequent deployment periods by CPH.

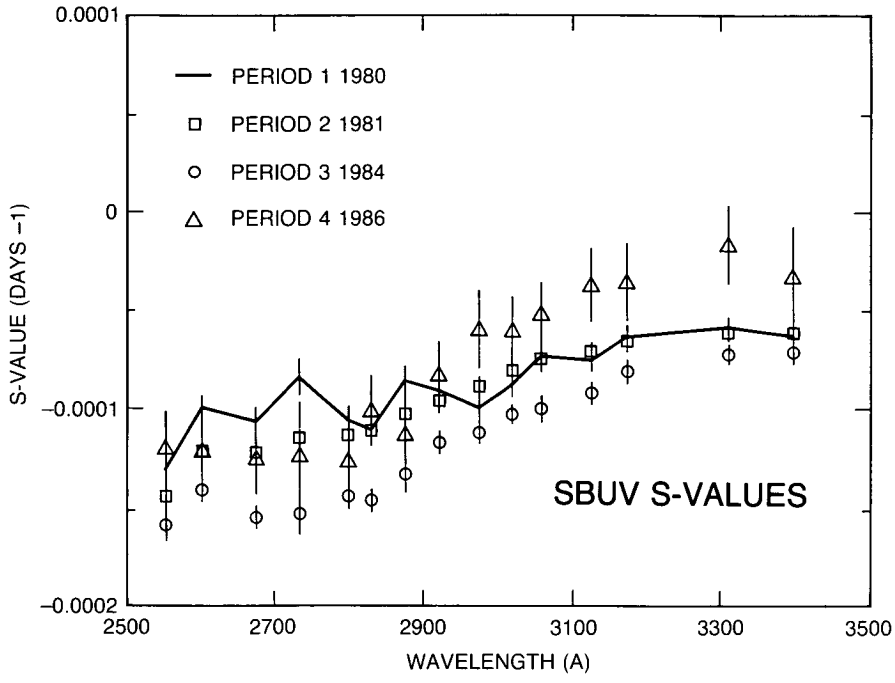

Figure 2.10 Values of $S(\lambda)$ determined during the four frequent deployment periods by CPH.

the four individual determination are shown in Figures 2.9 and 2.10. The formal uncertainty associated with $r(\lambda)$, based on the statistical fit of the solar flux data to the model, has been given as ~2 percent. Thus, at 273.5 nm (the wavelength contributing most to the 1 mb ozone retrieval), the total decrease in diffuser reflectivity over 7 years is 27 percent with a formal uncertainty of ±0.5 percent. Several arguments suggest that this formal error seriously underestimates the true uncertainty in $r(\lambda)$:

- In Figure 2.9, it is clearly seen that the $r(\lambda)$ values, particularly those from 1984 and 1986, differ significantly from the 1980–1981 values. The ozone retrievals use constant $r(\lambda)$ values derived from the 1980–1981 frequent solar observation periods. This is disturbing, as the deviation is largest in 1984–1986, the period of largest purported ozone decrease. The standard deviation of the data points for r at each wavelength is 6–13 percent (depending on wavelength), far greater than the formal 2 percent uncertainty in the 1980–1981 points.

- Values of $r(\lambda)$ derived from the TOMS data (see Table 2.2), are typically 13 percent higher than the SBUV $r(\lambda)$ values for wavelengths in common. This is statistically significant, despite the factor-of-two higher formal error than the SBUV $r(\lambda)$ values. While the TOMS FOV on the diffuser plate is smaller than that of SBUV, it is difficult to imagine an area-sensitive degradation mechanism that is capable of producing such an effect. (It has been suggested that the effect arises because the diffuser reflectivity has an angular dependence and TOMS views the diffuser at a larger angle from the normal, and that the frequent exposure periods were all at times that resulted in extreme angles. A deposit on the diffuser that changed the angular dependence might, in principle, lead to such an effect.)

Table 2.2 Comparison of SBUV and TOMS *r* Values for Combined Periods 1–2

λ	TOMS *r*-value	Sigma *r*	SBUV *r*-value	Sigma *r*
312.5	-3.63E–04	1.11E–05	-3.32E–04	5.04E–06
317.5	-3.76E–04	1.14E–05	-3.22E–04	5.80E–06
331.2	-3.17E–04	1.06E–05	-2.88E–04	4.38E–06
339.8	-3.01E–04	1.06E–05	-2.75E–04	4.92E–06
360.0	-2.50E–04	1.04E–05	-2.38E–04	4.16E–06
380.0	-2.28E–04	1.04E–05	-1.79E–04	4.44E–06

Note: The above uncertainties are based on the formal statistical error of the fit. The TOMS value is at the 65% confidence level, SBUV at the 90% confidence level.

λ	*R*-Value Diff. SBUV–TOMS	Comb. sigma (90% conf.)	Diff./Comb. sigma (90% conf.)
312.5	3.13E–05	1.93E–05	1.62
317.5	5.36E–05	2.00E–05	2.68
331.2	2.87E–05	1.83E–05	1.57
339.8	2.58E–05	1.85E–05	1.39
360.0	1.15E–05	1.80E–05	0.64
380.0	4.84E–05	1.81E–05	2.68
	Average		1.77
	Standard deviation		0.72

λ	Year 6 % Diff. @ E(t) = 600	Uncertainty in % Diff.	Year 8 % Diff. @ E(t) = 761	Uncertainty in % Diff.
312.5	1.90	1.18	2.41	1.50
317.5	3.27	1.24	4.16	1.58
331.2	1.74	1.11	2.21	1.42
339.8	1.56	1.13	1.98	1.44
360.0	0.69	1.09	0.88	1.38
380.0	2.95	1.12	3.75	1.43
Average	2.02	1.14	2.57	1.46
Standard deviation	0.86	0.05	1.10	0.07

Note: Again, the uncertainty in the % difference between the SBUV-based and TOMS-based *r*-values is calculated using only the formal statistical uncertainty in the fit, and does not include any possible systematic error. Specifically, the error in the TOMS *r*-values due to goniometric error is not included.

- The fit (Equation 7) to the degradation data that has been used to convert the SBUV radiance measurements in ozone amounts assumes that *r* and *s* are constants with respect to time. A comparison of this fit with the entire data record is shown by the dashed lines in Figure 2.8 and percent difference plots in Figure 2.11a,b for each wavelength. (Because the OPT adopted the CPU model, values obtained from it are labeled OPT in this and several subsequent figures. The two terms are interchangeable.) CPH argue that only the $\exp(-rE)$ portion of the fit is used in the ozone data reduction, and that the variation of *r*

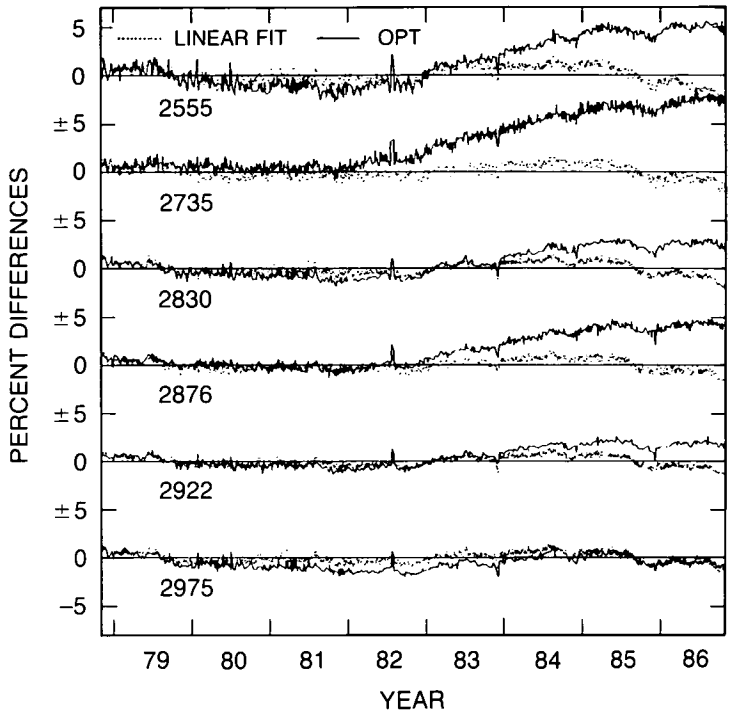

Figure 2.11a Percent difference between solar observation data and models. Horizontal line indicates 0 percent difference, solid line is OPT (CPH) model, and points are quasi-linear model (described below) for the six shortest wavelengths.

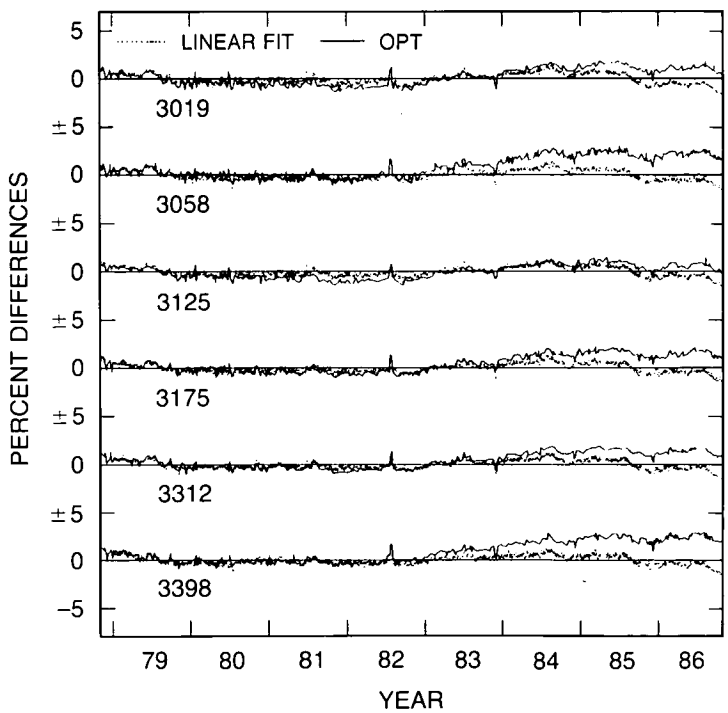

Figure 2.11b As in 2.11a, but for the six longest wavelengths.

calculated at each of the frequent deployment episodes is small. They interpret the small r variation as meaning that the form $\exp(-rE)$ correctly describes the diffuser plate degradation. To obtain an overall fit, they hold r constant in time and force the spectrometer constant, s, to vary. The variation of s with time calls into question the rationale for assuming Equation 7 as a unique form for describing the degradation. At best, it indicates that the formal statistical error given by CPH is probably too small.

The most critical assumption is the separation of the exponential model of the overall degradation into two components. CPH assumed the diffuser plate degradation is described for each wavelength by

$$D_\lambda(t) = e^{-r(\lambda)E(t)} \tag{8}$$

and the spectrometer by

$$S_\lambda(t) = e^{-s(\lambda)t}. \tag{9}$$

The rationale for putting all the exposure effect on the diffuser is that the diffuser plate is the only optical element directly exposed to the solar UV radiance and therefore is most likely to be the element affected by the amount of exposure time. The next element in the optical path, the depolarizer, is exposed to about 1 percent of the solar flux striking the diffuser plate. CPH assume that this amount of exposure would not contribute significantly to the exposure-dependent portion of the observed degradation (although, as noted above, it is continuously exposed). They claim that no exposure-correlated features are seen in the SBUV albedos to within 0.5 percent error. The rationale for assigning all the temporal variation to the spectrometer (Equation 9) is less clear.

The application of Equations 8 and 9 to the 339.8 nm radiance data is illustrated in Figure 2.12. The lower dash–dot line shows the raw solar irradiance, indicating that the SBUV response has decreased by about 28 percent after 8 years. The solid line shows the relative changes in the raw backscattered radiance, averaged from 20°S to 20°N, with seasonal variations removed. If the true backscattered radiance has not changed, the spectrometer has degraded by about 10 percent. The dotted line shows the decrease in F expected from the analysis. The ratio of these, the albedo, shown by the line of short and long dashes, is essentially constant over this period.

This demonstrates that the CPH approximations (including the use of r and s from 1980–1981 only) give reasonable results at this wavelength, but does not establish their applicability at other wavelengths.

One must be cautious about assuming that this approach is general, for at least two reasons:

- While A (340 nm) is sensibly a constant, other data (Cebula, private communication, 1988) indicates that this can vary by ±2 percent. It is not clear how large an uncertainty in D (340 nm) this would permit, and subsequently what part of the time-dependent degradation could be assigned to the diffuser.

- More important, even knowing what fraction of time-dependent degradation could be assigned to the diffuser at 340 nm, where degradation is relatively small, does not necessarily mean that the same fraction is relevant at the shorter wavelengths, where both components of the degradation are greater.

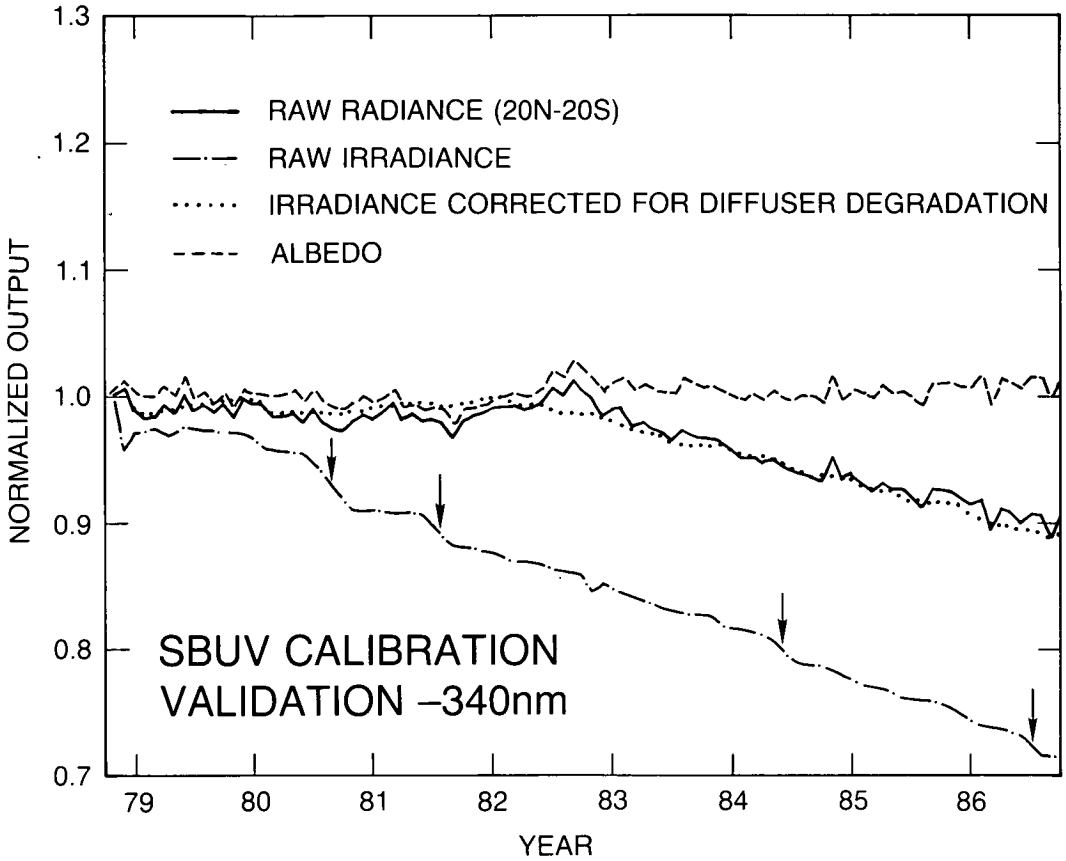

Figure 2.12 Comparison at 340 nm between the measured solar irradiance, irradiance corrected for diffuser degradation, Earth radiance from 20°N–20°S, and albedo, as a function of time.

An Alternate Empirical Model

Alternate empirical models can be derived that accurately describe the observed degradation (Herman and Hudson, private communication, 1988). These are of two types. The first and simplest is the observation that the data between 1978 and 1986 are well fit by linear or quasi-linear functions of the forms

$$D(t)S(t) = a + bt + cE$$

or

$$D(t)S(t) = a + bt + cE + dE(t)t \tag{10}$$

where $E(t)$ is the total accumulated exposure (hours) and t is the total elapsed time (hours) since day 307 of 1978. The linear expression fits quite well, with the largest differences during and after the last frequent deployment period. The second type is more closely based on a physical model of thin film formation on the diffuser plate and its optical effect on reflectivity (Madden, 1963; Smith et al., 1985). In this case, $D(t)$ is a function of the film thickness, real and imaginary parts of the refractive indices of a multilayer film over an aluminum substrate, and film deposition rate. $S(t)$ is an assumed empirical function that could be $\exp(-st)$. For both the quasi-linear and the thin film fits, the four parameters are determined by a least-squares procedure (nonlinear for the

thin film case). The solid line in Figure 2.8 represents Equation 10 plotted over the normalized data F/F_o. The fit is good over the entire period (1978–1986). The region of poorest fit is near the end of the data set, where the last rapid deployment occurred. The same problem occurs with the least-squares fitting procedure if the data are truncated just after the 1984 frequent deployment. If the data were extended into 1988, then the fitting problem would probably disappear. Percentage differences are shown by the solid lines in Figure 2.11.

Although the compressed scale makes the magnitude of the differences hard to see, it is clear that, at all wavelengths, the quasi-linear fit is closer to the data than the exponential model. This is perhaps not surprising in that a four-parameter (or three-parameter) model might be expected to fit better than a two-parameter model. However, it does illustrate the nonuniqueness of the form of the fit. The coefficients derived using Equation 10 are given in Table 2.3.

Table 2.3 Coefficients for the Quasi-Linear Model

Wavelength (nm)	A	B (hr-1)	C (hr-1)	D (hr-2)
255.5	9.900E–01	-5.048E–06	-4.785E–04	2.584E–09
273.5	1.004E+00	-4.623E–06	-4.155E–04	2.110E–09
283.0	1.002E+00	-4.194E–06	-3.907E–04	1.646E–09
287.6	1.007E+00	-4.012E–06	-3.674E–04	1.448E–09
292.2	1.001E+00	-3.683E–06	-3.625E–04	1.417E–09
297.5	1.002E+00	-3.404E–06	-3.542E–04	1.276E–09
301.9	1.001E+00	-3.209E–06	-3.316E–04	1.036E–09
305.8	1.003E+00	-3.009E–06	-3.186E–04	9.008E–10
312.5	1.002E+00	-2.721E–06	-3.042E–04	6.779E–10
317.5	1.006E+00	-2.565E–06	-2.864E–04	5.153E–10
331.2	1.005E+00	-2.235E–06	-2.593E–04	2.312E–10
339.8	1.006E+00	-2.270E–06	-2.498E–04	1.127E–10

$F/F_0 = A + B*t + C*E + D*E*t$ fit to full data set of 2303 points (1978 to 1986).

The quasi-linear fit is not based on any physical model and therefore cannot be extrapolated beyond the domain of the data (1978–1986). Eventually, the degradation data, F/F_o, would have to deviate from the quasi-linear form. Such a deviation might have helped in constructing a physical model based, for example, on thin film optics. In the discussion that follows, different factorization of the quasi-linear model can be shown to yield different rates of degradation for the diffuser plate and spectrometer. One of the many possible cases indicates that the decreasing ozone trend at 1 mb is much smaller (perhaps zero) than that calculated by the OPT using Equation 8, and another case shows a larger decrease than that found by OPT. The point of this exercise is to demonstrate the large uncertainty in any ozone trend analysis based on the presently archived data.

Case M: Diffuser degradation more than exponential model (which will result in higher derived ozone concentration, or more ozone).

Equation 10 can be written as

$$D(t)S(t) = (A + kE)\left(1 + \frac{Bt + DEt + hE}{A + kE}\right) \tag{11}$$

where

$$h = C - k$$

Let

$$k = f\frac{C}{1 + (B/A)t} \tag{12}$$

then assume that

$$D(t) = A + kE$$

and

$$S(t) = 1 + \frac{Bt + DEt + hE}{A + kE} \tag{13}$$

The factor f in Equation 12 is an arbitrary scale factor selected to produce a particular value of the calculated SBUV albedo.

Case L: Diffuser degradation less than the exponential model (which will result in lower derived ozone concentration)

An alternate division of terms is

$$D(t)S(t) = (A + ht)\left(1 + \frac{CE + DEt + kt}{A + ht}\right) \tag{14}$$

where

$$k = B - h.$$

Let

$$h = B \tag{15}$$

then assume the factors can be identified as

$$D(t) = 1 + \frac{CE + DEt + kt}{A + ht} \tag{16}$$

and

$$S(t) = A + ht$$

In Case M, the diffuser and the spectrometer degradation depend on both E and t. In Case L, the diffuser term depends on E and t, while the spectrometer term depends on t alone.

Comparisons between the diffuser degradation using the CPH constant r(smooth) shown in Table 2.1 and the quasi-linear diffuser degradation (Case M $f=1$ is Case M1, $f=0.9$ is M2 and Case L) are shown in Figure 2.13a,b for all 12 wavelengths used in the ozone retrieval algorithm. Figure 2.14a,b shows the corresponding degradation of the spectrometer.

Using Equation 4, the different rates of the diffuser plate degradation can be used to calculate the percent change in albedo relative to the CPH formulation. Results of such a comparison are shown in Figures 2.15a,b. Each line labelled with the wavelength is the zero reference line. Case L generally has a larger albedo at the end of 8 years, while Case M has a smaller one. In terms of ozone, a negative (positive) albedo difference means more (less) ozone than the OPT model based on the CPH exponential fit would predict. (Henceforth, this will be referred to simply as

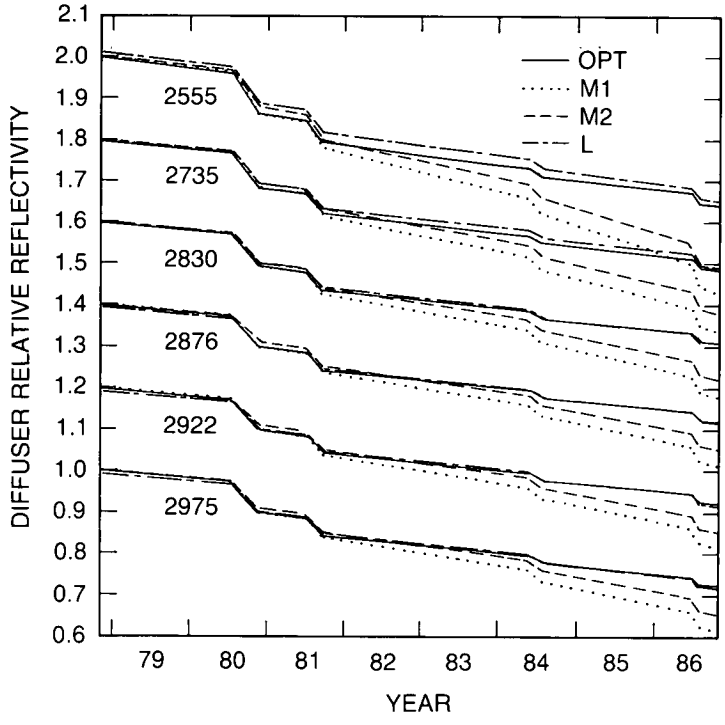

Figure 2.13a Relative diffuser reflectivity as a function of time for the OPT (CPH) and quasi-linear models, for the six shortest wavelengths.

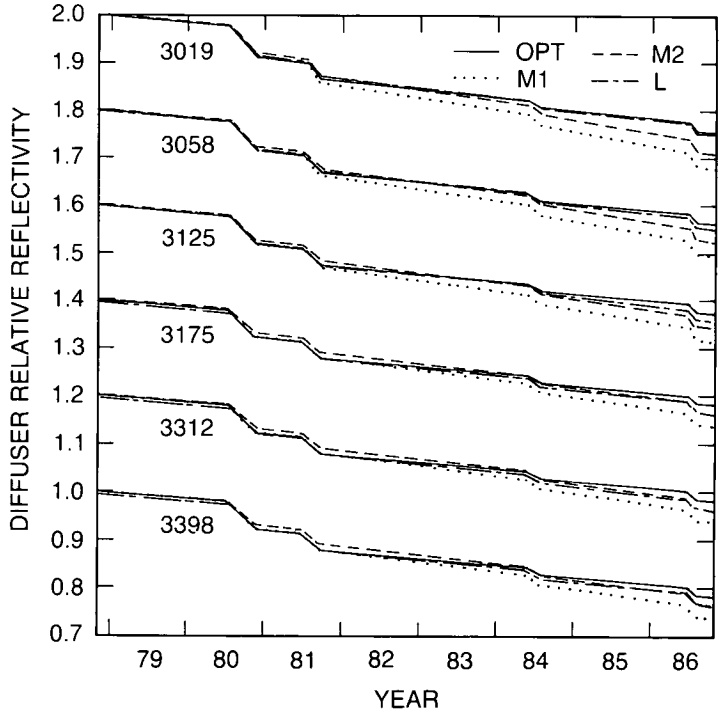

Figure 2.13b As in 13a, but for the six longest wavelengths.

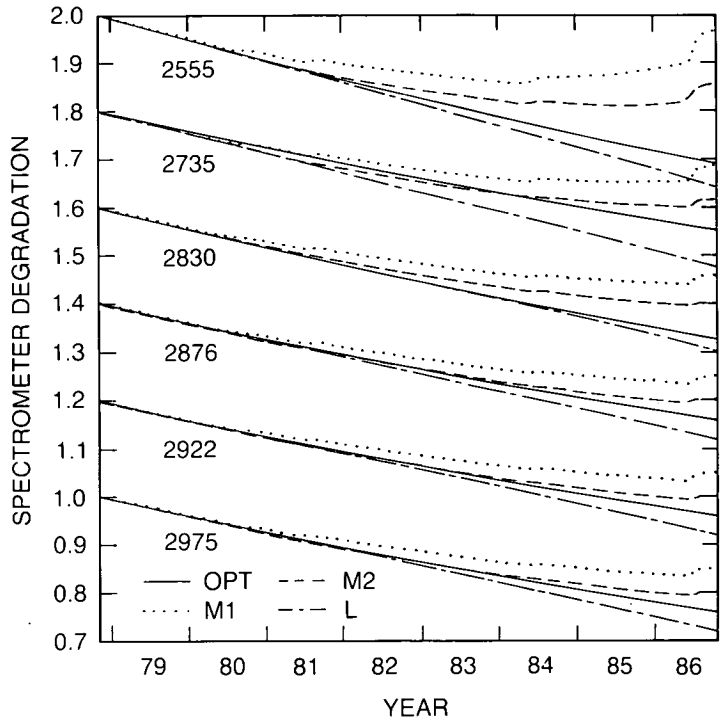

Figure 2.14a Relative spectrometer degradation as a function of time for the OPT (CPH) and quasi-linear models, for the six shortest wavelengths.

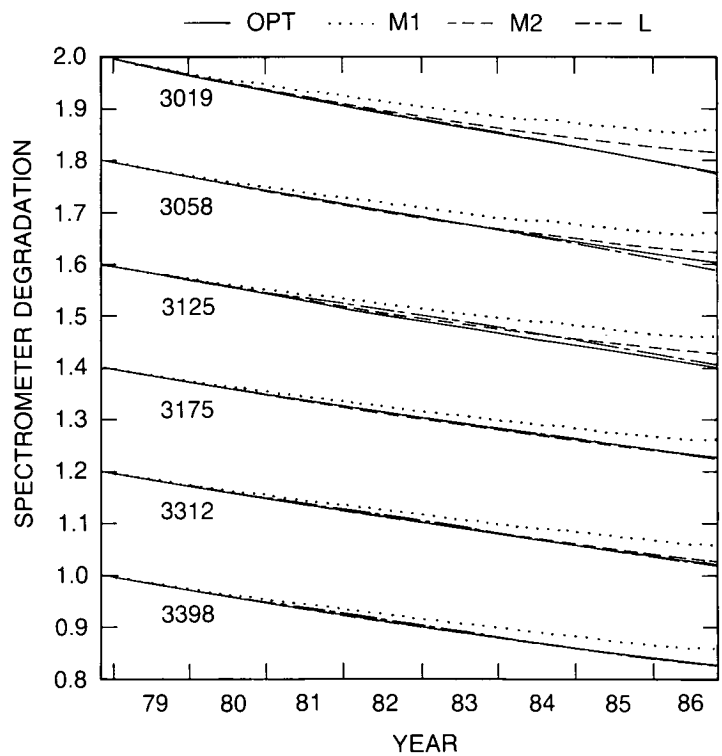

Figure 2.14b As in 14a, but for the six longest wavelengths.

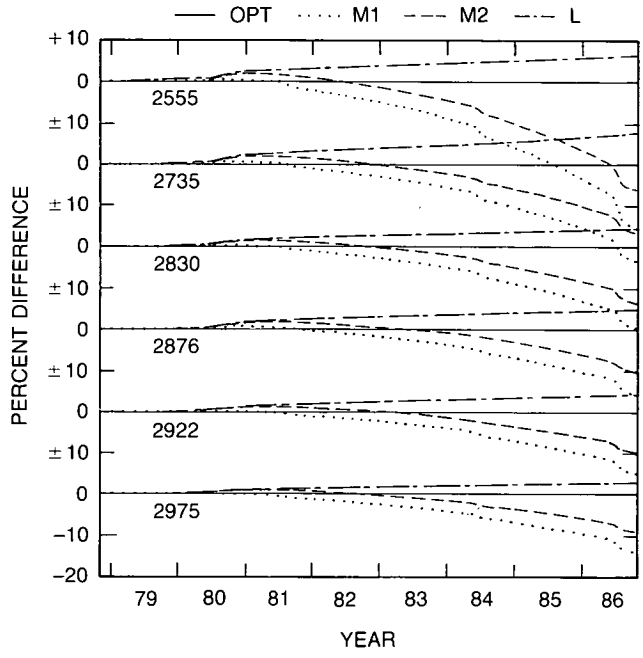

Figure 2.15a The percent difference in the calculated albedo between the quasi-linear models and the exponential (CPH) fits for the six shortest wavelengths. The exponential fit as used in the OPT model is the reference, % diff. = (model - OPT)/OPT. Each line labeled with the wavelength is the zero reference line. In terms of ozone, positive albedo difference means less ozone than the OPT exponential fit would predict. Since 0.1 units = 10%, the 273.5 nm deference for case M2 implies about 14–16% more ozone than OPT. This reduces the reported ozone decrease at 1 mb to about 5% from 1978–1987. Case M1 would yield no decrease over this period, while case L would give a slightly larger decrease than the OPT results.

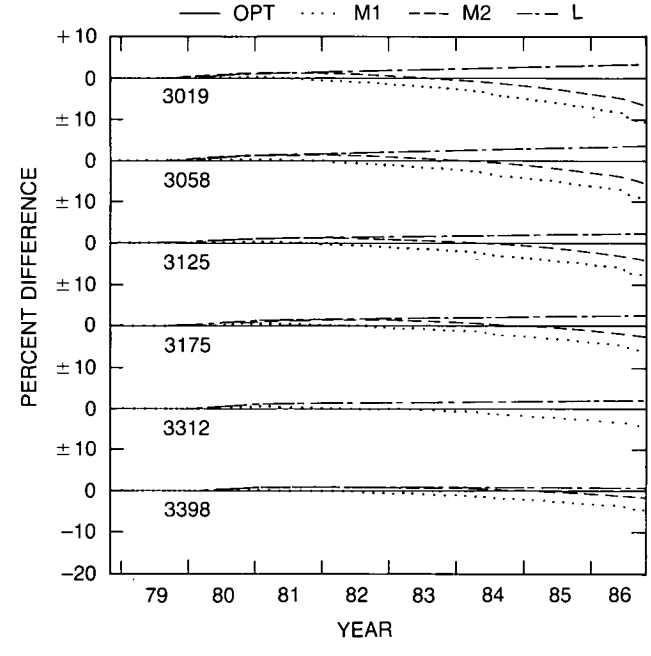

Figure 2.15b The same as 15b, but for the six longest wavelengths. Note that the longest wavelength channel, 339.8 nm, is almost independent of the model chosen to fit the degradation of the instrument or its separation into diffuser plate and spectrometer degradation. This means that the long-wavelength channels cannot be used to determine S(t) and D(t) for the shorter wavelengths (cf. Fig. 2.12).

the OPT model.) Since 0.1 units = 10 percent, the 273.5 nm difference for Case M2 implies about a 14–16 percent smaller albedo than OPT, or about 27 percent more ozone over the 8-year period. The conclusion is that the variation of albedo and ozone amounts can be very large, depending on the way the $D(t)S(t)$ product is factored. Clearly, a critical question is whether there is any way to select one separation over another.

2.3.7 Validation of Diffuser Degradation Models

Comparison With Dobson Network Results

Comparison with the Dobson network results is a way of checking the total ozone results and, therefore, the longer wavelength channels, and will be deferred to the next section, which will discuss TOMS as well. For profile data, i.e., wavelengths shorter than 312.5 nm, it has not been possible to obtain data that would distinguish between the various choices for $D(t)$ and $S(t)$. It might be expected that the inclusion of $E(t)$ in the spectrometer degradation portion of Case M would lead to structure in the radiance observed at 339.8 nm over the tropical regions of Earth. As can be seen from Figure 2.14, no structure corresponding to the frequent deployment periods is present in any of the three forms of $S(t)$, and the magnitudes are sufficiently close as to be within the experimental error. Thus, these data do not point to a preferred model.

Earthshine Data

An additional source of data was critically reviewed. This was the series of diffuser Earth-view studies, during which backscattered radiance of Earth was observed directly, and off the diffuser. The ratio of the diffuser view to the direct view gives a measure of diffuser-relative reflectivity, as other instrument sensitivities and Earth radiance cancel out. By periodically repeating the measurements, it was hoped that a time history of the relative reflectivity could be obtained, and used to compare with and check the model predictions.

The geometry of this experiment is illustrated in Figure 2.16. The diffuser was deployed continuously on December 6 or 7 in the years 1978 and 1983–1987. The data were then ratioed to the average of the direct view on the prior and following days. An example of the results for 1978 in Figure 2.17 illustrates some of the problems. The rapid rise at a subsatellite latitude near 20°N is due to the direct solar illumination of the diffuser, while the drop near 85°S suggests that the FOV is partially in an unilluminated region. However, for the region between, the latitudinal variation is not understood. This is partly because the area of the atmosphere seen by the diffuser is very large and poorly defined. The signal received must include many rays taking long paths at large zenith angles through the atmosphere. The effective backscattered radiance from the atmosphere will thus depend on the ozone amount and distribution. However, neither the complete radiative transfer problem nor the sensitivity to instrumental effects (e.g., the angular dependence of the diffuser reflectivity) has been analyzed in detail. Therefore, there may be systematic errors in the reported values, for which no estimate can now be given. In addition, there are appreciable random errors, due to cloud variability at long wavelengths and to the low signal levels (2.5 percent of the direct signal) and poor signal to noise ratios at the short wavelengths. These are at the 1–2 percent level.

At this time, only data for 1978 and 1983–1985 have been reduced. Figure 2.18a,b,c compares the model used by the OPT and quasi-linear predictions of the degradation from 1978 to 1983–1985 with the "earthshine" results. The rough magnitude and the general trend for greater degradation at shorter wavelengths agree, giving greater confidence in these features. However,

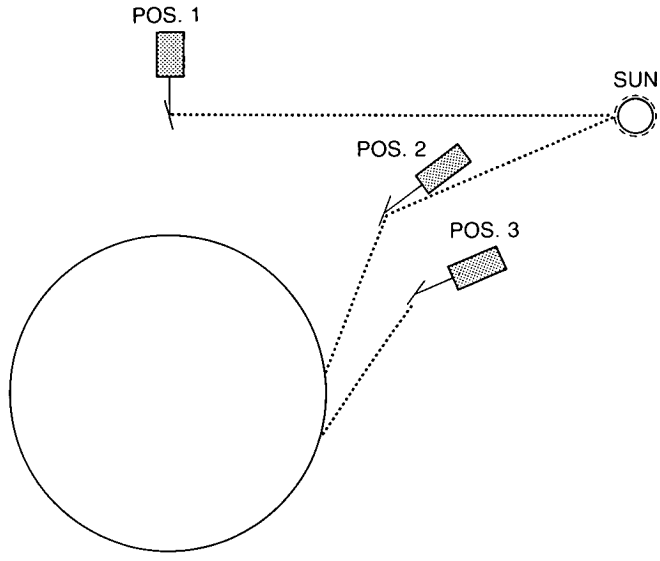

Figure 2.16 Geometry of the earthshine observations.

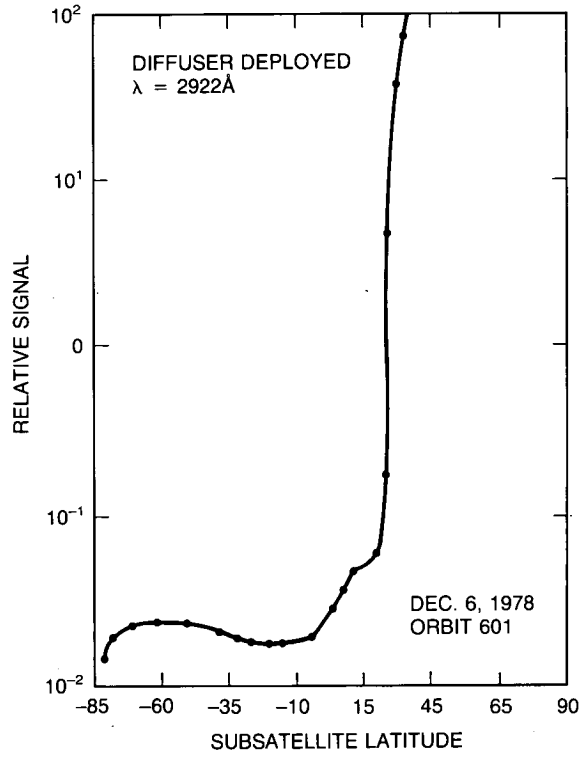

Figure 2.17 Example of ratio of earthshine signal to direct solar irradiance as a function of subsatellite latitude.

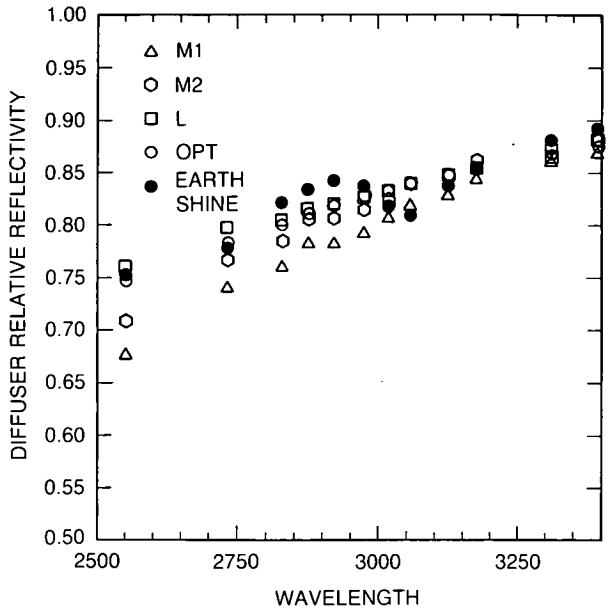

Figure 2.18a Comparison of diffuser reflectivity relative to 1978 versus wavelength, determined from earthshine measurements, and given by the models, for December 1983.

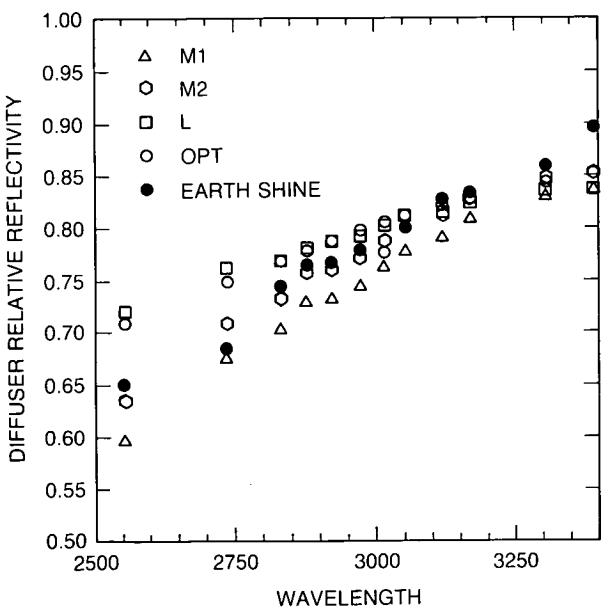

Figure 2.18b As in 18a, but for December 1984.

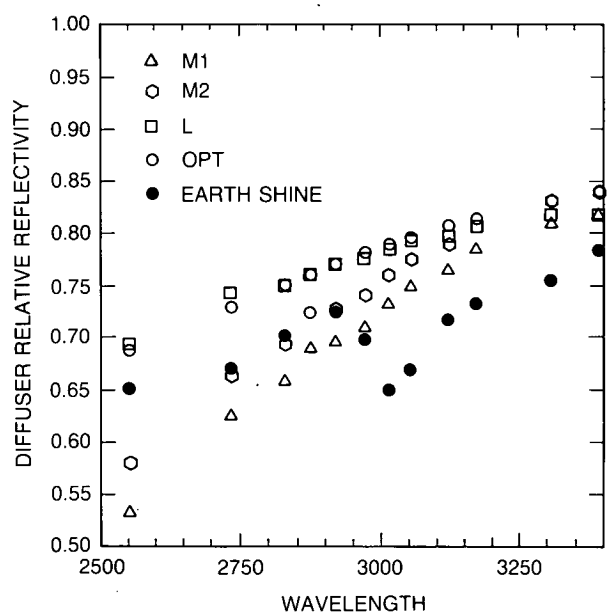

Figure 2.18c As in 18a, but for December 1985.

the earthshine results have a curious local minimum near 303 nm each year that is not suggested by the other results. Taken at face value, the "earthshine" data also indicate a faster degradation with time than either of the models, with greater degradation by 1985 than predicted by the CPH model.

However, because the interpretation of the "earthshine" values is not clear, the only conclusions that can be drawn at this time are that the earthshine data do not consistently or unambiguously favor one model over another, and perhaps disagree with all those discussed here. This could indicate that the assumption that the coefficients are constant with time is not valid. More probably they should be interpreted only as not contradicting the general magnitude and trend with wavelength derived from the models.

Total Ozone Determinations From the D-wavelength Pair

Another piece of internal information from the SBUV experiment indicates strongly that the OPT corrections for the diffuser degradations are not adequate. In a recent study, Bhartia (private communication, 1988) has compared total ozone determined from the D-wavelength pair to archived total ozone in the Tropics. Figure 2.19 shows schematically the SBUV wavelengths involved. Operationally, major reliance is placed on the A and B pairs, with C being used in high latitudes where the solar zenith angle is large and the total ozone amount is large (See Chapter 3).

The D pair uses wavelengths that are only 6.7 nm apart, compared to 18.7 nm for the A pair. Thus, if diffuser degradation is roughly linear in wavelength, the D pair should be $1/2.8 = 0.36$ times as sensitive to diffuser drift as the A pair. In addition, because the difference in ozone absorption coefficients is larger for the D pair than for the other pairs, results then are estimated to be only $1/4.5 (= 0.22)$ times as sensitive to diffuser drift than the archived "best ozone," which is based on a weighted sum of the A, B, and C pairs.

The limitation is that, because the ozone absorption coefficients at the D wavelengths are large, this pair can give results only for the small solar zenith angles, i.e., in the Tropics.

Figure 2.20 shows the difference between the archived "best ozone" and the D pair ozone, between 20°N and 20°S, as a function of time. The points in this plot are monthly averages determined each March and September and show a downward drift of the archived ozone

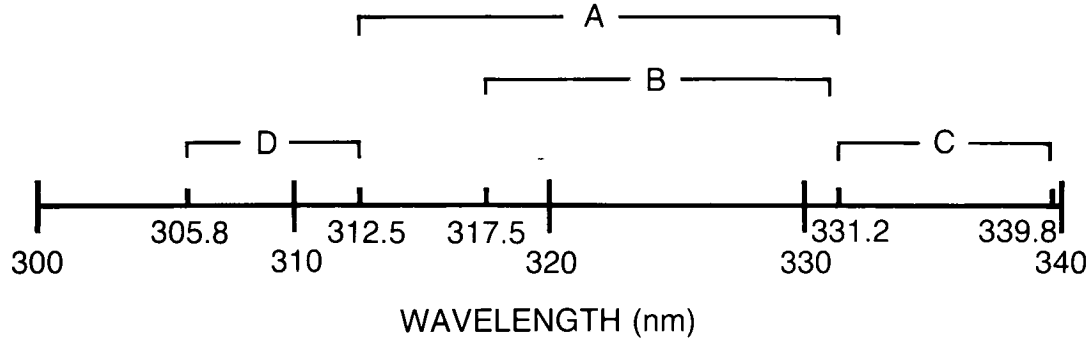

Figure 2.19 Wavelength pairs for total ozone determination.

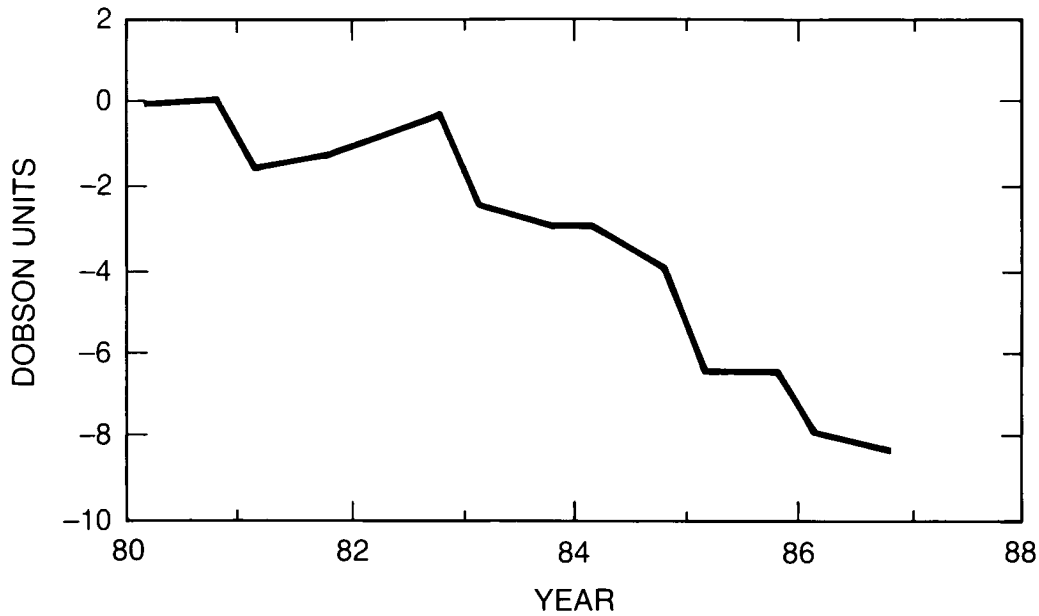

Figure 2.20 Archived SBUV total ozone minus total ozone determined from SBUV D-pair wavelengths, 1980–1987 (from Bhartia, unpublished).

relative to the less sensitive D-pair ozone. The data indicate a small drift, if any, between the archived and D-pair ozone from launch until late 1982, followed by a rapid downward drift of archived ozone. This suggests that the model used to correct for diffuser drift did not display any obvious problems for the first 4 years, but seems to have departed from the actual diffuser thereafter. The change shown in Figure 2.20 is similar to the comparison between SBUV and Dobson results in Chapter 4. This lends further support to the stability of the D-pair ozone, and to the failure of the OPT model to follow diffuser degradation very well after 1982, at least at the longer wavelengths.

2.3.8 Assessment

Section 2.3.6 has shown that a linear or quasi-linear form for the dependence of the degradation on t and E fits the observed degradation of the solar observations somewhat better than an exponential form. The form used by CPH is not only not unique, it is not as good as some others. Section 2.3.6 also pointed out that the product of $D(t)S(t)$ could be factored in an infinite number of ways, leading to large differences in the estimated diffuser reflectivity; again, the form used by CPH is not unique. Section 2.3.7 shows that there are no known data that allow a selection of one factorization over another at the short wavelengths used for ozone profile determination. Thus, the true value of any instrument change (and any ozone trend) is subject to large uncertainty.

Certainly, more complex models of diffuser and spectrometer degradation are possible, but are not amenable to verification from the available data and observing sequences used. The crucial factor is that none of the proposed models has a physical justification for its uniqueness, nor is it possible to show from the data that any one model is the only one compatible with the observations.

Values of D for the quasi-linear and OPT models after 8 years are compared in Table 2.4, along with the percent differences in D between Case M1 or Case M2 and Case L. These percent differences can be used to calculate the uncertainty in ozone change in each Umkehr layer, as described in Chapter 3. These uncertainties are plotted in Figure 2.21. Clearly, the uncertainty in the ozone amounts is quite large after 8 years, as expected from the large uncertainty in the diffuser characteristics. The uncertainties in the trends, or rate of change, are shown in Figure 2.22.

Table 2.4 Model Values of Diffuser D After 8 Years

Wavelength (nm)	M1	M2	OPT	L	Ratio 1*	Ratio 2*
2555	.4276	.4848	.6426	.6508	0.414	0.292
2735	.5349	.5814	.6875	.6977	0.264	0.182
2830	.5800	.6220	.7110	.7020	0.191	0.122
2876	.6147	.6533	.7224	.7162	0.152	0.092
2922	.6286	.6658	.7334	.7297	0.149	0.092
2975	.6469	.6822	.7458	.7346	0.127	0.074
3019	.6748	.7073	.7551	.7453	0.099	0.052
3058	.6939	.7245	.7626	.7523	0.081	0.038
3125	.7146	.7432	.7748	.7577	0.058	0.019
3175	.7362	.7626	.7830	.7649	0.038	0.003
3312	.7674	.7906	.8021	.7780	0.014	-0.016
3398	.7755	.7980	.8128	.7780	0.003	-0.025

*Ratios 1 and 2 are the differences L – M1 and L –2 M2, respectively, divided by their average value.

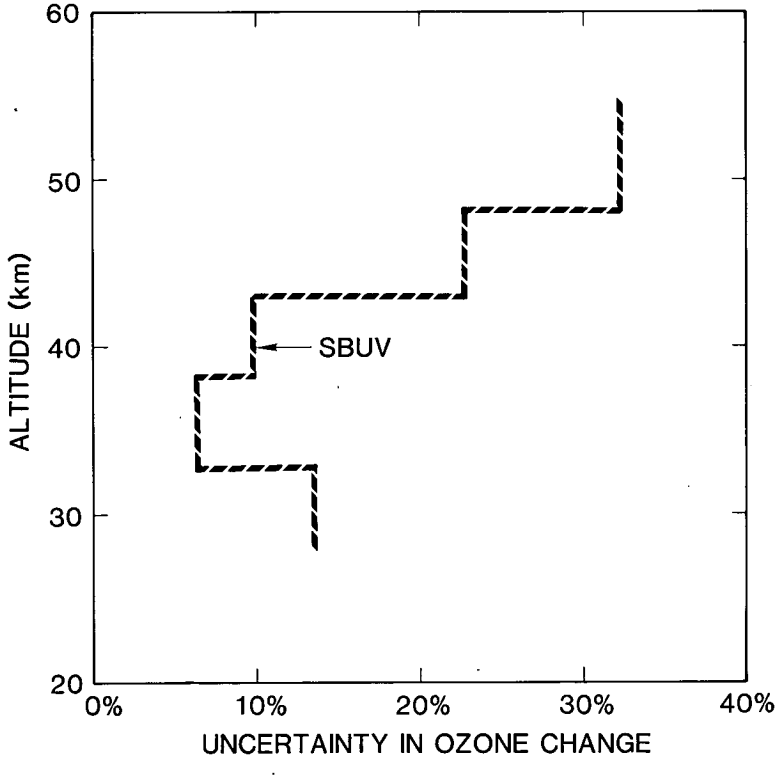

Figure 2.21 Uncertainty in ozone change determined from SBUV data over 8 years.

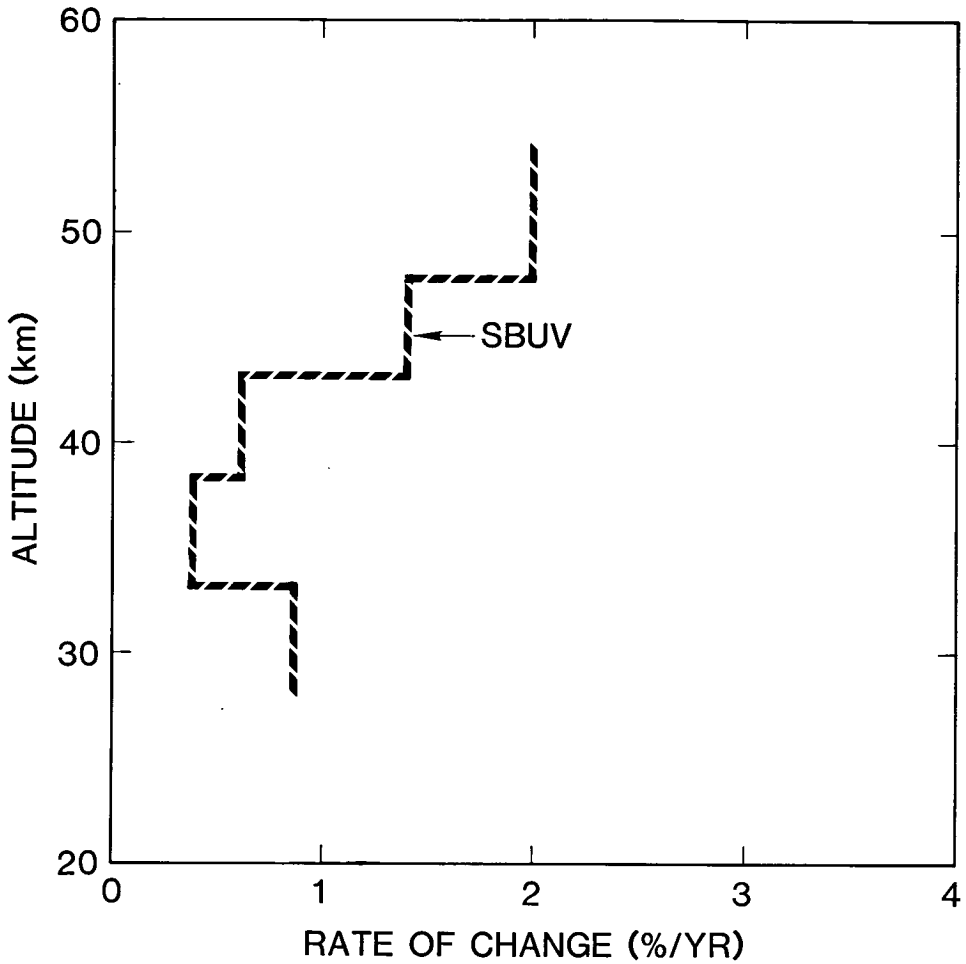

Figure 2.22 Uncertainty in rate of ozone change determined from SBUV data over 8 years.

Table 2.4 and Figure 2.18c also illustrate that the D(OPT) is close to Case L, at the top end of the range, and results in ozone values close to the minimum likely values (i.e., largest decrease). The ozone changes determined using the OPT model, and those determined from cases L, M1, and M2, are compared in Table 2.5 and Figure 2.23. Clearly, the models indicate that the change in ozone is unlikely to have been larger, and may have been considerably smaller, than suggested by the archived OPT data. In fact, there may have been no change or trend at all.

Table 2.5 Midlatitude Ozone Changes (1978–1986) for Different Diffuser Degradation Models

Umkehr Layer	OPT*	L	M2	M1
10	-25	-30	+3	6
9	-22	-24	-3	5
8	-14	-11	-7	-3
7	-9	-8	-4	0

*Different analyses and latitude ranges will lead to slightly different values for the ozone decrease.

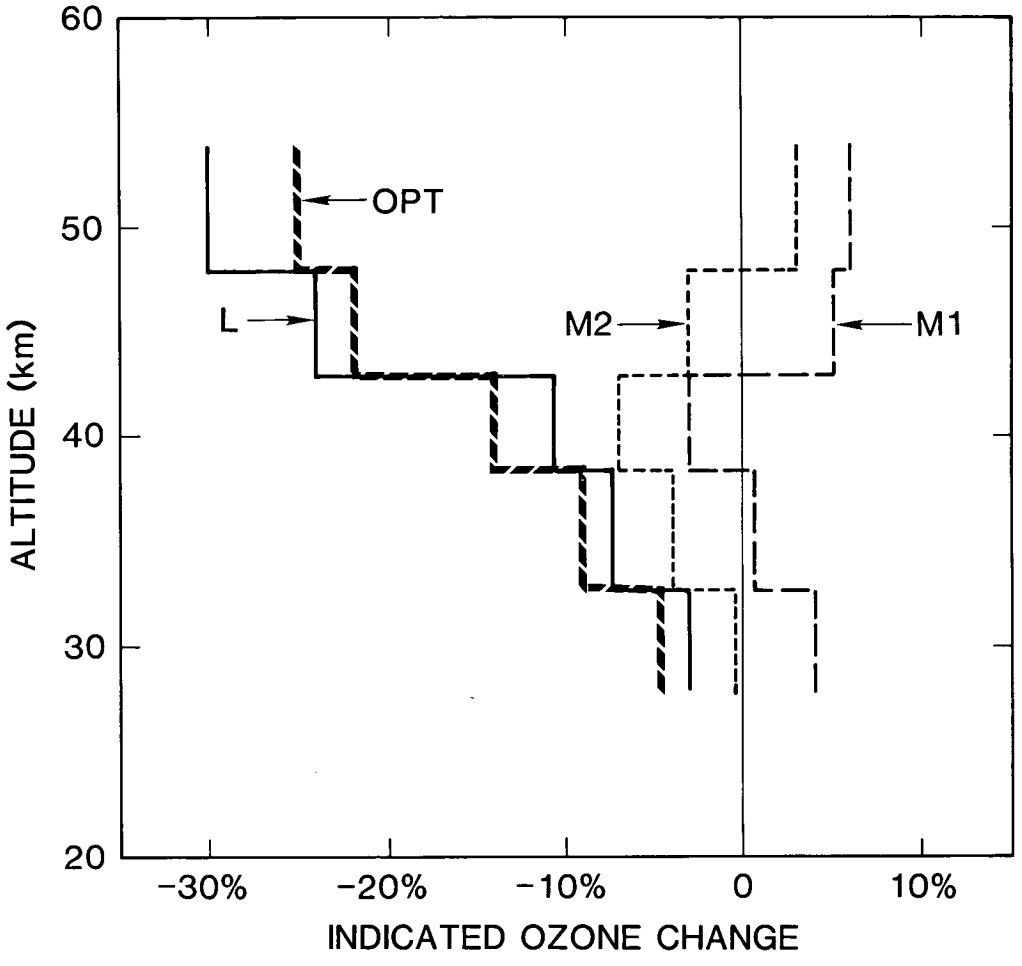

Figure 2.23 Midlatitude vertical distributions of ozone change from 1978–1986 determined from SBUV data, for several models of diffuser degradation. Curve marked OPT used the model employed in producing the data archived as of 1987. Curve L was calculated using a model with less diffuser degradation; M1 and M2 were derived using models with more diffuser degradation than the SBUV archive model.

2.4. THE TOTAL OZONE MAPPING SPECTROMETER (TOMS)

TOMS is an ozone-mapping instrument mounted adjacent to the SBUV instrument on the Nimbus–7 satellite (Heath et al., 1975 and 1978 [UG]). The primary measurement goal of TOMS is to obtain contiguous mapping of the total column ozone density on a latitude–longitude grid on the Earth's surface (Bowman and Krueger, 1985; Schoeberl et al., 1986). To achieve this, TOMS step scans across the orbital track, sampling radiation backscattered from swaths that pass from side to side through the nadir. By comparison, the SBUV observes solar radiation backscattered only in the nadir.

Although TOMS is an independent optical–mechanical ozone sensor, it shares with the SBUV the diffuser that is deployed for direct solar observations. Because the four longest SBUV wavelengths, which are used for total ozone determination, are the same as those used by TOMS, total ozone trend uncertainties for both instruments are treated in this chapter.

2.4.1 Physical Principles

TOMS employs the same measurement principle as the SBUV instrument (see Section 2.3.1). Ozone column amounts are inferred by utilizing the wavelength dependence of Earth's ultraviolet albedo at the wavelengths between 312.5 nm and 380 nm, in the region of the Huggins band of the ozone absorption spectrum. The TOMS raw data, like the SBUV, are measurements of the intensities of direct and backscattered solar UV radiation. TOMS, however, makes measurements in only six fixed wavelength channels (380.0, 360.0, 339.8, 331.2, 317.5, and 312.5 nm), the last four of which are used in pairs to provide three estimates of the total column ozone concentration by the differential absorption method. The remaining two channels, which are free of ozone absorption, are used to determine the effective background albedo. Mathematically, the measurement quantity required for the determination of the total ozone concentrations is (with reference to Equation 1),

$$\frac{I(\lambda_1)}{F_o(\lambda_1)} \Big/ \frac{I(\lambda_2)}{F_o(\lambda_2)} \tag{17}$$

with appropriate corrections for the background albedo and cloud cover. In particular, the so-called A-pair data, which are the ratios of the albedos at 331.2 nm and 312.5 nm, are analyzed to provide low-latitude total ozone concentrations. Since the retrieval of total ozone amounts from the measured raw data is determined from ratios of the albedo of Earth plus atmosphere divided by these wavelengths, the TOMS measurement technique is, in principle, capable of highly reliable determination of the ozone column. The OPT has conducted sensitivity studies that indicate that a 1 percent wavelength-dependent uncertainty in the measured albedos leads to a 1 percent uncertainty in total ozone, whereas a 1 percent wavelength-independent albedo uncertainty results in an uncertainty of only 0.3 percent in total ozone. (For a more complete discussion, see Chapter 3.)

Again, the plan for determining long-term stability is implicit. Most important, as discussed in Section 2.3 with respect to SBUV, no provision was made to monitor the reflectivity of the diffuser during flight. However, the TOMS monochromator wavelengths and the electrometers' gains have been measured during the mission. Unlike the SBUV experiment, the gain of the TOMS photomultiplier has not been monitored, on the assumption that such changes are wavelength independent and therefore cancel in the ratio of the albedos.

2.4.2 Instrument Description

Optical

TOMS measures the direct solar UV irradiance and the UV radiance backscattered by Earth's atmosphere at each of its six fixed wavelengths with a spectral pass band of 1 nm. Four of these wavelengths, those used in ground-based Dobson spectrometer ozone determination, are in common with the SBUV instrument. The principal optical components (Figure 2.24) involved in a TOMS radiance measurement are a depolarizer, mirror system for scanning the Earth "scene," monochromator, and photomultiplier. Radiation backscattered from a given Earth "scene" selected by the scan mirror is depolarized by a calcite Lyot type depolarizer (note that this is different from the SBUV depolarizer), transferred via a mirror to the entrance aperture of a single Ebert–Fastie monochromator (which is a close replica of the first monochromator of the SBUV spectrometer), and dispersed by a fixed grating onto an array of exit slits. A rotating wavelength

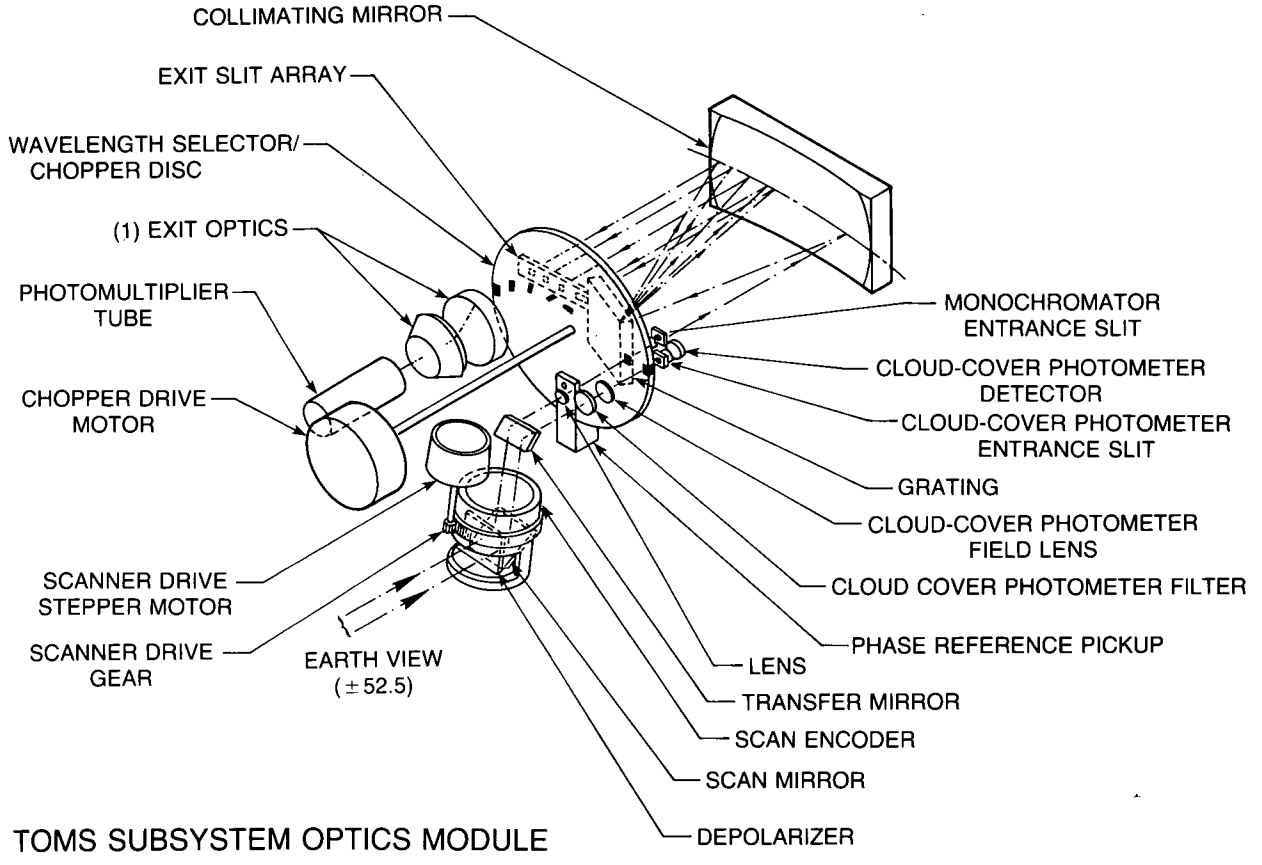

Figure 2.24 TOMS optical diagram (from Heath et al., 1975).

selector is used to gate the dispersed light from the desired exit slit to the detector, which is the same type as that used in the SBUV instrument. This same disc also chops the incident light at the entrance slit to provide dark intervals between the wavelength gates at the exit slit.

When nadir-looking, TOMS, like the SBUV instrument, views radiation backscattered by the underlying atmosphere and Earth along the track of the Nimbus–7 spacecraft. By mechanically scanning its 3° × 3° FOV (by comparison, the SBUV FOV is 11.3° × 11.3°) through the subsatellite point, perpendicular to the orbital plane, TOMS also measures the UV radiation backscattered from along a 105-degree swath (± 52.5 degrees, in 35 sequential steps of 3 degrees each) across the spacecraft track (Figure 2.25). At each scan step, TOMS measures the signal in each of the six wavelength channels. From the data acquired during these scans (achieved by a scan mirror driven by a stepper motor), a contiguous mapping of the total ozone can be created, since the scans of consecutive orbits overlap; the scan geometry provides total Earth coverage somewhat more than once per day. For direct solar irradiance measurements, which TOMS makes once per week, the same diffuser used by SBUV is deployed; TOMS views a central part of this diffuser, which SBUV views in its entirety.

Electronics/Signal Processing

TOMS has its own detector power supply, first-stage signal processing amplifier, and calibration generator. A small bias is designed into the electrometer amplifier that is additive to

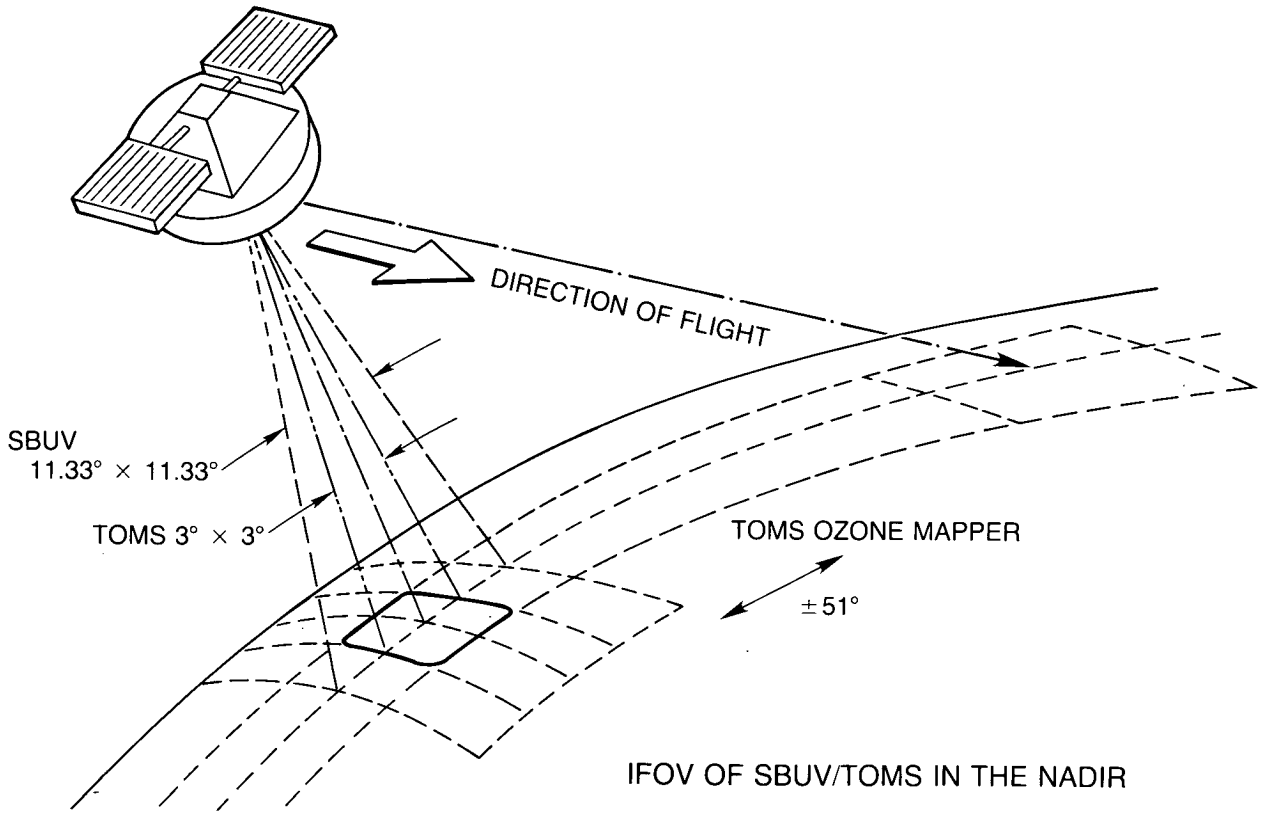

Figure 2.25 Diagram of TOMS scanning swath (from Heath et al., 1978).

the PMT dark current. This bias ensures that the electrometer signal remains onscale during the spacecraft operation lifetime, thus eliminating the need for zero correction circuits. This bias is subtracted along with the dark current by the digital demodulation techniques.

The bulk of TOMS signal processing electronics is performed by the electronics module that TOMS shares with SBUV, and is described in detail in the UG.

Operating Modes

TOMS has five scanner modes: scan off mode, single-step mode, normal scan mode, stowed mode, and view diffuser mode. These are described in the UG.

Inflight Calibration

The techniques used for inflight monitoring of the wavelength calibration of the TOMS monochromator and the gain stability of each electrometer range are described in the UG.

Scientific and Engineering Data Output

The TOMS radiance values at specified wavelengths for each instrument field of view (IFOV) along each orbit, together with housekeeping data such as the PMT bias, temperature, and diode detector bias, as well as the solar, satellite, and Earth reference data, are available on magnetic tape.

2.4.3 Prelaunch Calibration

Analogous to the SBUV prelaunch calibration (see Section 2.3.3 and the UG), TOMS calibration comprises three primary parts: irradiance and radiance radiometric calibrations and system linearity determination. The dynamic range of the TOMS signal is 10^3, and the linearity over this range is assumed to be better than 2 percent (which is the maximum measured SBUV nonlinearity). Stray light rejection is estimated to be better than 10^3, which allows the minimum signal to be measured with 1 percent accuracy. TOMS polarization sensitivity was measured prior to launch, and is discussed in the UG. Unlike the SBUV, TOMS sensitivity to diffuser angle was not determined prior to launch.

2.4.4 Results in Orbit

There is a difference of approximately 3 percent between the absolute total ozone concentrations measured just after launch by TOMS and SBUV, with TOMS data yielding the higher values. The origin of this bias is attributed to differences in the respective prelaunch absolute calibrations of the two instruments, and is not understood by the experimenters.

During the first 7 years of TOMS operation, the drift in the wavelength calibration of its monochromator was less than 0.01 nm. Consequently, the TOMS experimenters do not consider wavelength-drift-induced errors to be a significant source of uncertainty in the TOMS measurements.

The maximum electrical calibration change detected during the first 7 years of operation was less than 0.3 percent, with the typical change being less than 0.1 percent, which is within the measurement noise. Therefore, electrical calibration drift-induced errors are not considered to be a significant source of uncertainty in the TOMS measurements. However, the range 3 to range 4 gain ratio was increased by 0.55 percent after an annual oscillation of 1 percent peak to peak was observed in the ratio of the solar irradiance measurements at the A-pair (331.2 nm, 312.5 nm) wavelengths. This is an effect related to the changing angle of solar illumination of the diffuser. Although this oscillation cancels in the albedo, it compromises the determination of diffuser degradation parameters (the r values discussed in Section 2.3) from the TOMS solar signals for comparison with those determined from the SBUV solar signals (see below). Adjusting the gain ratio removed the A-pair oscillation, but had no impact on the ratios of the B (331.2/317.5 nm) and C (339.8/331.2 nm) pairs.

After the removal of the diffuser degradation, there is an overall increase in the TOMS solar and backscattered signals (e.g., 5 percent at 340 nm). In part, this is considered to be due to an overall increase in photomultiplier gain. However, this does not explain the wavelength dependence of this increased sensitivity.

Since February 1984, the chopper nonsync flag condition has occurred in approximately randomly spaced episodes. This has caused both a relative change and an increase in the scatter in the TOMS-measured solar signal. The B-pair ratio (which is used for high-latitude ozone determination) has been affected more than the A-pair ratio (used for lower latitude ozone determination). In particular, a plot of the B pair ratio vs. time (McPeters, private communication, 1987) shows that since 1984 it has oscillated between two separate values. The nonsync condition is considered to be the cause of drifts in the bias between TOMS and SBUV total ozone concentrations: from launch to 1986, the TOMS A-pair-derived ozone has drifted upwards, from

3 percent to 3.5 percent, compared to SBUV total ozone, and the TOMS B-pair-derived ozone has drifted downward, from 3 percent to less than 1.5 percent. The overall result of this is a downward drift in the bias between TOMS and SBUV total ozone concentrations of 2 percent to 3 percent at high latitudes during winter, and of <1 percent at the Equator.

2.4.5 Mechanisms of Drift

Many of the same kinds of drift mentioned for SBUV (Section 2.3.5) are also relevant to TOMS. Aside from the wavelength dependence of the diffuser degradation, two particular possible sources of wavelength-dependent drifts in the measured TOMS albedos are drifts in the wavelength calibration of the monochromator and in the electrometer gain ratios (since measurements at different wavelengths are made on different gain settings). However, both have been monitored in orbit and are not considered to be major sources of uncertainties in the measured long-term ozone trends.

Changes in instrument throughput (such as PMT gain and reflectance of optical surfaces, which may affect the measured irradiance and radiance) cancel, since the albedo is the ratio of these quantities.

Thus, the primary source of uncertainty in the long-term ozone trends reported by TOMS is the uncertainty in the reflectivity of the diffuser TOMS shares with SBUV. Changes in the wavelength dependence of the diffuser reflectivity (specifically at each of the wavelengths used to form the albedo pairs) affect the measured albedos directly, while uncertainties in the absolute reflectivity at the longer wavelengths (cf. Eck et al., 1987) generate uncertainties in the background albedo that are propagated through the data reduction algorithm (see Chapter 3). Since the diffuser degradation parameters determined from SBUV data are used in the production of total ozone values from TOMS data, the critical evaluation of the diffuser reflectivity degradation parameters, discussed with reference to SBUV in Section 2.3, is also pertinent here.

2.4.6 Estimates of Diffuser Plate Degradation Effects on Total Ozone

Calculations of diffuser degradation at the TOMS wavelengths for the models discussed in Section 2.3 are shown in Figure 2.26 and tabulated in Table 2.6. Since it is clear that the diffuser degradation is wavelength dependent, it is necessary to consider how uncertainties in the spectrum of the change in diffuser reflectivity may affect the total ozone trends derived from the

Table 2.6 Model Values of Diffuser D After 8 Years

Wavelength (nm)	D(OPT)	D (M2)	D (M1)	D (L)%	Diff. D(M1)–D(OPT)	% Diff. D(L)–D(OPT)
312.5	.7767	.7447	.7161	.7592	-8.1	-2.8
317.5	.7827	.7672	.7407	.7695	-5.5	-1.7
331.2	.8032	.7946	.7713	.7820	-4.1	-2.7
339.8	.8112	.8028	.7802	.7827	-3.9	-3.6
360.0	.8343	.8409	.8225	.8105	-1.4	-2.9
380.0	.8727	.8851	.8717	.8241	-0.11	-5.7
Ratio 312.5/ 331.2	0.9670	0.9372	0.9284	0.9708		

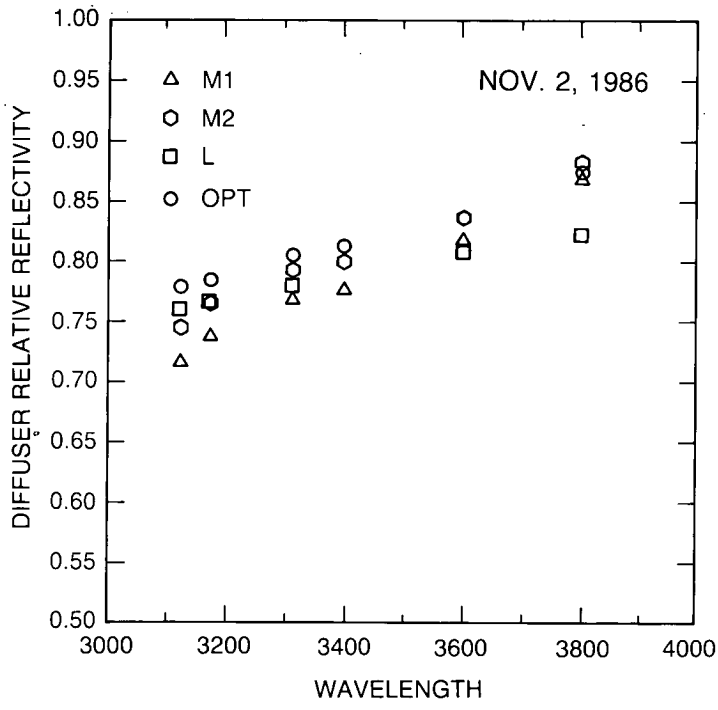

Figure 2.26 Diffuser reflectivity vs. wavelength; comparison of model predictions for TOMS wavelengths.

TOMS data. Three qualitative estimates at the A-pair wavelengths (331 nm and 312 nm) were obtained as follows:

- The diffuser degradation parameters were determined separately for four different frequent deployment periods, using the OPT model. The *r* values are shown in Figure 2.9. For there to be no associated uncertainty in the derived total ozone values, the diffuser degradation at 331 nm must remain the same, relative to the degradation at 312 nm, for each of the four determinations. However, after 650 hours of exposure (i.e., 7 years), the diffuser reflectivity at 331 nm calculated using the 1984 *r* values is 1.1 percent lower than when calculated with the 1981 *r* values (when normalized at 312 nm). This wavelength-dependent uncertainty in the measured albedos would correspond to a similar uncertainty in the derived total ozone.

- Because TOMS views one fifth of the diffuser area seen by SBUV, and does so at a larger angle, the changes in reflectivity determined for the entire diffuser surface from the SBUV data may not be completely appropriate for reduction of TOMS data. The degradation at the center of the diffuser was determined using the OPT diffuser degradation model discussed in Section 2.3.6 and the TOMS raw solar signal. The results were presented in Table 2.2; the TOMS-determined *r* values are about 2 percent higher than the SBUV-determined *r* values. The TOMS-derived values are considered to be less reliable because 1) it was not possible to correct the raw solar signal for changes in the PMT gain because this was not monitored on TOMS and 2) the angle-related annual oscillation noted above interfered with the raw signal during the frequent-deployment time period. Converting the *r* values to D's results in a wavelength-independent shift of 2.3 percent, which translates to an uncertainty of 0.7 percent in the derived total ozone. The wavelength dependence does not differ significantly from the SBUV value.

- Table 2.6 presents the D values for the various total ozone wavelengths for the quasi-linear and OPT models and the A-pair ratios after 8 years. Comparing Cases M1 and M2 with Case L indicates uncertainties of 3.6–4.6 percent in total ozone over the 8 years, or an uncertainty in the rate of change of 0.57 percent per year.

2.4.7 Assessment

Because TOMS views the same diffuser as that used by SBUV, and because the TOMS total ozone values are obtained by using diffuser degradation parameters determined from SBUV data, the long-term total ozone trends measured by TOMS are very similar to those obtained by SBUV. They cannot be considered as independent determinations of the total ozone trends. For the reasons discussed in Section 2.3, there is no information available with which to uniquely determine the partitioning of degradation between the diffuser and the spectrometer. Estimates of the relative D value uncertainties are given in Table 2.6.

An approximate value for the total ozone uncertainty can be obtained by multiplying the D value uncertainties by the sensitivity factors from Chapter 3, Table 3.1. The resulting uncertainty in total ozone, after 8 years of diffuser degradation, is given in Table 2.7.

Table 2.7 Range of Uncertainty in Total Ozone

	Zenith Angle	
	0°	51°
Case M2–Case L	+ 2.2%	+ 2.1%
Case M1–Case L	+ 3.9%	+ 3.3%
Case M1–OPT	+ 4.2%	+ 3.1%

Thus, the range of total ozone, based on the uncertainty in D values, is a few percent. The OPT values suggest the lowest values of total ozone: 4.2 percent below Case M1, or 2.5 percent below Case M2, and even 0.3 percent below Case L for small zenith angles.

Over the 8 years of data, the OPT values are decreasing 0.53 percent per year faster than M1, 0.31 percent faster than M2 and 0.04 percent per year faster than L, again for small zenith angles. Fleig et al. (1986) found OPT TOMS trends lower than the Dobson network by 0.37 percent per year. The Dobson results clearly point toward a larger diffuser degradation than that given by the OPT formula, and suggest values much closer to those given by Case M of the quasi-linear model. This also gives some support to the larger Case M degradation at the shorter profiling wavelengths discussed in Section 2.3.

2.5 THE SAGE–I AND SAGE–II INSTRUMENTS

SAGE–I and SAGE–II are both satelliteborne multiwavelength radiometers employing solar occultation techniques to determine concentrations of stratospheric aerosols and gases. Ozone profiles are determined from measurements of absorption in the most intensely absorbing part of the Chappuis band, at 600 nm. SAGE–I was launched aboard the dedicated Application Explorer Mission–B (AEM–B) spacecraft on February 18, 1979. It operated continuously for 34 months, until November 1981, when the spacecraft power subsystem failed. SAGE–II was launched from shuttle aboard the Earth Radiation Budget Satellite (ERBS) on October 5, 1984. It has operated continuously since that time without problems. Both are in approximately 600 km circular orbits

with inclination angles of 56° and 57° for SAGE–I and SAGE–II, respectively, such that the latitudinal coverage is almost identical.

2.5.1 Physical Principles

In the solar occultation technique, measurements are made of the solar radiation transmitted through the atmosphere as the Sun sets behind it.

Mathematically, the atmospheric transmission value $T_\lambda(h)$ at tangent height h and wavelength λ is expressed as a ratio between the solar radiance observed within the atmosphere to the radiance outside the atmosphere as

$$T_\lambda(h) = I_\lambda(h)/I_{o\lambda} \tag{18}$$

where $I_\lambda(h)$ is the solar radiance at wavelength λ observed at tangent height h and $I_{o\lambda}(h)$ is the measured extraterrestrial solar radiance at λ. Ozone concentration profiles can then be retrieved from the atmospheric transmission profile as described in the algorithm chapter or by Chu and McCormick (1979), Mauldin and Chu (1982), or Chu (1986).

The measured data at the different wavelength channels are converted to transmission values by ratioing a scan across the Sun, obtained when the FOV is transversing the atmosphere, to a reference Sun scan. The reference Sun scan for each channel is obtained from the high-altitude scans with tangent altitudes above 100 km, where no atmospheric attenuation is present. Tangent altitudes of the measured data were previously determined differently for SAGE–I and SAGE–II. The SAGE–II algorithm used spacecraft and solar ephemeris data to calculate tangent altitudes, while the SAGE–I algorithm determined the tangent altitude by fitting the calculated Rayleigh transmission with the short-wavelength channel measurements. For the purpose of these studies of ozone trends, SAGE–I data have been reinterpreted using tangent altitudes determined in the same way as they were for SAGE–II.

It is important to note that the measurements performed by SAGE–I and SAGE–II are self-calibrating, in that only atmospheric transmission or relative radiance measurements are required to determine the concentration of atmospheric species such as ozone, and, therefore, no absolute radiance calibration is performed. The only requirement is that the instrument with all its various components retain constant responsivity for the duration of each measurement event—i.e., a spacecraft sunrise event or sunset event. A typical measurement event duration is about 100 seconds, in which time the instrument configuration is kept nearly constant except for the scan mirror, which views the Sun at an elevation angle that varies slightly with time. The primary consideration is, thus, to keep the instrument at a constant temperature such that no thermal drift can occur during the measurement events.

2.5.2 Instrument Summary

Both the SAGE–I and SAGE–II instruments share the same design, illustrated in Figure 2.27, with similar optical components. Each instrument is composed of three major subsystems, i.e., a scanhead assembly, a telescope, and a spectrometer. The scanhead assembly consists of a scan mirror together with a Sun-presence sensor and an azimuth Sun sensor. The telescope is a spherical Cassegrain with a 152.4 cm effective focal length and an f-number of 30. The telescope is mounted in a graphite–epoxy composite telescope barrel to minimize thermal effect. The spectrometer consists of a concave holographic grating with detector assemblies located at the

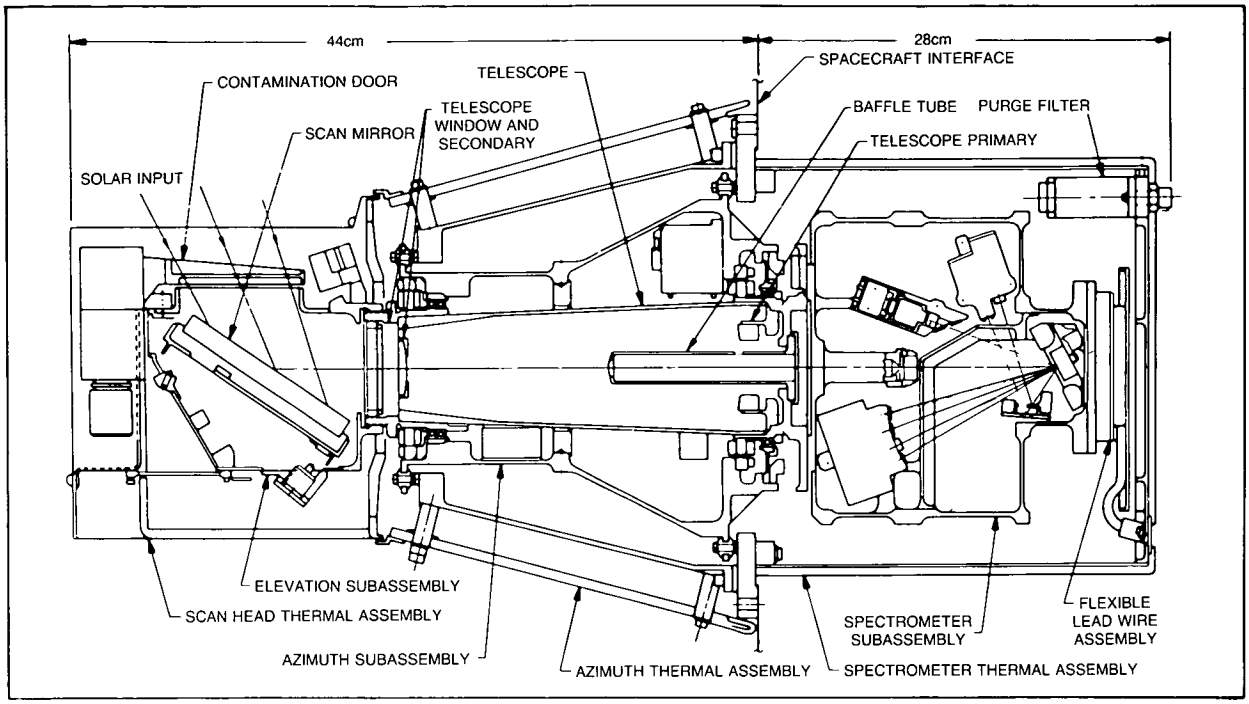

Figure 2.27 SAGE–II sensor assembly (from Mauldin et al., 1985a,b).

zero- and first-order reflection of the grating. The difference between SAGE–I and SAGE–II instruments is primarily in the number of spectral channels employed. For SAGE–I, there were four spectral channels at 1.0, 0.6, 0.45, and 0.385 micron center wavelength, with silicon photodiode detectors located at the first-order reflection of the grating on the Rowland Circle. For SAGE–II, there are seven spectral channels at 1.02, 0.94, 0.6, 0.525, 0.453, 0.448, and 0.385 microns. All of the channels use silicon photodiode detectors, with five located on the Rowland Circle, while the 0.94 and the 0.453 micron channels are situated at the zero-order reflection of the grating. The SAGE–II spectrometer layout is shown in Figure 2.28. The spectral bandwidth for the four channels on SAGE–I was about 30 nm. For SAGE–II, all the channels have a bandwidth of 15 nm except for the 0.448 and 0.453 micron channels which have bandwidths of 2 and 3 nm, respectively.

Another difference between SAGE–I and SAGE–II instruments is the scan mirror coating. SAGE–II uses a simple quartz-coated silver substrate mirror, while SAGE–I used a multilayer dielectric-coated silver mirror that was specially designed for minimizing the change in reflectivity across the scanning angular range. Both coatings were designed to produce changes in reflectivity of not more than 0.1 percent per degree mirror rotation over the operational angular range. Preflight measurements were not sufficiently accurate to verify the designed specifications, but placed an upper bound of 0.5 percent change per degree mirror rotation.

Detailed descriptions of the SAGE–I and SAGE–II instruments have been given elsewhere (McCormick et al., 1979; Mauldin et al., 1985a,b). A comparison of the characteristics of the two instruments is shown in Table 2.8.

During each spacecraft sunrise or sunset event, the instrument is activated when the Sun-presence sensor indicates a Sun intensity of at least 1 percent relative to the unattenuated

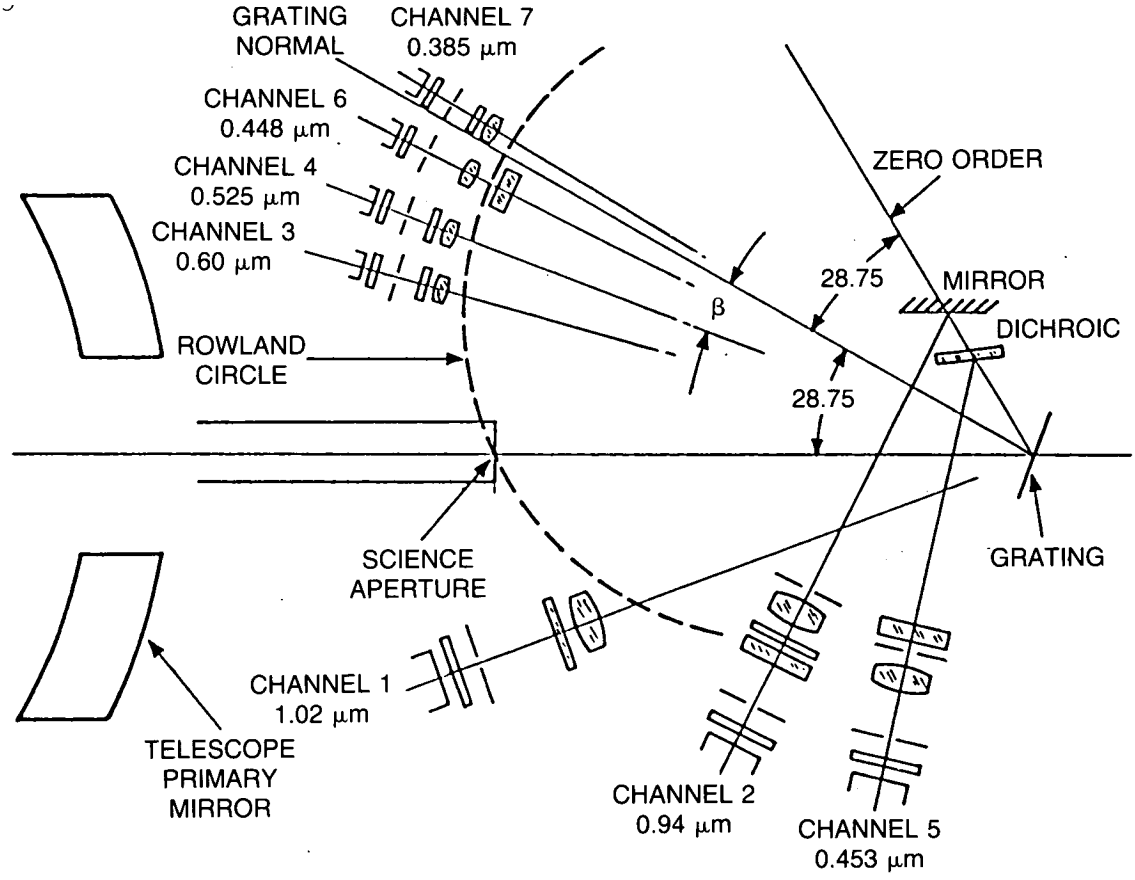

Figure 2.28 SAGE–II spectrometer layout (from Mauldin et al., 1985a,b).

Table 2.8 Sage Instrument Characteristics

Subsystem	SAGE–I	SAGE–II
Telescope	5.1 cm dia F/30 cassegrain	5.1 cm dia F/30 cassegrain
Scan Rate	15′/sec	15′/sec
Instantaneous Field of View	0.5′ dia.	0.5′ elevation 2.5′ azimuth
Azimuthal Pointing Accuracy	0.5′	0.5′
Sample Rate	64/sec (4/km)	64/sec (4/km)
Wavelength Separation (at 600 nm)	Holographic Grating Spectrometer 30 nm	Holographic Grating Spectrometer 15 nm
Detector	Silicon Photodiode	Silicon Photodiode

Sun. The instrument then searches for and locks onto the Sun in azimuth within 1′ of the radiometric centroid. The scan mirror fast scans (3°/s) in elevation until the Sun is acquired in elevation, then it scans vertically across the face of the Sun at a rate of 15′/s, reversing itself each time a Sun limb crossing occurs. Figure 2.29 illustrates a typical data-taking sequence for a sunset event. The two solid lines denote the image position of the top and bottom of the solar disk as viewed from the spacecraft with atmospheric refraction properly included. The left vertical ordinate denotes relative angle measured from the spacecraft coordinate system in arc-minutes, while the right vertical ordinate denotes the corresponding vertical tangent altitude. The horizontal abscissa denotes event time in seconds for nominal orbital geometry. The dashed line represents the up-and-down scan of the IFOV with respect to Earth's horizon. Radiometric data for each channel are sampled at a rate of 64 samples per second.

2.5.3 Prelaunch and Inflight Instrument Characterization

Both SAGE–I and SAGE–II instruments underwent extensive preflight testing. Component and system-level tests that were performed include scan mirror reflectivity, telescope modulation transfer function, grating efficiency, detector spectral response, detector response temperature sensitivity, spectrometer wavelength calibration, individual channel spectral bandpass (in-band and out-of-band) responses, stray light test, scan mirror linearity test, and full-Sun scan on the ground. Considerable effort also went into the setting of the gain for both SAGE–I and SAGE–II instruments to ensure that the full-scale count level for each channel would be neither saturated nor too low.

As stated previously, absolute calibration of the measured radiance is not necessary since all the measurements are nearly self-calibrating. To reduce any thermal change during the measurement, large thermal inertia has been built into the hardware; both instruments have demonstrated less than 0.3 K change in temperature during measurement events.

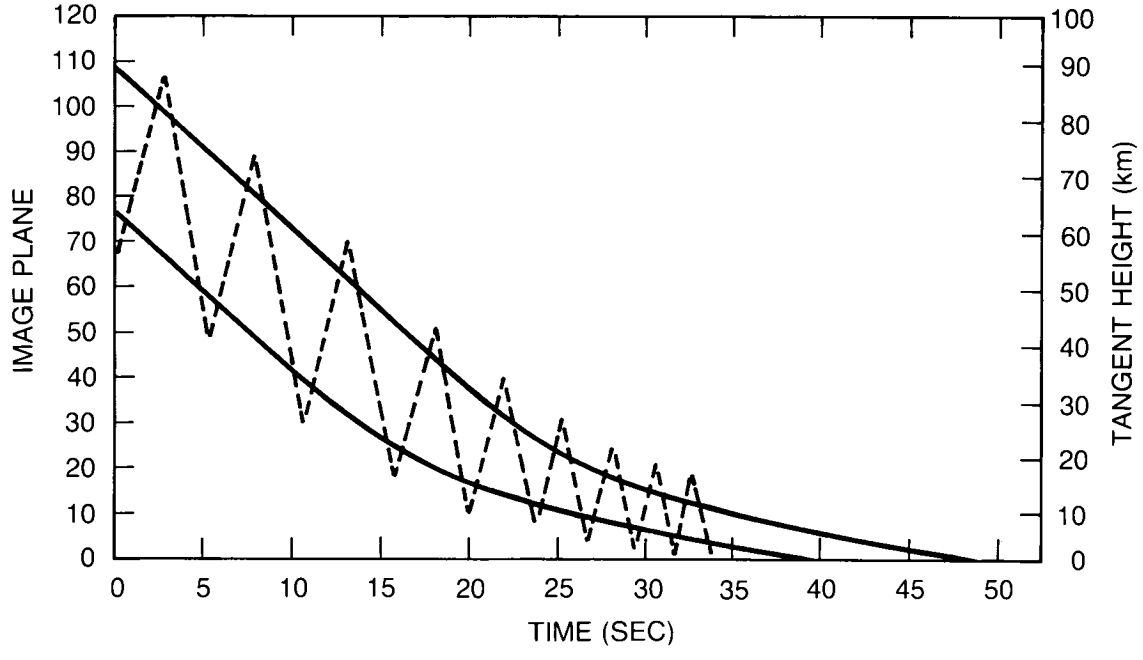

Figure 2.29 Data acquisition mode for solar extinction experiment during sunset event (from Mauldin et al., 1985b).

Changes in mirror reflectivity with angle during the occultation are also a potential source of error. For SAGE–II, a simple quartz coating over a silver substrate was used; the ERBS spacecraft is periodically turned upside down so that the scan mirror reflectivity can be tested across its entire angular range using the unattenuated Sun. Results of the measurements have been used to correct the radiance data for any change in reflectivity with mirror angle. These corrections, however, are very small (between 0.02 to 0.1 percent per degree).

The coating for SAGE–I is a multilayer dielectric over a silver substrate designed to minimize the change in reflection versus scan angle. Inflight testing of the SAGE–I scan mirror over the observing view angles was not possible, however, because the spacecraft could not be maneuvered to view the unattenuated Sun at all scan angles. The SAGE–I scan mirror did measure the unattenuated Sun from tangent height of 100 km to about 250 km. By analyzing the scan mirror reflectivity over the restricted angular range, and assuming linear extrapolation is justified, the results suggest that the SAGE–I scan mirror reflectivity change with angle for the ozone channel is about the same as the SAGE–II scan mirror.

2.5.4 Sources of Error in Ozone Profiles Derived From the SAGE–I and SAGE–II Measurements

This section has been generated from a careful study of all error sources in both the measurement and retrieval processes. Most error sources considered here can be quantified with careful analyses of the known engineering parameters or other measurement parameters. If insufficient information was available for assessing the uncertainty magnitude, then a conservative approach was taken to estimate the error. For error parameters that could be magnified by propagation through the retrieval process, the sensitivity of the retrieved ozone accuracy to those error sources was then determined by a simulation and retrieval study.

The characteristics of the error sources can generally be classified into two distinct categories: systematic and random components. Accuracy in trend determination is usually limited only by the magnitude of any varying part of the total systematic error, and should not be susceptible to the random-error component. However, random-error is unimportant in trends determination only if sufficient sampling of the measurements can be obtained such that the averaging process (or any other statistical means) can be used to reduce the random-error component to an insignificant level. There is also an error component that is partly random and partly systematic. An example of this type of uncertainty is errors with long correlation times. The effect of this type of error for measurements with limited sampling is difficult to assess unless the complete statistic of the error is known. It is possible that the uncertainty in reference height determination for the SAGE–II algorithm belongs to this type of error.

In the following, individual error sources for the SAGE–I and SAGE–II ozone measurements are discussed, and the derivation of the ozone sensitivity factors is explained. The ozone error sensitivity factors discussed here apply only to the retrieved ozone concentration versus geometric height data, and not to any other derived parameters such as ozone-mixing ratio on pressure levels.

Ozone Absorption Cross-Section Error

The ozone Chappuis band absorption coefficient data used in the SAGE–I and SAGE–II processing are those measured by Penney (1979). The precision of the absorption data was estimated by the experimenter to be about 2 percent. However, the room temperature Hg line

measurements in the UV at 296.7 nm and 302.15 nm showed a 6 percent difference from Hearn's (1961) results. Thus, the ozone cross-section values used by SAGE–I and SAGE–II could be associated with a 1σ error of 6 percent.

There is also an uncertainty of 0.5 percent in the Rayleigh cross-section used at 600 nm, which is insignificant compared to the ozone cross-section error. Neither of these varies with time.

Scan Mirror Calibration

Calibration of the SAGE–II scan mirror reflectivity versus angle was possible during the spacecraft pitch 180° exercise (spacecraft titled upside down in orbit). The resulting data have been least-squares fitted to determine the linear coefficients for the correction of mirror reflectivity with scan mirror viewing angle. In all seven channels, the data show small reflectivity changes with angle, and the estimated errors on those coefficients are about the same order of magnitude. To assess the sensitivity of the retrieved ozone to the scan mirror calibration factors, a typical measurement event has been processed with and without the scan mirror reflectivity correction factors. The difference between the two retrievals is illustrated in Figure 2.30, showing a small difference below 40 km altitude and about 1 percent difference above 45 km altitude.

For SAGE–I measurements, scan mirror calibration was impossible to perform in orbit. The only way to assess the scan mirror reflectivity change is by analyzing the mirror reflectivity when the Sun is high above the atmosphere. Using mirror reflectivity data between 160 km and 100 km tangent altitude, no observable change was found. Assuming that one can extrapolate the mirror reflectivity behavior to viewing angles corresponding to atmospheric heights, one should expect very small changes in mirror reflectivity. Therefore, a doubling of the error for SAGE–II scan mirror reflectivity uncertainty has been assigned to the SAGE–I scan mirror reflectivity change.

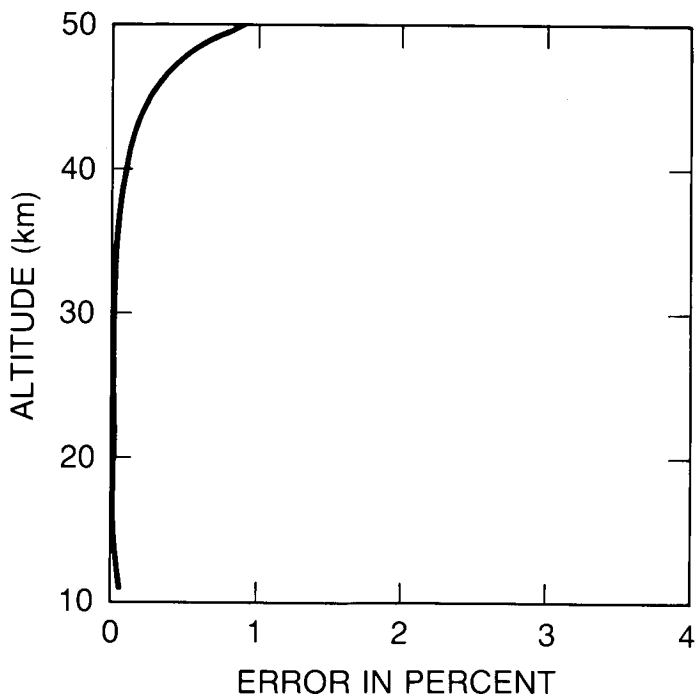

Figure 2.30 Sensitivity of ozone retrieval to variation of scan mirror reflectivity variation with angle.

Aerosol Interference

Due to the overlapping of aerosol signature in the ozone channel at 600 nm, a small residual aerosol contamination of the ozone profile at heights where high aerosol concentrations occur could exist. Error analyses based on simulation and retrieval studies of the aerosol interference in the SAGE–II ozone profile have been performed for typical 1985 aerosol profiles (Chu et al., 1989). The results indicated that, for altitudes above the aerosol (typically above 25 km), aerosol interference in the ozone profile is insignificant. However, for altitudes below 25 km, where the aerosol content is high, up to a 4 percent error in the retrieved ozone could be contributed by the aerosol signature. A similar study on the SAGE–I measurements shows approximately the same size error, even though the aerosol content during 1979–1981 was lower by a factor of five. This is caused by the inaccurate characterization of the aerosol extinction versus wavelength behavior obtained when only SAGE–I's two wavelength channels for determining aerosol properties are available.

Reference Height Uncertainty

Due to the high vertical resolution of the SAGE measurements, the sensitivity of the retrieved ozone profile to height determination becomes important. Figure 2.31 shows a simulation and retrieval study of the ozone profile sensitivity to reference height error. Based on an error study on the determination of reference height from the calculation of orbital and solar ephemeris data (J. Buglia, unpublished report, 1987), it is estimated that the SAGE–II reference height error is approximately 0.2 km, and for SAGE–I it is about 0.35 km. However, the SAGE–I processing algorithm also included a slight adjustment on the reference height by fitting the measured atmospheric airmass data to those computed from the National Meteorological Center (NMC) temperature-versus-height data. Thus, the reference height error on SAGE–I should be approximately the same as the SAGE–II error, even thought the statistic of this error for the two experiments will be very different because of the readjustment process in the SAGE–I algorithm.

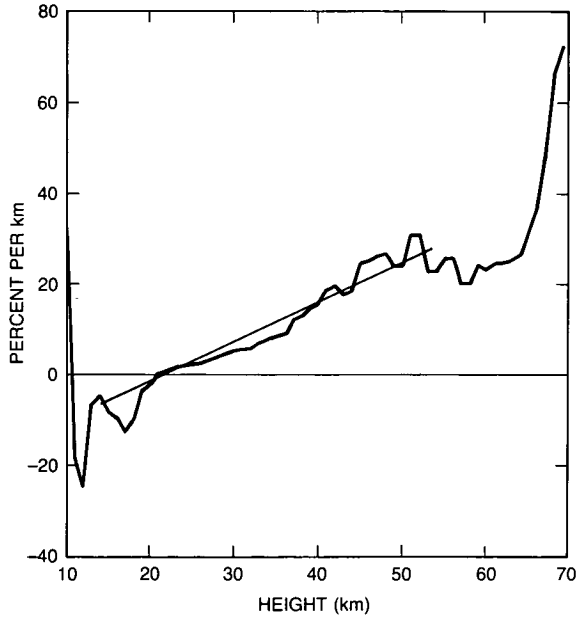

Figure 2.31 Sensitivity of SAGE–II ozone retrieval to reference altitude errors (%/km), as a function of altitude.

In comparing SAGE and SAGE–II ozone data, a possible systematic error component could exist due to the different reference height determination schemes applied to the two satellite systems. These errors arise partly from offsets in the NMC data sets used between the SAGE–I and SAGE–II time frames, and partly from an offset between the NMC data and the ephemeris data. Preliminary results from the analyses of the SAGE–I and SAGE–II data indicated that this error is small and is bounded by a maximum height difference of 60 meters. This would introduce at most a 1 percent systematic error in the SAGE–I to SAGE–II ozone comparison at about 40 km altitude and makes no significant contribution to the total error when root-mean-squared with other error sources. In addition, according to Buglia (unpublished report, 1987), the errors on the SAGE–II reference height calculated from the ephemeris data are generally correlated over a 7-day period coincident with the periodic updating of the spacecraft orbital tracking data. This would imply that the reference height errors on SAGE–II can be treated as systematic errors for ozone data covering spans of approximately 7 days, and can be treated as random errors for data covering spans of several weeks or more.

Random Error

The random errors for the retrieved ozone consist of contributions from the measurement errors of the atmospheric transmission data, the Rayleigh component calculated from the NMC temperature-versus-height data, and random error contributed from the aerosol measurements. Aerosol analyses based on the propagation of uncertainties in the SAGE–I ozone retrieval (Chu et al., 1989) have been used to estimate the precision of the SAGE–I and SAGE–II ozone profiles. It is found that the measurement error is the dominating source of uncertainty in limiting the precision of the SAGE–I and SAGE–II ozone values to a level of about 10 percent between cloud top to 60 km (SAGE–II), and to 50 km (SAGE).

Budget for Trend Errors in SAGE–I and SAGE–II

Combining the independent systematic errors cited above in the first four items results in the total errors shown in Table 2.9 and plotted in Figure 2.32. (The more conservative altitude registration error of 0.35 km is used for SAGE–I.) These are the values relevant in a comparison with other instruments. However, these are dominated by the constant ozone cross-section error. Removing this, and considering that the mirror or altitude registration error could vary by the amounts indicated over 2 years, gives the uncertainty in observed changes, which are also shown in Table 2.9 and in Figure 2.33. These are dominated by altitude registration uncertainties, which seem more likely to be random than characterized by a trend, so these errors, too, are probably conservative.

It should be emphasized that these errors do not necessarily represent the changes that could be seen by SAGE–I and SAGE–II over their 2-year periods of operation. To determine such a change requires a sufficiently large number of observations at a given location under similar seasonal conditions, with a meteorological situation that allows a representative longitudinal average to be obtained. The limited data taken by SAGE–I or SAGE–II do not necessarily fulfill these conditions. The numbers in Figure 2.33 should be regarded as suggestive. However, as SAGE–II continues in operation, the same total errors will apply over a longer period with more data and, presumably, improved sampling, allowing it to observe any changes of this magnitude.

Table 2.9 Errors of SAGE–I and SAGE–II (all errors in percent)

Altitude	Ozone Abs. Cross-Section	Mirror	Altitude Registration	Aerosols	Total Error	Error in Changes
			SAGE–I			
20	6	0	0	4	7.2	4
25	6	0	1.5	1	6.3	1.9
30	6	0	2.9	.5	6.7	2.9
35	6	.1	4.4	.2	7.4	4.4
40	6	.2	5.8	0	8.3	5.8
45	6	.5	7.3	0	9.5	7.3
50	6	2	8.8	0	10.8	9.0
			SAGE–II			
20	6	0	0	4	7.2	4
25	6	0	.8	1	6.1	1.3
30	6	0	1.7	.5	6.3	1.8
35	6	.05	2.5	.2	6.5	2.5
40	6	.1	3.3	0	6.8	3.3
45	6	.25	4.2	0	7.4	4.2
50	6	1	5.0	0	7.9	5.1

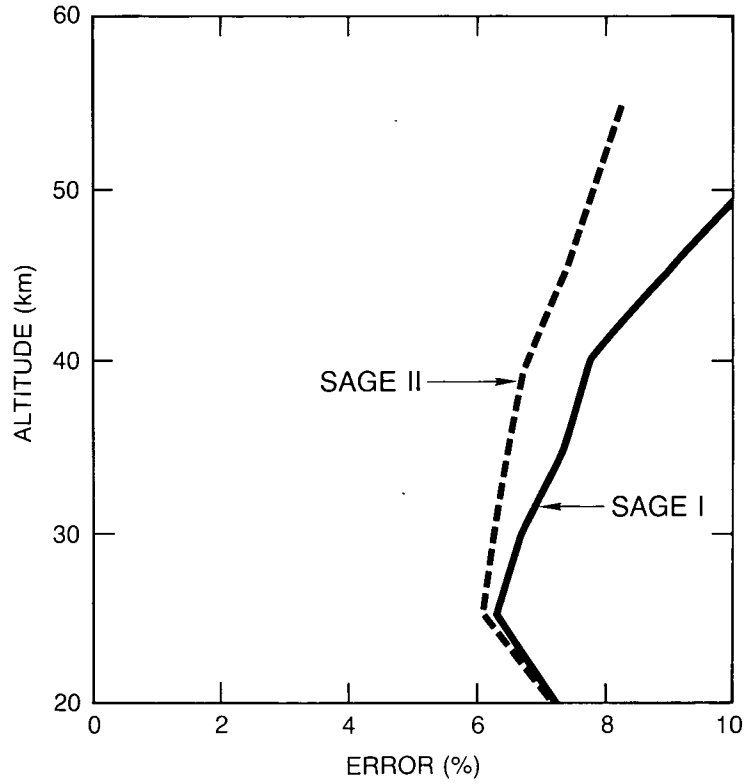

Figure 2.32 Combined systematic errors in SAGE ozone profiles.

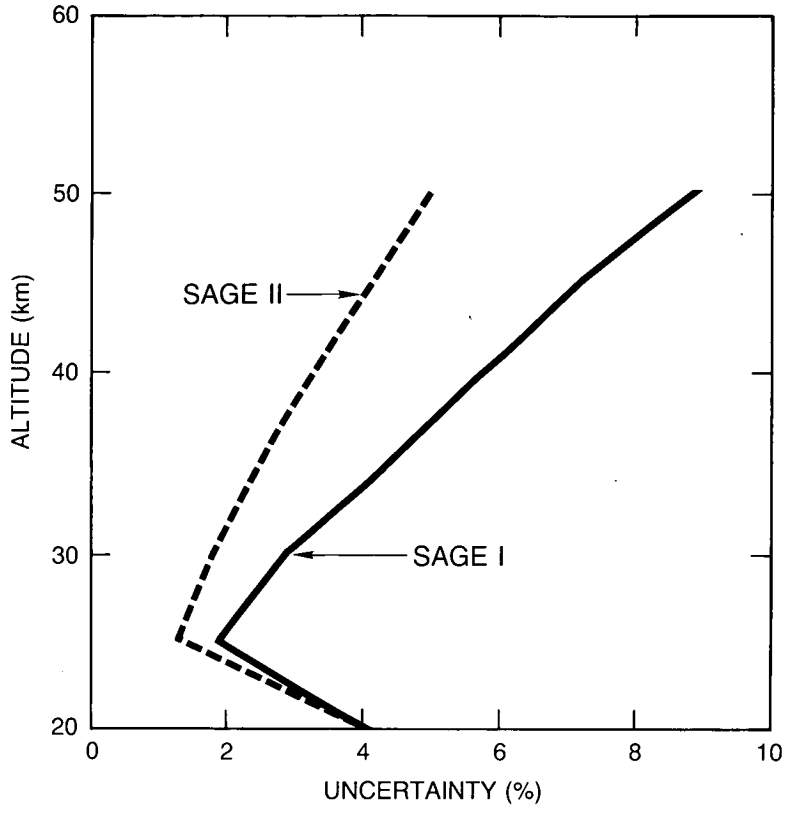

Figure 2.33 Uncertainty in SAGE ozone changes.

2.5.5 Error Budget of the Difference Between SAGE–I and SAGE–II Ozone Retrievals

There are three error sources that can produce a consistent difference between SAGE–I and SAGE–II ozone results besides the aerosol interference, which is transient in nature. These error sources are the relative uncertainties in the mean ozone absorption cross-sections for the two instruments, the scan mirror calibrations, and any systematic difference in the reference height.

Relative Uncertainty in the Mean Ozone Absorption Cross-Section

The ozone channels for SAGE–I and SAGE–II are both nominally centered at 600 nm, with nominal widths of 30 nm and 15 nm, respectively. The factor that affects the ratio of SAGE–I to SAGE–II ozone determinations is the ratio of the two mean absorption cross-section values R, defined as

$$R = \bar{\sigma}_1/\bar{\sigma}_2 \tag{19}$$

$$= \frac{\int_{w_1}\sigma(\lambda)d\lambda/w_1}{\int_{w_2}\sigma(\lambda)d\lambda/w_2}$$

where σ_1 and σ_2 are the mean ozone absorption cross-sections over the bandwidths w_1 and w_2 for SAGE–I and SAGE–II, and $\sigma(\lambda)$ is the ozone absorption cross-section.

By partitioning w_1 into regions w_2, w_S, and w_L, where the latter are regions within w_1 at wavelengths shorter and longer than w_2, respectively, and introducing δ for the uncertainty in the absorption cross-section, Equation 19 may be written

$$R + \delta R = \tag{20}$$

$$\frac{\frac{1}{w_1}\int_S[\sigma(\lambda) \pm \delta(\lambda)]d\lambda + \frac{w_2}{w_1}\cdot\frac{1}{w_2}\int[\sigma(\lambda) \pm \delta(\lambda)]d\lambda + \frac{1}{w_1}\int_L[\sigma(\lambda) \pm \delta(\lambda)]d\lambda}{\frac{1}{w_2}\int_S[\sigma(\lambda) \pm \delta(\lambda)]d\lambda}$$

$$= \frac{1}{\bar{\sigma}_2}\left[\frac{w_2}{w_1}\bar{\sigma}_2 + \frac{1}{w_1}\int_{w_S}\sigma(\lambda)d\lambda + \frac{1}{w_1}\int_{w_L}\sigma(\lambda)d\lambda \pm \frac{1}{w_1}\int_{w_S}\delta(\lambda)d\lambda \pm \int_{w_L}\delta(\lambda)d\lambda\right]$$

Note that any uncertainty in the $\sigma(\lambda)$ that is used in w_2 has no effect, because the identical values are used in that part of w_1.

In $w_{S,L}$ we can define

$$\bar{\sigma}_{S,L} \equiv \frac{1}{w_{S,L}}\int_{S,L}\sigma(\lambda)d\lambda \equiv a_{S,L}\bar{\sigma}_2 \tag{20a}$$

In the last two terms in Equation 20, expressing the uncertainty, if δ has the same sign at all frequencies in S or L (a worst case), then

$$R = \frac{w_2}{w_1} + \frac{w_S}{w_1}a_S + \frac{w_L}{w_1}a_L \tag{20b}$$

and

$$\delta R^1 = \pm\frac{\delta_S}{\bar{\sigma}_2}\frac{w_S}{w_1} \pm \frac{\delta_L}{\bar{\sigma}^2}\frac{w_L}{w_1} \tag{20c}$$

Since $w_{S,L}/w_1 \simeq 0.25$, and Penney (1979) indicates that $\delta/\delta_2 \simeq 0.02$, then, very conservatively, $\delta R^1 = 0.01$.

There is another uncertainty, δR^2, because the widths w_1, w_2, w_S, and w_L are not known exactly, but subject to the constraint that $w_2 + w_S + w_L \equiv w_1$. Evaluating the relevant expression gives $\delta R^2 = 0.0045$.

The errors δR^1 and δR^2 are independent; their RSS is 1.1 percent. To be conservative and allow for other possible small terms, we take 1.2 percent as the uncertainty in the relative cross-sections in Table 2.10 below.

Uncertainty in the Scan Mirror Calibration

The systematic retrieval errors due to the mirror for SAGE–II are shown in Figure 2.30. The mirror reflectivity effects for SAGE–I are estimated to be about twice as large. These values are presented again in Table 2.10.

Table 2.10 Errors in the Difference Between SAGE–I and SAGE–II (all errors in percent)

Altitude (km)	Ozone abs. Cross-section Difference	Mirror SAGE–II	Mirror SAGE–I	Alt. Registration Difference	SAGE–I Aerosol	SAGE–II Aerosol	Root Sum Square
20	1.2	0	0	0	4	4	5.8
25	1.2	0	0	.25	1	1	1.9
30	1.2	0	0	.50	.5	.5	1.5
35	1.2	.05	.1	.75	.2	.2	1.5
40	1.2	.1	.2	1.0	0	0	1.6
45	1.2	.25	.50	1.25	0	0	1.8
50	1.2	1	2	1.5	0	0	3.0

Systematic Differences in SAGE–I/SAGE–II Reference Height

As noted above, there may be a maximum error between the reference heights of SAGE–I and SAGE–II of 60 m. Combining this with the sensitivity curve in Figure 2.31 results in the uncertainties given in Table 2.10.

Combined Instrumental Error of SAGE–I/SAGE–II Differences

The errors noted in the three items above, plus contributions due to aerosols, are given in Table 2.10. Their combined value, treating the errors as independent, is given in the last column, and plotted in Figure 2.34. It should be noted again that there may be errors resulting from the sampling and data sparseness.

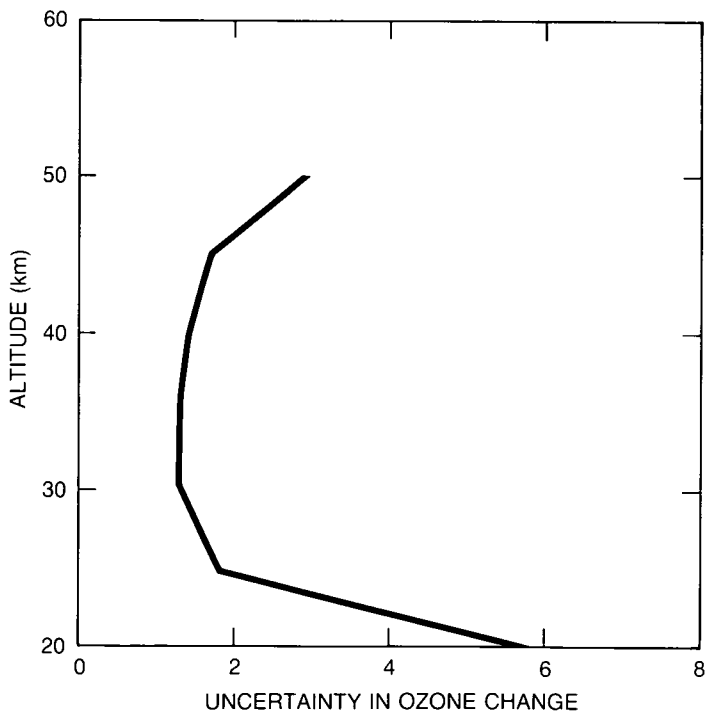

Figure 2.34 Uncertainty in ozone change determined from SAGE–I/SAGE–II differences.

The differences reported in Chapter 5 were obtained by pairing soundings taken at the same latitude and season during 2 years of operation of each instrument. This does not entirely eliminate the possibility of a systematic error due to the interaction of the sampling and the interannual variability, but the magnitude of such an effect has not been quantified at this time. The errors given in Table 2.10 and Figure 2.34 are the instrumental errors associated with the differences.

2.6. SOLAR MESOSPHERE EXPLORER (SME) UV OZONE AND NEAR INFRARED (NIR) AIRGLOW INSTRUMENTS

The SME UV Ozone and Near Infrared Airglow instruments were launched aboard the SME satellite on October 6, 1981. The satellite is in a polar orbit that is Sun synchronous and spins once every 12 seconds. The instruments take data from sunrise to sunset when the IFOV's are at the limb. Ozone data are recovered from 48–70 km from the UVS and from 50–90 km from the NIR. The two instruments overlap their altitude coverage by approximately 20 km, allowing an internal comparison of the ozone trend to be made. Data are taken at Earth's limb with an altitude resolution of about 4 km over a slant path hundreds of kilometers long. Figure 2.35 shows the observing geometry of both instruments. Ozone is deduced by independent physical means from the two instruments; however, satellite parameters, such as altitude of the observations, are common to both instruments.

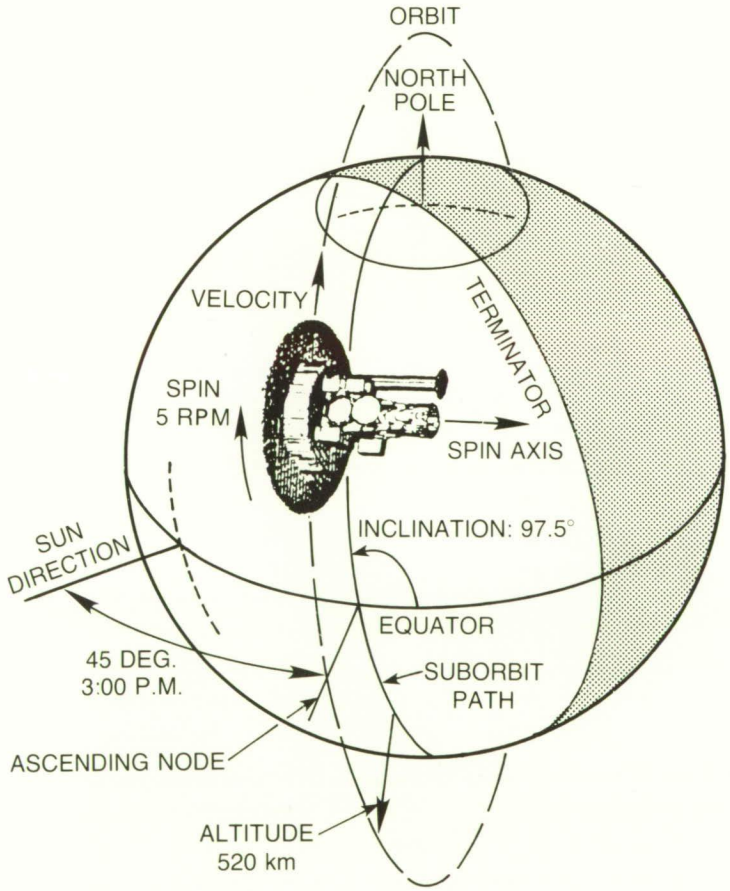

Figure 2.35 SME orbit and scan geometry.

SME experienced two problems after launch that had an unplanned effect on the two ozone instruments. First, the operating temperature of the instruments was approximately 40°C less than was anticipated. This resulted in operational problems with the diffraction grating drives, and the decision was made early on not to move them more than was necessary. This did not cause serious problems for the NIR as it was designed to work mainly at a single wavelength. The UV instrument science was restricted however, since the atmospheric altitude band of the ozone retrieval is very wavelength dependent. The instrument operates over the Hartley ozone region. Wavelengths with large ozone cross-section give good ozone retrievals at high altitudes where the ozone abundance is small, and wavelengths with small ozone cross-section give good results where the ozone abundance is large. It had been hoped to move the wavelengths over the entire Hartley band to give full altitude coverage. Instead, the mission was accomplished at a single wavelength pair that corresponded to ozone recovery in the 1.0–0.1 mb (48–70 km) altitude regions.

The second problem was the inability of the passive cooling device on the long wavelength infrared radiometer to reduce the detector temperatures to the point where they could provide an accurate pressure altitude for the coaligned instruments on board. This resulted in a serious problem in recovery of the all the IFOV altitudes at the limb. The altitudes are now derived approximately from the spacecraft bus IR horizon sensors that are part of the spacecraft attitude control system and then further refined using the actual data from each horizon scan from the UV ozone instrument. Final determination of altitude accuracy of the FOV at the limb is stated to be approximately 1 km. The derived altitude of the FOV of the UV ozone instrument was used for all the instruments on board the satellite. The UV ozone and NIR instruments were turned off in December 1986.

2.6.1. UV Spectrometer

2.6.1.1 Physical Principles

The technique is described by Rusch et al. (1984) and in User's Manual (Mount, 1982). Figure 2.36 illustrates the geometry and the physical processes. The radiance measured by the UVS at wavelength λ, I_λ, looking at an altitude z_0, can be written as

$$I_\lambda(z_o) = F_\lambda \sigma_\lambda \phi(\psi) \int_{-\infty}^{\infty} T_{\lambda s}(s)[T_{O_3}(s,\infty)]N[z(s)]ds \qquad (21)$$

where F_λ is the solar flux, and σ and $\phi(\psi)$ are the Rayleigh scattering cross-sections and phase function for scattering angle ψ. $T_s(s)$ is the transmittance of solar radiance to the scattering point s, $N(s)$ is the volume density of Rayleigh scatters at s, and T_{O_3} and T_R are the transmittances after attenuation by ozone absorption and Rayleigh scattering, respectively, between the scattering point and SME, taken to be at $+\infty$. Only single scattering is included for the altitudes of interest.

As the data are now reduced, data from the long wavelength channel (296.4 nm) are used to determine the density at a level where ozone absorption is negligible ($T_{O_3}(s,a) = 1$). In this case, I/F depends only on the number of scatterers (i.e., the density) that can be related to an approximate height using the proposed COSPAR International Reference Atmosphere (CIRA) model atmosphere (Barnett and Corney, 1985). This incorporates climatological latitudinal and seasonal variations, but not the effects of short-period disturbances or systematic longitudinal variations. The density level selected corresponds to an altitude of about 65 km. The exact altitude depends on the ratio of the absolute calibrations of the UVS and the separate solar instrument (Rottman et al., 1982) as well as on meteorological effects.

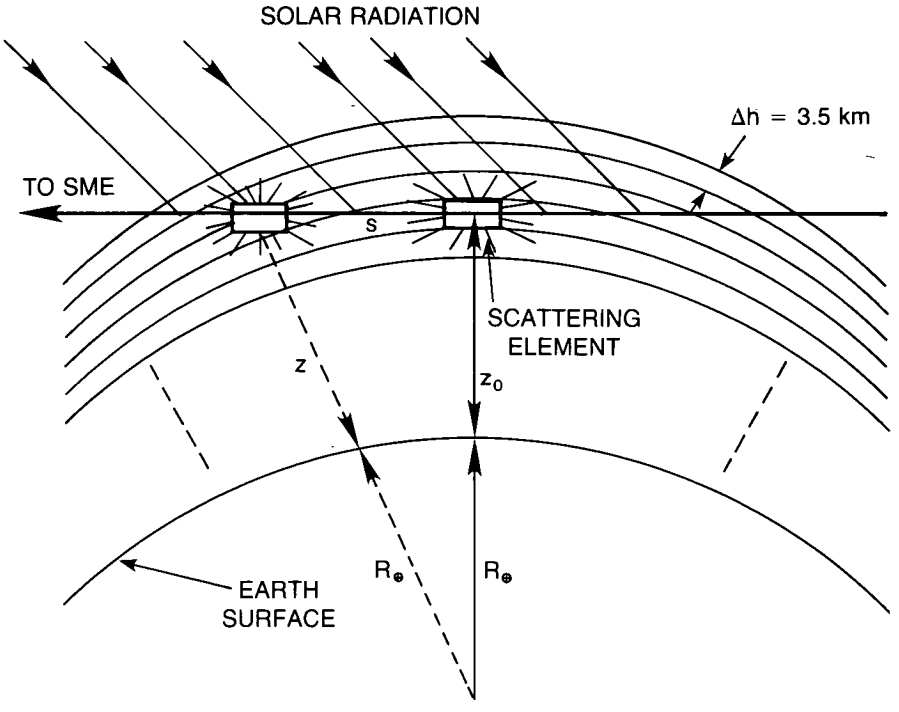

Figure 2.36 The geometry of limb viewing with the UVS on SME. Z_o is the minimum ray height of the 3.5 km vertical resolution of the measurement (from Rusch et al., 1984).

With the density and altitude point determined from the long wavelength channel, the short wavelength channel (265.0 nm) radiance profile is then adjusted in magnitude to force agreement with the model Rayleigh scattering at 76 km altitude where the short wavelength channel ozone absorption is negligible. Only the relative shapes of the radiance profiles from the short wavelength channel are needed to deduce ozone abundance once these shifts are made, and the shapes depend only on atmospheric Rayleigh scattering and ozone abundance. It is very important to note that the absolute calibration of only the long-wavelength channel is required in the determination of ozone abundance. Neither the absolute nor the relative calibration of the short wavelength channel plays a role.

There was no plan for long-term calibration, since the mission was originally specified to last for 1 year. The expectation, apparently, was that there would be no serious degradation over this period, and the experimenters were directed not to plan for longer instrument life. The UV instrument did not incorporate an internal calibration lamp. Two features helped to reduce degradation over the 5 years in orbit. First, the SME was a very clean spacecraft, resulting in less outgassing that could contaminate the optical surfaces. Second, the UVS did not view the Sun, so solar dissociation and fixing of contaminants on the optics could not occur.

2.6.1.2. Instrument Description and Prelaunch Testing

The instrument and its testing have been described by Rusch et al. (1984) and in User's Manual (Mount, 1982). The collecting telescope is a nonobscured f/5, 250-mm focal length off-axis parabola. The telescope feeds an f/5, 125-mm Ebert–Fastie spectrometer employing a 3600 l/mm diffraction grating. Spectral resolution is approximately 1.5 nm. Dual channel detectors are EMR 510–F–06 photomultiplier tubes. Figure 2.37 shows a schematic diagram of the

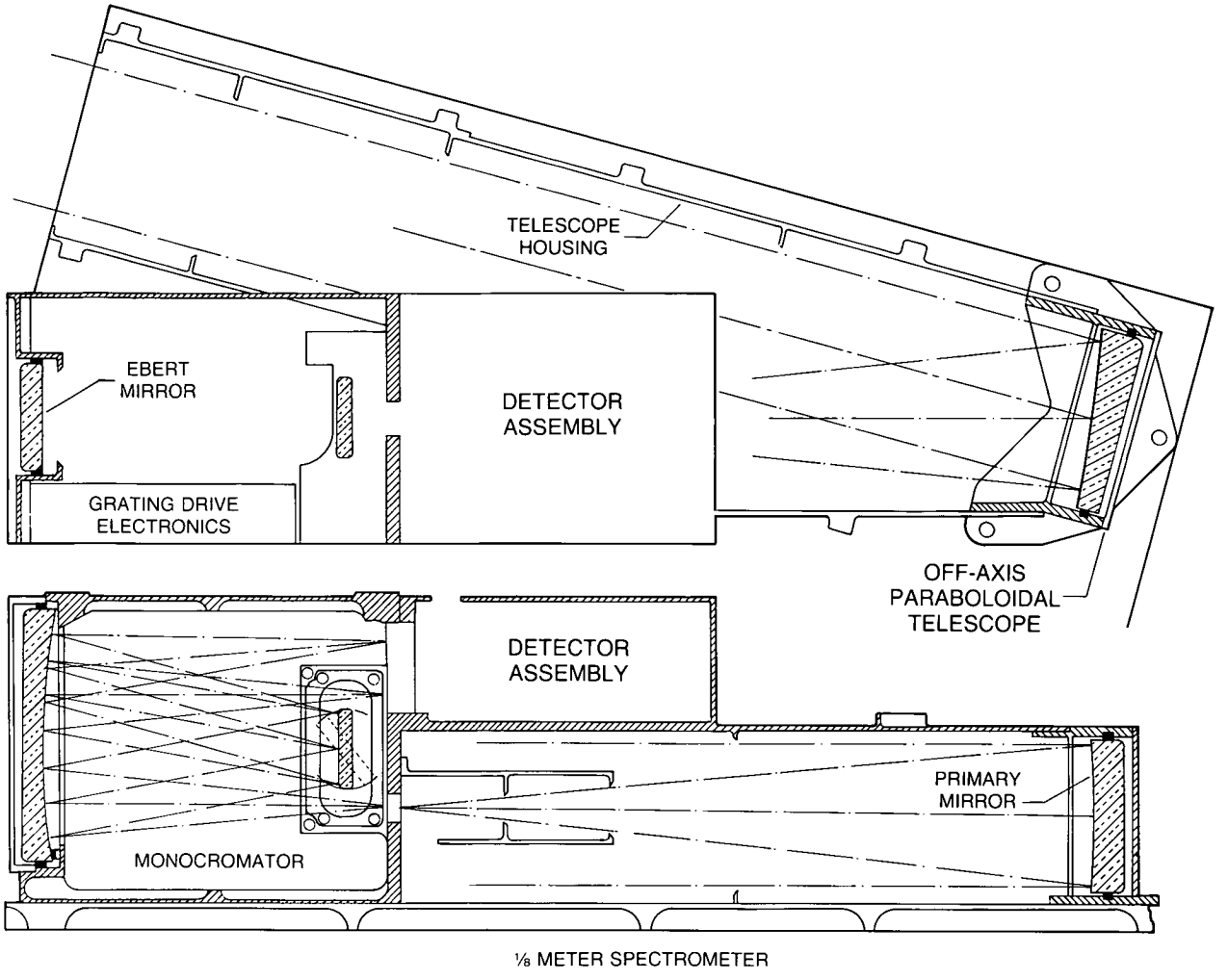

Figure 2.37 Schematic drawing of the SME UV spectrophotometer. Two views are shown rotated 90° with respect to each other. The detector assembly houses two photomultiplier tubes and pulse-counting electronics (from Rusch et al., 1984).

UV ozone instrument. Calibration tests performed on the instrument and its components were grating efficiency, grating scatter and ghosts, grating polarization, mirror efficiency, mirror off-axis scatter, mirror RMS surface roughness, detector dead time, detector efficiency, detector sensitivity maps, absolute instrument efficiency, instrument off-axis scatter, instrument wavelength calibration, instrument polarization, FOV sensitivity variation, and spectral bandpass.

The instrument absolute calibration for wavelengths of less than 260 nm was made using a system similar to the Johns Hopkins CTE, which utilizes NBS photodiodes and transfer photomultiplier tubes as the standards. For wavelengths greater than 240 nm, NBS standard tungsten strip filament lamps were used, either focused directly onto the ozone spectrometer entrance slit (with telescope removed) or onto a $BaSO_4$ scattering screen with the telescope on the instrument. The resulting (one sigma) error budget was wavelength less than 240 nm: ±25 percent; 240–270 nm: ±12 percent; 270–320 nm: ±10 percent; and greater than 320 nm: ±15 percent. Wavelengths used in flight were 265.0 nm and 296.4 nm, and so the absolute calibration for the retrieval wavelength pair was about ±10 percent (one sigma). These wavelengths provide

information on ozone from about 1 mb–0.1 mb. A relative sensitivity shift of the two channels, noted after launch, results in an absolute sensitivity determination of about 20 percent (one sigma).

Figure 2.38 shows the altitude-dependent errors resulting from the inversion process for each indicated calibration measurement. The UV ozone instrument retrieves the ozone abundance in

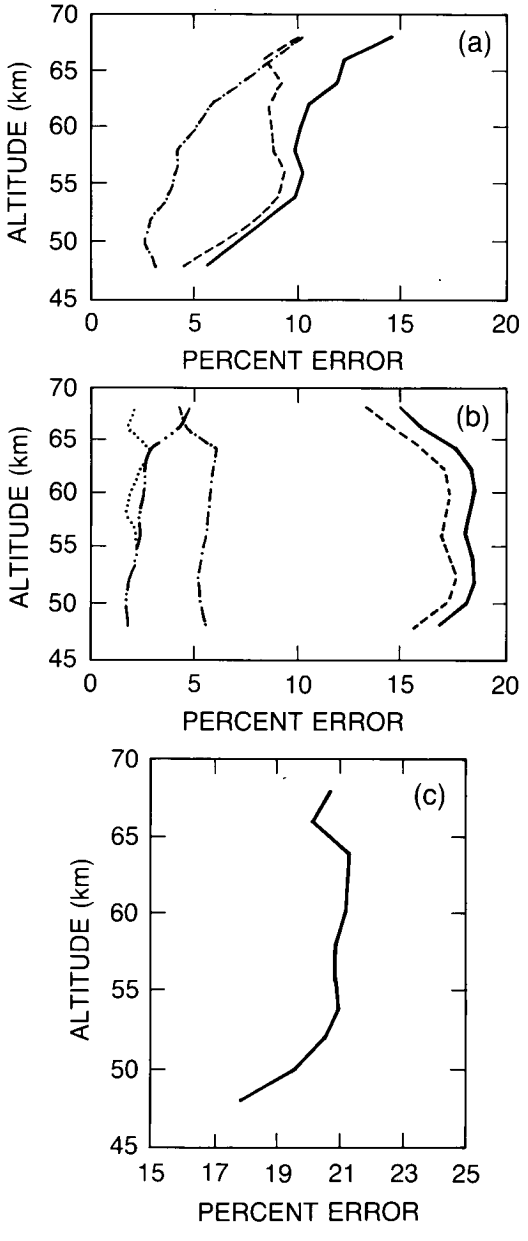

Figure 2.38 (a) Random altitude-dependent errors associated with noise and data compression (dashed dot line) and temperature and pressure (dashed line). The solid line is the rms sum. (b) Systematic altitude-dependent errors associated with uncertainties in instrument sensitivity (dashed line), instrument polarization (dash-dot-dot-dash), dead-time constants (dotted line), and ozone cross-sections (dash-dot-dash). The solid line is the rms sum. (c) The altitude-dependent error from combined random and systematic errors (from Rusch et al., 1984).

the 1–0.1 mb region with an overall accuracy of approximately 21 percent (one sigma), which includes errors caused by using model atmosphere that may differ from the real atmosphere, although the differences are not expected to be significant from year to year. The use of temperatures determined from Wallops Island (U.S.) rockets fired during satellite overpasses results in insignificant changes in the retrieved ozone from the model assumption.

FOV limb altitudes are determined by comparison of the Rayleigh-scattered radiance measured with that calculated from modeling this signal using the relevant solar fluxes, cross-sections, and the proposed CIRA model. The normalization in altitude is done at 65 km in the long-wavelength channel (296.4 nm), where no ozone absorption is detectable and the Rayleigh scattering is optically thin. The altitude is then considered by the SME science team to be determined with an accuracy of approximately 1 kilometer, based on uncertainty in the absolute calibration, with a repeatability of 0.3 km. Figure 2.39b (taken from Barth, Rusch, Clancy, and Thomas [BRCT], unpublished report, 1987) shows the required corrections to the spacecraft IR horizon sensors for a particular orbit and the limb sensor altitude determinations themselves (Figure 2.39a). Sensitivity to the long-wavelength channel absolute calibration is about 1 km per 15 percent change in long-wavelength channel calibration.

Several factors affect the ability of the UV ozone instrument to detect ozone abundance trends: changes in the absolute calibration of the long-wavelength channel of the instrument, since it determines the model normalization at 65 km, which in turn determines the absolute altitude of the FOV; reliance on a model atmosphere that has seasonal and latitudinal changes, but that is assumed to be the same every year and has no local spatial or rapid temporal variability; drift in the wavelength drive, resulting in incorrect use of ozone cross-sections and solar fluxes; changes in the solar flux at the long-wavelength (296.4 nm); and changes in instrument polarization as a function of time.

2.6.1.3 Performance in Orbit

The UV ozone instrument incorporated no internal calibration lamp. The tropical background radiance was monitored for about a year after launch; there was no apparent change in either of the two channel radiances, other than the expected seasonal changes, to a level of about 10 percent.

The wavelength drive has been checked regularly since launch, and shows a very small and easily corrected change that is known to a very high degree of accuracy from wavelength scans of the scattered solar light. Based on the SME solar instrument measurements of solar flux, no correction is applied for a time-dependent solar flux.

Since launch, there has been an observed time-dependent trend in the altitude correction deduced from the UV instrument relative to the spacecraft IR limb sensors that can be explained by a 9 percent per year change in total instrument sensitivity. Observation of the altitude shifts over time since launch indicate that these shifts are correlated with the roll angle of the spacecraft and with the resulting tilt of the entrance apertures of the instruments, which were designed to operate on a tangent to Earth's limb. The orbit was optimized for operation during the first year after launch, and orbit precession has increasingly tilted the projected slits relative to the tangent. Determination of the altitude shifts during June of each year, when the roll angle is near zero, indicates a 6 percent per year change in the instrument sensitivity. Thus, 3 percent can be removed as having been caused by the changing roll angle of the spacecraft.

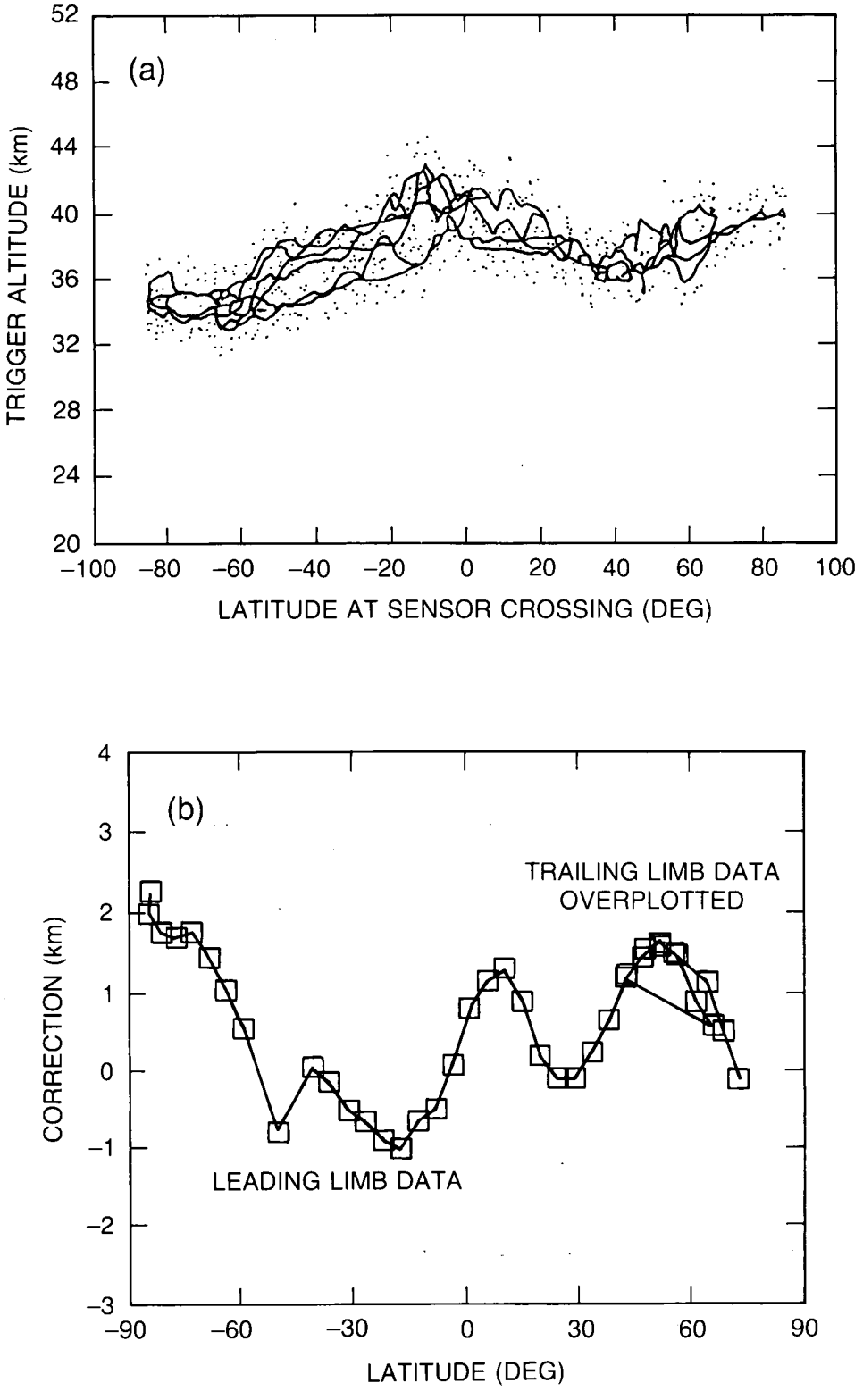

Figure 2.39 (a) Example of IR horizon sensor trigger altitudes vs. latitude. (b) Altitude corrections vs. latitude (from BRCT).

There is a dual channel visible light spectrometer (VIS) on board SME that measures NO_2 near 440 nm (Mount et al., 1984). The detectors used are dual silicon photodiodes, which are etched in the same active material in the rectangular shape of the "exit slits." The instrument scans the altitude range from about 100 km above to 20 km below the horizon. Assuming that the wavelength-dependent scattering properties of the atmosphere at 48 km have not changed since launch and that there is no measurable NO_2 absorption in the visible spectrum at 48 km (a good assumption), then it is determined that the relative drift of the diodes with respect to each other is 0.4 percent/year. This is quite reasonable, since the diodes are physically located only a few millimeters apart. The absolute calibration of the diodes and the associated analog electronics is not known, but the relative drift of the two diode channels relative to each other is expected to be small since the diodes are from the same piece of silicon. No onboard electronics test of standard current levels was provided. There is evidence that the electronics drift is less than 1 percent per year, since the electronic offset added to the electrical signal from the photodiodes has remained very stable over the 5-year life of the mission.

2.6.1.4 Assessment of Instrument Drift and Its Effects

The following discussion is based in part on BRCT. Assuming that the VIS diodes have not drifted in absolute calibration, and ratioing their observed signal near 440 nm at 48 km to the observed signal from the UV spectrometer long-wavelength channel at 76 km altitude (where ozone absorption should be negligible), leads to a deduced change in the UV instrument long-wavelength channel sensitivity at 296 nm of -4.8 percent/year ± 1.4 percent/yr. This change in sensitivity then translates into an ozone change at 0.75 mb (53 km) averaged over 0–60°N latitudes in the summers of $+1.6$ percent/year since launch, with a range from $+4.1$ percent/year (for smaller instrument degradation) to -0.7 percent/year (greater instrument degradation). These error bars are a measure of the statistical variation in the summer data from each year and do not include algorithm-related errors in the ozone retrieval. The SME UVS shows an ozone trend bounded by a range $+4.1$ percent/year to -0.7 percent/year assuming no change in the absolute calibration of the visible spectrometer photodiodes.

The ozone trend determined from this method depends on the assumptions that there will be:

- No change in the absolute calibration of the visible instrument photodiodes.
- No change in the calibration of the analog electronics that convert the photodiode signals to data numbers.
- No shift in the positions of the two instrument fields of view in relation to each other.
- No nonseasonal changes in atmospheric albedo and temperature effects between 48 and 76 km between 1982 and the present.
- No nonseasonal systematic drifts of atmospheric shape with time.

While changes in the VIS photodiode sensitivity are expected to be small, there is no way to verify that this is, indeed, the case. The SME science team feels that it would detect changes in the diode sensitivities of the order of several percent per year since this would change the response to NO_2. There is also no way to measure changes in the analog electronics. The relative sensitivity drift of the two photodiode channels is 0.4 percent/year, indicating that the diodes

and their absolute sensitivity could well be changing in a similar manner. There has been very little stress on the diodes, since the operating current is six decades below the nonlinear operating point. The diodes are operated in photovoltaic mode, so there is no voltage stress on them. No increase in noise level has been observed. Measurements of polar albedo (which is expected to remain fairly constant) taken in the nadir indicate approximately a 10 percent change in 5 years. Assuming no change in albedo due to aerosols (El Chichón) and other factors, this gives a 2 percent/year photodiode sensitivity change. There is no reason to expect that the FOV's have shifted relative to each other. Atmospheric effects should be small, but are again not verifiable. Therefore, the SME science team has set a limit on the change of the photodiode calibration at 1 percent per year ±1 percent per year; in this assessment, the worst case value of 2 percent per year has been used.

There is evidence from the SME solar instrument that SME is a particularly clean satellite because there is no evidence of significant degradation of the optical surfaces in that instrument. It is reasonable to conclude that it has not occurred in other instruments. Thus, any sensitivity degradation in the UV spectrometer is assumed to be mostly in the photomultiplier tubes. The tubes were used in the pulse-counting mode, which makes them initially insensitive to changes in gain with increasing total count rate. The tubes were used in orbit at rates of several hundred thousand counts per second, which are conservative rates. The long-wavelength channel photomultiplier would suffer count-rate degradation first, since its count rate is more than twice that of the other channel. This is in agreement with the determination above. The changes in solar flux have been negligible at these wavelengths, and there is no reason to suspect that the polarization of the optics has changed. It is important to repeat that only the long-wavelength channel absolute calibration is required for the altitude determination, and even the relative calibration between the two channels is not needed for ozone determination.

2.6.2. Near Infrared (NIR) Instrument

2.6.2.1 Physical Principles

The physics of the ozone retrieval on the NIR instrument is quite different from the UV instrument, which measured relative absorption in two channels. The approach is described by Thomas et al. (1984). The most important processes are indicated in Figure 2.40. Photodissociation of ozone by solar radiation

$$O_3 + h\nu(210 < \lambda < 310\text{nm}) \rightarrow O_2(^1\Delta_g) + O(^1D) \tag{22}$$

and other processes lead to the formation of $O_2(^1\Delta_g)$. Some of these molecules are quenched, while others radiate. The NIR measures the emission by $O_2(^1\Delta_g)$ at 1.27μm. Deduction of the ozone from the $O_2(^1\Delta_g)$ emission depends on ozone absorption, O_2 absorption, ozone photodissociation, the solar flux in the UV and visible/red, and quenching of excited oxygen. Rate constants and cross-sections must be known, photochemistry must be correct, and a correct background atmosphere must be used.

In particular, the signal will depend on solar radiation and its spectral variations and on atmospheric temperature. The retrieval is made from approximately 50–90 km. The retrieval requires that the absolute radiance at 1.27μm emerging from the atmosphere be measured. Again, planning for long-term operations was not part of the preflight strategy, but the NIR included an inflight calibration source to allow measurement of, and correction for, instrument drift.

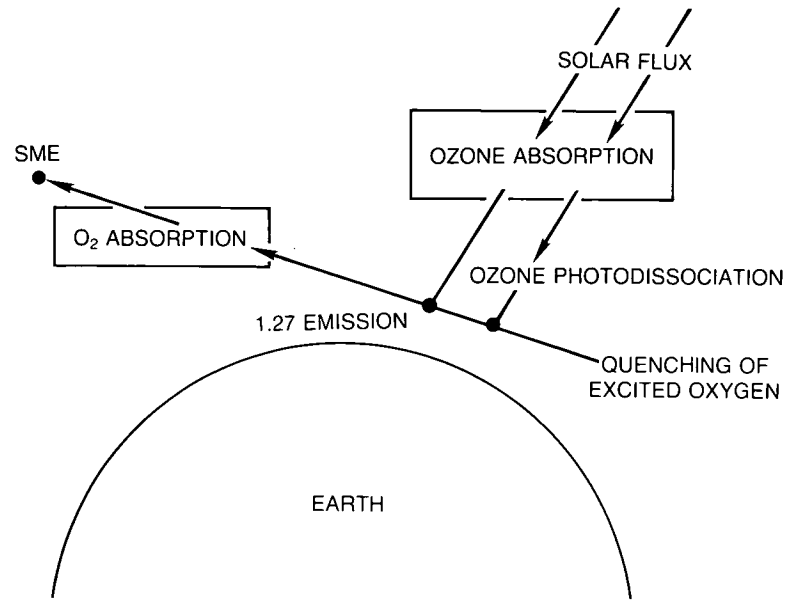

Figure 2.40 NIR physical processes (from Thomas et al., 1984).

2.6.2.2 Instrument Description and Prelaunch Testing

The optics of the NIR instrument are very similar to those of the UV spectrometer; Figure 2.41 shows a schematic diagram of the NIR. The detectors are chopped lead sulfide photoconductors with immersion lenses cooled by radiation to space. The following quantities were measured during calibration: absolute sensitivity, spectral bandpass, polarization, wavelength scale, FOV, off-axis scatter, time response, out-of-band leakage, linearity, and thermal characteristics. The absolute sensitivity was determined with an NBS-calibrated tungsten strip filament lamp. The filament was focused on a barium sulfate screen producing a diffuse light of known intensity. Absolute calibration was accurate to about 20 percent.

The NIR spectrometer had an onboard calibration source. A small tungsten lamp, a silicon photodiode, and a thermistor were placed at the edge of the f/5 telescope beam near the entrance slit of the spectrometer (Figure 2.41). Light scattered from the baffles enters the spectrometer, and, if the time-dependent calibration of the system is understood, the relative time-dependent response of the instrument (not including telescope) can be deduced. The brightness of the lamp depends on its operating conditions (such as temperature and voltage) and changes as it ages. The photodiode measures the lamp brightness; since it is temperature sensitive, a thermistor is placed next to the diode. The system is not a precise calibration for short-term use, but should detect major short-term changes. For long-term changes it is very useful.

2.6.2.3 Performance in Orbit

One hundred forty-nine calibrations were performed after launch. The following conclusions have been drawn from the calibrations: comparison of the two NIR detector channels indicate that the brightness changes of the lamp are changes in the black-body temperature of its filament, and the photodiode output has been determined and shows that the change in its sensitivity over the mission is small. Normalized sensitivity of the 1.27μm detector is shown in Figure 2.42. The result is an increasing sensitivity of only 0.28 percent ±0.15 percent per year.

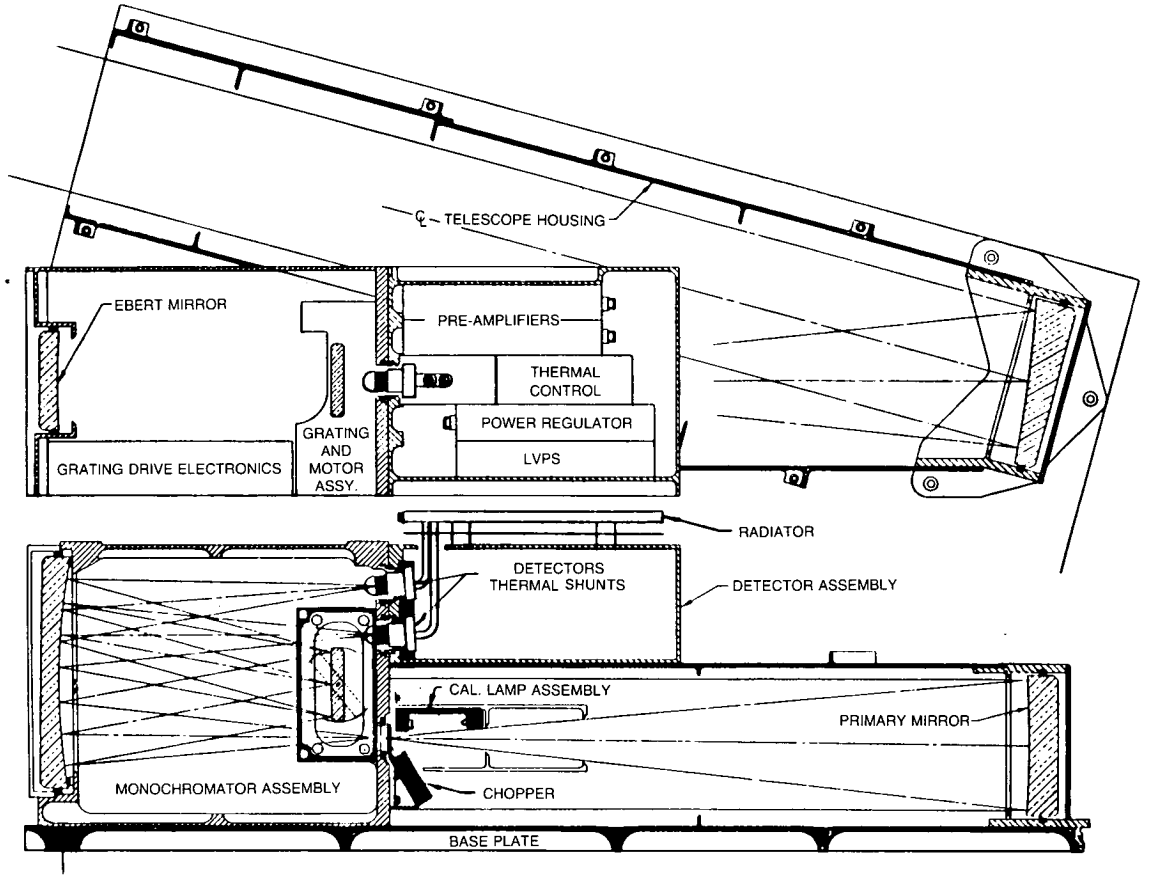

Figure 2.41 Optical scheme of the near-infrared spectrometer. Light enters the telescope through a baffle assembly. The light is focused onto the entrance slit and chopper. In the monochromator, the chopped light is collimated by the Ebert mirror onto the grating. The Ebert mirror then focuses the dispersed light onto the detectors, which define the exit slit. The detectors are passively cooled by a radiator on the outside of the instrument (from Thomas et al., 1984).

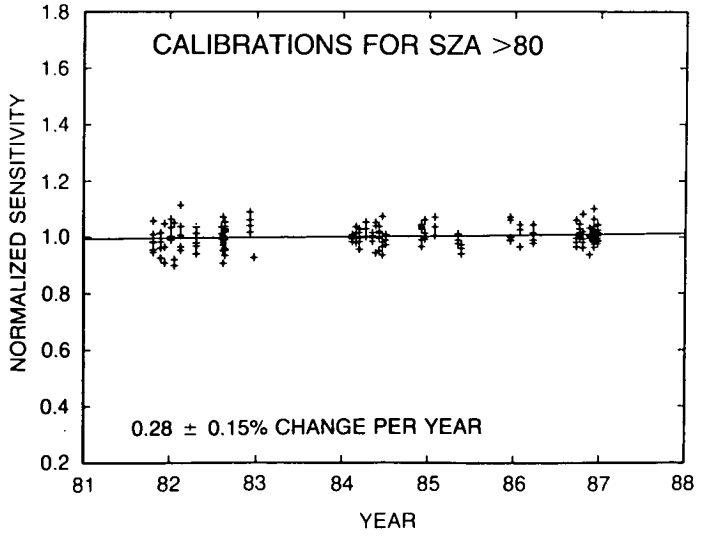

Figure 2.42 Normalized NIR photodiode sensitivity through the mission (from BRCT).

Thus, from the inflight calibration checks it appears that the instrument was very stable over time.

The derived ozone profiles from the NIR spectrometer overlap those determined from the UV ozone instrument in the 50–65 km region. The NIR results were adjusted by 10 percent to force a match between the two instruments for the time period immediately after launch. This adjustment has been used since then without change. The trends from the two instruments have diverged since launch if the preflight calibration values are assumed.

2.6.2.4 Sources of Instrument Drift

Systematic errors due to errors in rate or cross-sections, poor background atmospheric models, and instrument calibration errors result in a 50 percent error near 1 mb and a 30 percent error near 0.001 mb. Total systematic errors are shown in Figure 2.43 as a function of altitude.

Although the systematic errors are large, they will not change with time and will not introduce drifts in the inferred ozone. A detailed discussion is contained in Chapter 3. Errors that introduce trends into the data are changing instrument calibration, drifts between the real and model background atmosphere, changes in the assumed solar irradiance in the UV and the red, and dependence on the UV instrument for the altitude determination of the FOV. In this chapter, only the effects of changing calibration and altitude determination are addressed.

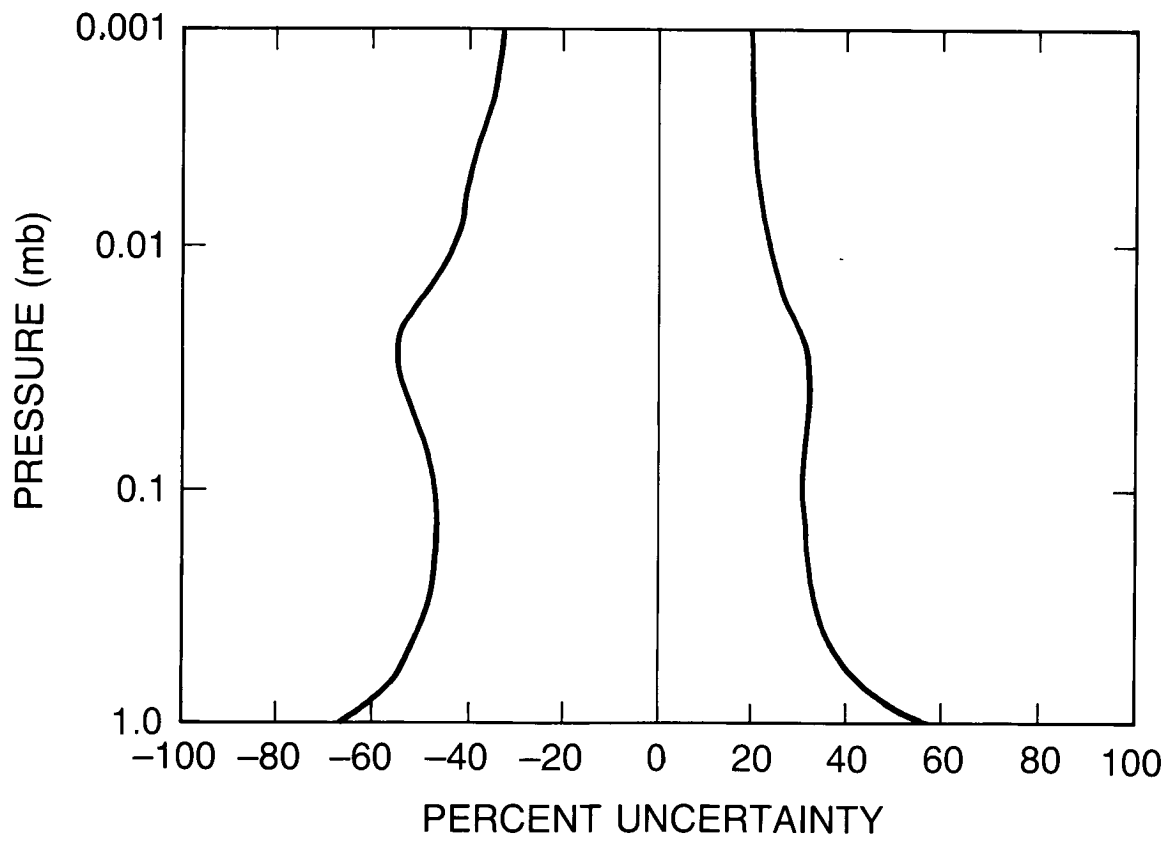

Figure 2.43 Total systematic error on ozone data estimated from input errors (from Thomas et al., 1984).

2.6.3 UVS and NIR

2.6.3.1 Comparison of Ozone Trends From the Two Instruments

Using the standard UVS altitude corrections for both the UVS and NIR instruments with no allowance for any changes in UV sensitivity produces the ozone trends for June shown in Figure 2.44a,b for 0.75mb averaged over 0°–60°N latitude. These changes are +13.2 percent per year for the UV instrument and +2.4 percent per year for the NIR instrument. These are the data in the NSSDC data base as of September 1987.

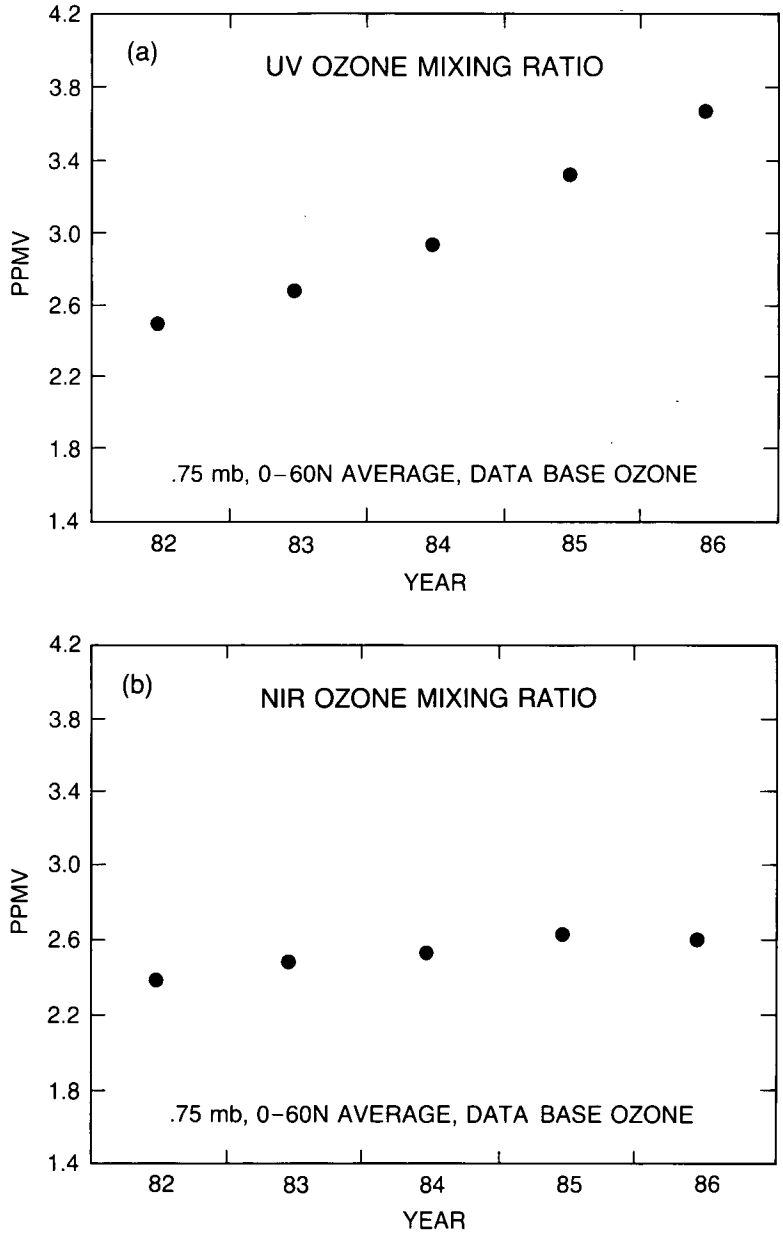

Figure 2.44 UV and NIR 0.75 mb mixing ratio with time. No correction for sensitivity drift of UV LW channel (from BRCT).

Figure 2.45a,b shows plots of the 0.75mb data for the derived change in UV instrument long-wavelength channel sensitivity of -4.8 percent per year as described earlier (assuming no degradation of the visible spectrometer photodiodes). The NIR data are calculated using the altitude shifts derived from the changed long-wavelength channel UV sensitivity. The calculated ozone changes, 1.57 percent per year for the UV and 1.6 percent per year for the NIR, are in close agreement.

Using the spacecraft bus IR CO_2 horizon sensors, an FOV determination independent of the UV instrument can be made for the NIR Airglow instrument. The altitude pointing determined this way is noisier, but provides a useful check on ozone that is independent of the UV instrument. Figure 2.46 shows the trends in ozone for the NIR instrument using this technique.

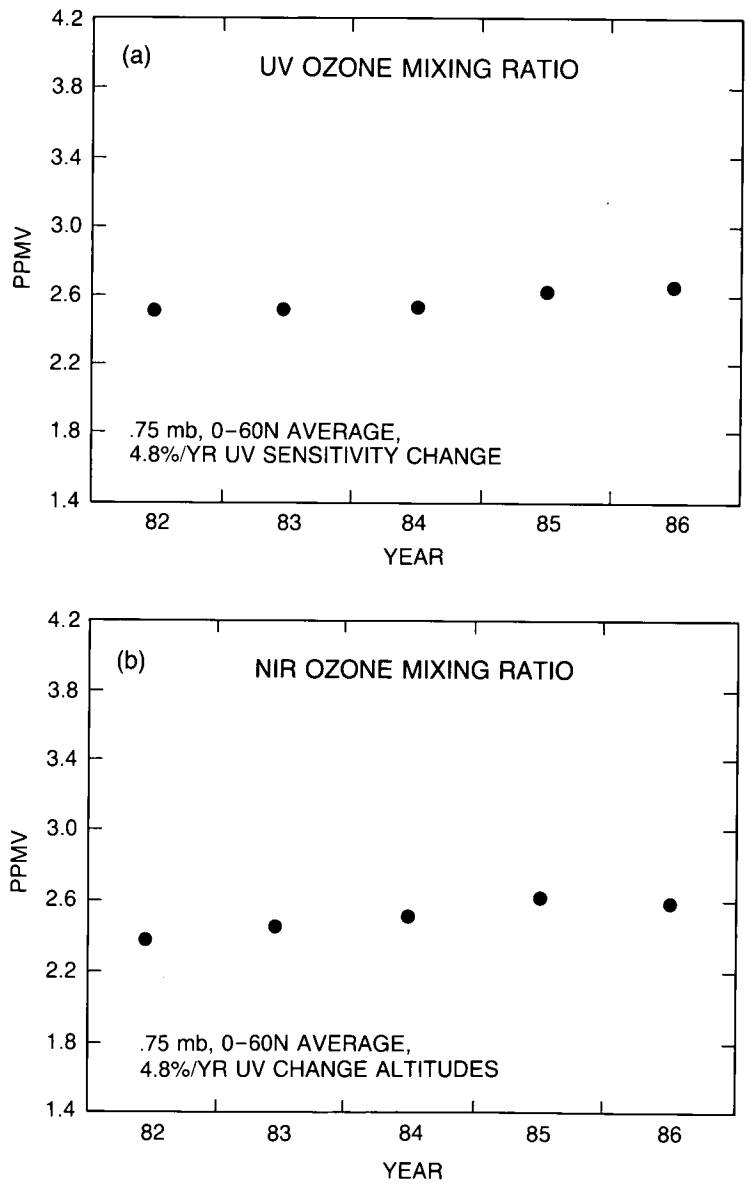

Figure 2.45 UV and NIR 0.75 mb mixing ratio with time. Correction for sensitivity drift of UV LW channel (from BRCT).

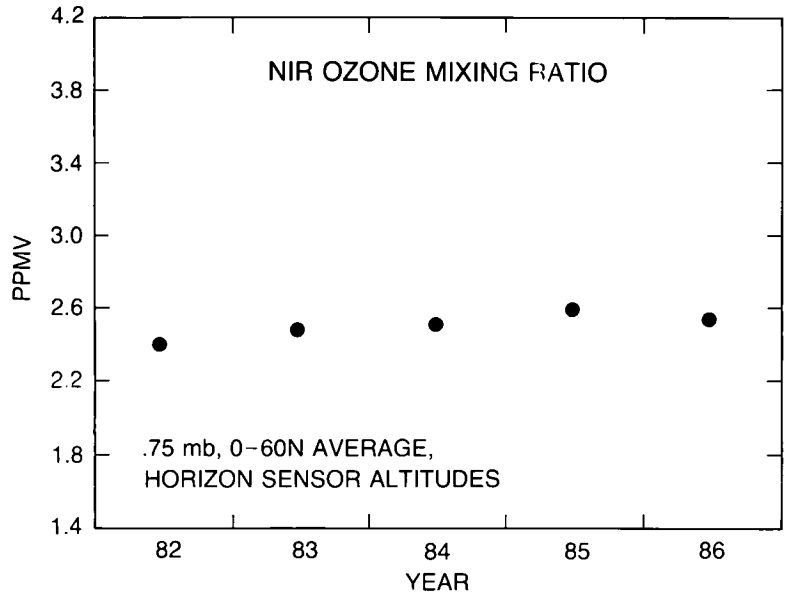

Figure 2.46 NIR 0.75 mb mixing ratio with time using the bus horizon sensors (from BRCT).

Note that the trend in ozone derived from this method (1.8 percent per year) is very nearly equal to that derived from using the UV altitude shifts shown in the previous figure. The 0.75 mb ozone-mixing ratios from the NIR instrument are only slightly affected by changes in the altitude determinations, since the broad maximum of the 1.27μm airglow is near this altitude.

Figure 2.47 shows the range in the trends for 0°–60°N for June 1982–1986 that results from inverting the UV data using two standard deviation uncertainties in the UV long-wavelength

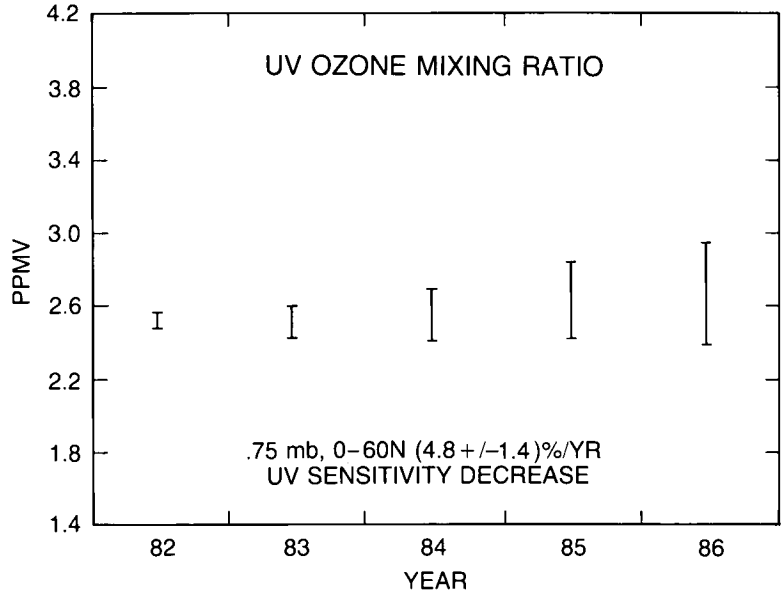

Figure 2.47 Ozone mixing ratios for June 1982–1986 for the UV instrument. The error bars denote the range of the data resulting from the uncertainty in the determination of the UV sensitivity change as a function of time assuming no algorithm retrieval error and no visible spectrometer photodiode drift with time (from BRCT).

channel sensitivity, assuming the algorithm physics is correct and assuming the visible photodiodes have not drifted with time. The values for the ozone change at the extremes of the sensitivity changes are -0.7 percent per year and +4.1 percent per year. When the possibility of visible spectrometer photodiode degradation of 2 percent per year is taken into account, the range of possible ozone trend is +4.1 percent per year to -3 percent per year for 0°–60°N in June.

2.6.3.2 Assessment

The accuracy of the absolute calibration of the SME UVS long-wavelength channel determines the accuracy to which the altitude of the FOV of this instrument can be determined. The ozone abundance and ozone trend depend crucially on this determination. The SME science team has used the photodiode channels on the SME visible spectrometer to correct the absolute calibration of the UV long-wavelength channel for drift over the 5-year period in orbit. The change in the UVS absolute calibration relative to the visible instrument photodiodes is -4.8 percent per year ±1.4 percent per year*. An observable limit to the degradation of the visible instrument photodiodes, on which the UV calibration is based, is 2 percent per year. Including this limit in the absolute calibration uncertainty, the ozone trend derived from the SME UV instrument is +4 percent per year to -3 percent per year.

A detailed analysis of the long-term drift of the NIR instrument was presented, and a convincing case for only small calibration drifts during the 5 years in orbit was made. However, although the NIR instrument has a reasonably determined calibration drift, which is small, the altitude of its FOV, and hence its ozone determination, is dependent upon the absolute calibration of the UV ozone instrument, which determines the altitude used in its inversion. This dependence is very small at the 0.75 mb pressure level. The range of uncertainties, including uncertainties in both calibration and altitude, is ±0.7 percent per year. Thus, the ozone trend determination from this instrument at the 0.75 mb level is +2 percent per year ±0.7 percent per year.

A determination independent of the UVS altitude corrections was made from the NIR instrument using the altitude determination from the spacecraft bus IR horizon sensors; this analysis gave a trend of +1.8 percent per year.

2.7 THE LIMB INFRARED MONITOR OF THE STRATOSPHERE (LIMS)

LIMS is a six-channel infrared limb scanning radiometer on the Nimbus–7 spacecraft. The experiment and its calibration have been described in detail by Gille and Russell (1984); previous discussions are contained in Russell and Gille (1978) and Gille et al. (1980).

*Note added in proof. Subsequently, Rusch and Clancy (1988) have claimed an accuracy in trends of ±1.3%/year. These authors reference an *oral* presentation by Barth, Rusch, and Thomas at the 1987 spring AGU meetings as the source of the ±1.3%/year trend determination accuracy. However, it was clearly stated in the meetings that this report is based on the ±1.3%/year number reported at AGU *assumed* that the visible diode instrument experienced no drift in sensitivity. In fact, it experienced a 0± 1% drift as described in Figure 2.47 above, which must be included in the total trend error budget, as has been carefully done in this report.

2.7.1 Principles of the Technique

The viewing geometry is the same as that shown in Figures 2.36 and 2.40, except that LIMS measures the infrared radiation emitted by the atmosphere as it scans across the limb. At any given measurement during the scan, when the instrument is viewing tangent altitude h above the surface, it receives a radiance in the ith channel given by

$$N_i(h) = \int_{-\infty}^{\infty} B_i(T,x)\frac{d\tau_i(\mu_i)}{dx}\,dx \tag{23}$$

where

B is the Planck function,
T is the temperature,
τ is the transmittance, and
x is the distance along the line of sight from the instrument through the tangent altitude h.
μ_i is the mixing ratio of the gas that absorbs in this channel.

The general strategy is to measure N_i for channels in which CO_2 is the emitting gas. Because its mixing ratio is known, τ and $d\tau/dx$ may be calculated, allowing B and thus the temperature T to be derived. This temperature is then used to calculate B for the ozone channel (indicated by subscript 3); from N_3 and B_3, the distribution of the ozone-mixing ratio, μ_3, can be derived through the dependence of τ_3 on μ_3.

From this discussion it is clear that the solution depends on the absolute value of the N_i, resulting in a requirement for accurate calibration of the measurements.

More exactly, Equation 23 should be written

$$N_i(h_j) = C_i \int_{h_i}^{h_2}\int_{\nu_{i_1}}^{\nu_{i_2}}\int_{-\infty}^{\infty} \phi(h - h_j)\psi_i(\nu)B(\nu,T(x)) \times \frac{d\tau}{dx}(\nu,x,h_j)dx\,d\nu\,dh \tag{24}$$

where h_j denotes the jth tangent height,
C_i is a calibration constant, relating the output from the instrument to the input radiance,
$\phi(h\text{-}h_j)$ is the relative spatial response,
$\psi_i(\nu)$ is the relative spectral response.

In addition, we note that

$$h_o + j\cdot\Delta h$$

where h_0 is an (initially) unknown reference height, and measurements spaced Δh apart are made on a vertical scale relative to it.

Thus, the quantities C, ϕ, and ψ must be known in order to determine the absolute radiance, and the spacing Δh must be known to perform the retrievals.

2.7.2 Instrument Description

The instrument has been described by Gille and Russell (1984), referred to below as GR. Here, a very brief summary is given, with emphasis on those features most important for determining the calibration and its stability during orbital operation.

A schematic of the optical train is shown in Figure 2.48. Radiation from the limb is reflected off the scan mirror to the primary mirror, an off-axis parabola that brings the light to a focus where it is chopped. A parabolic secondary recollimates the beam and directs it through a Lyot stop to a folding mirror, from which it passes through relay optics, interference filters that define the spectral response of the channels, and an FOV-defining mask, and onto mercury–cadmium–telluride detectors. The optics from the Irtran 6 lens through the detectors are cooled to about 61 K by the primary cryogen, solid methane. The optical train out to the thermal mask was maintained at about 152 K by the solid ammonia second-stage cryogen. The amount of methane in the cooler limited the experiment life to 7 months.

In operation, the scan mirror caused the line of sight (LOS) to traverse the limb at a rate of 0.25 degree per second. The mirror position is controlled by a low-resolution sensor, but accurate relative positions are obtained from a 15-bit optical encoder on the scan mirror shaft, which nominally puts a pulse into the data stream for every 79.1 arc seconds of LOS motion, or approximately every 1.4 km. The encoder was used to determine Δh.

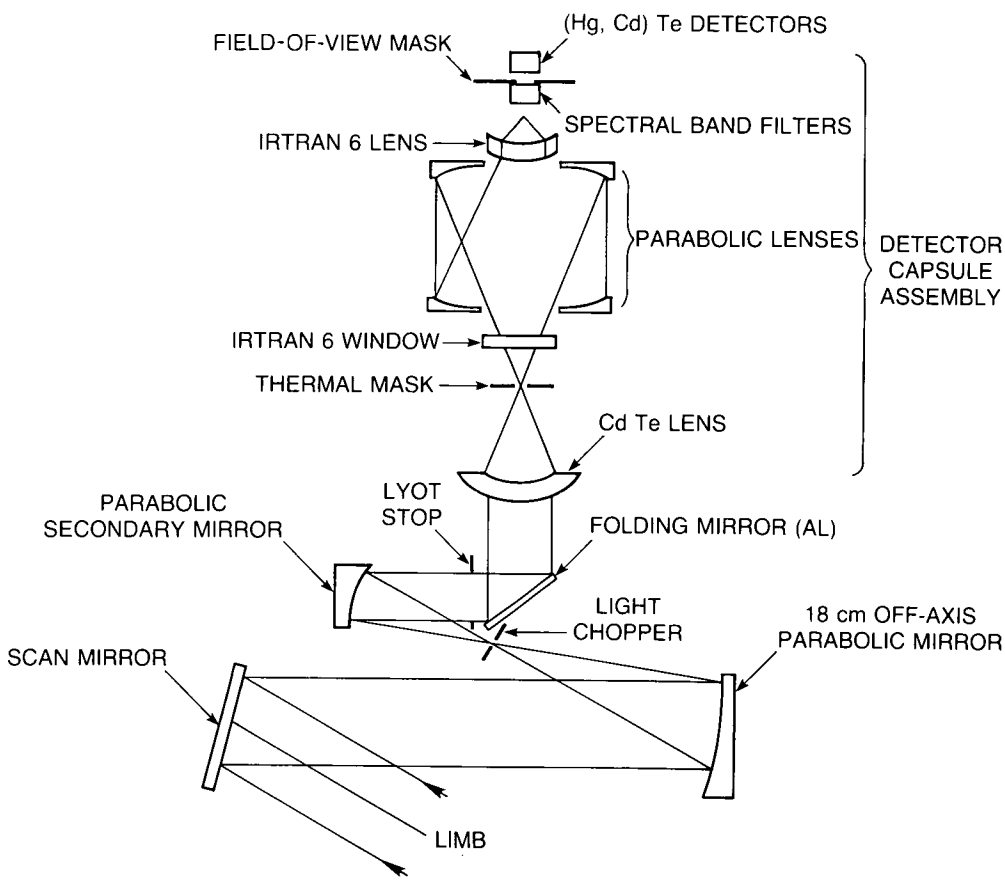

Figure 2.48 Schematic drawing of LIMS optical train (from Gille and Russell, 1984).

To ensure that all channels scanned high enough to see cold space and low enough to view the hard Earth, the total scan was 3 degrees, making each down or up scan 12 seconds. After every second up-down scan pair, the scan mirror scanned up so that a small off-axis blackbody cavity in the focal plane adjacent to the chopper, at the focus of the primary, was reflected from the scan mirror back through the optics, in the same way a signal would be. The temperature of the cavity was held at 308 K, and its temperature was monitored by a platinum resistance thermometer and a backup thermistor. The cavity design should be relatively insensitive to changes in the condition of its surface. The calibration of this inflight calibrator (IFC) will be discussed further below.

After viewing the source for ~2 seconds, the mirror scanned down to a position in which all channels were viewing above the detectably emitting atmosphere, and viewed space for 1 second, to get a cold radiometric calibration point. The scan sequence then began again.

2.7.3 Preflight Calibration

The ability to obtain retrievals required that the absolute radiances be measured, which in turn required that the instrument characteristics defined by Δh, $\phi(h)$, $\psi(\nu)$, and C(N) be known accurately. The first three are not expected to change from the laboratory to orbit, and were measured on the ground. The radiometric response depends on a number of factors, including detector temperature and possible degradation in the optics, which require inflight calibration. The latter requires that the characteristics of the IFC under different instrument conditions be known.

Encoder Spacing

The repeatability of a given pulse position was determined to be 1–2 arc seconds. The average pulse spacing, 80.4 arc seconds, was slightly larger than the nominal 79.1 arc seconds, and there was an unexpected small oscillation of the mean spacing of the pulse positions (these deviations were subsequently used in the data calibration software to get a better relative vertical registration of the radiance samples).

Field of View

The instrument was mounted in a protected enclosure purged with dry nitrogen for most of the optical tests. The FOV shape was measured by scanning the radiometer very slowly across a hot wire, which had an angular width about 0.1 that of the CO_2 and O_3 channels. The normalized results of these scans are shown in Figure 2.49. For reference, one milliradian translates to ~3.6 km at the limb.

The major peaks correspond to the positions of the channels on the FOV mask. The response of one channel seen at the position of another channel is an unwanted side lobe feature. Other tests showed that these side lobes were not caused by radiation outside the spectral passband of the channel, but are believed to be due to internal reflections between the interference filters and the concave rear side of the final lens; the negative values result from the 180° phase difference in chopping of the narrow and wide channels. These are extremely important for interpreting the measurements, since when a main lobe is viewing weak radiance at 50 km, even a small side lobe viewing the large tropospheric radiance can provide a significant fraction of the received signal.

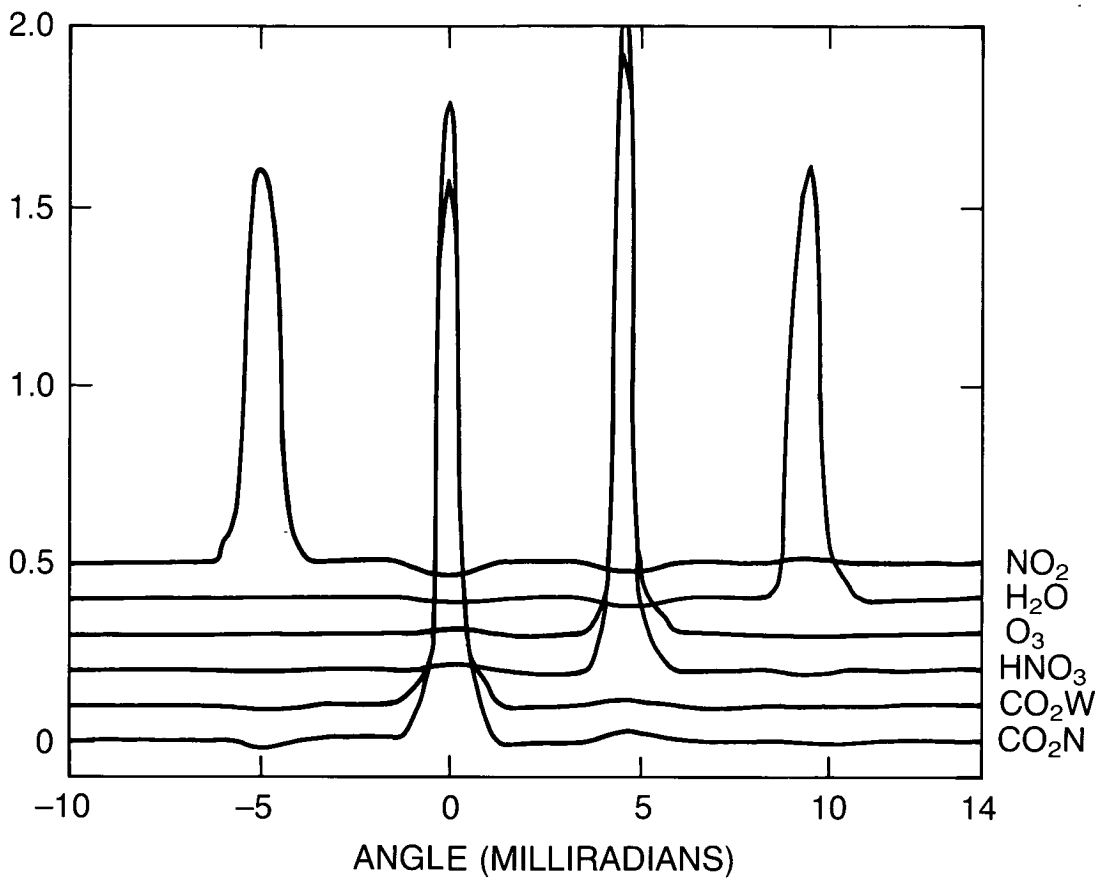

Figure 2.49 Normalized instantaneous FOV functions for the six LIMS channels. The response of a channel at the position of another channel is a side lobe. Toward the left is the downward (Earthward) direction on a scan (from Gille and Russell, 1984).

To correct for this effect, the shapes of the side lobes were taken from the hot wire scans, but the magnitudes were determined from scans across a knife-edge target, for which there was a better signal-to-noise ratio. The corrected spatial response function was Fourier transformed (to yield the transfer function of the optics and FOV mask) and multiplied by the electronics frequency response to give the system modulation transfer function. This was used in the spatial frequency domain to remove side lobe effects and to partially deconvolve the effects of the FOV on the radiance scan, as outlined in GR and described by Bailey and Gille (1986).

Spectral Response

The relative spectral response $\phi(\nu)$ of the instrument was determined by aligning a monochromator having 1–2 cm^{-1} resolution on a given detector and measuring the response of the instrument as the monochromator scanned in frequency. Three in-band measurements of spectral response were made at two perpendicular orientations of a polarizing screen, and the resulting values were averaged. Individual runs generally differed by less than 0.01 at a given frequency. Monochromator output was calibrated against a thermocouple bolometer that was traceable to a spectrally flat, black standard.

Wavelength calibration of the monochromator was performed, using a HeNe laser line seen in high-order reflection from the grating, with CO_2 and H_2O lines from the small amount of room air in the protective enclosure, to define the frequency scale, estimated to be known to be ≤ 0.7 cm^{-1}.

The shapes of the relative spectral responses are shown in Figure 2.50, while the cuton and cutoff points (5 percent response) are tabulated in Table 2.11.

Table 2.11 Characteristics of LIMS Channels*

Channel	Emitting Gas	Bandpass 5% Relative Response Points cm^{-1}	Field of View at Limb, km Vertical	Horizontal	Noise Equivalent Radiance (W/m^2sr)
1	NO_2	1560–1630	3.6	28	0.00055
2	H_2O	1370–1560	3.6	28	0.0023
3	O_3	926–1141	1.8	18	0.0037
4	HNO_3	844–917	1.8	18	0.0015
5	CO_2W	579–755	1.8	18	0.0055
6	CO_2N	637–673	1.8	18	0.0014

*From Gille and Russell, 1984

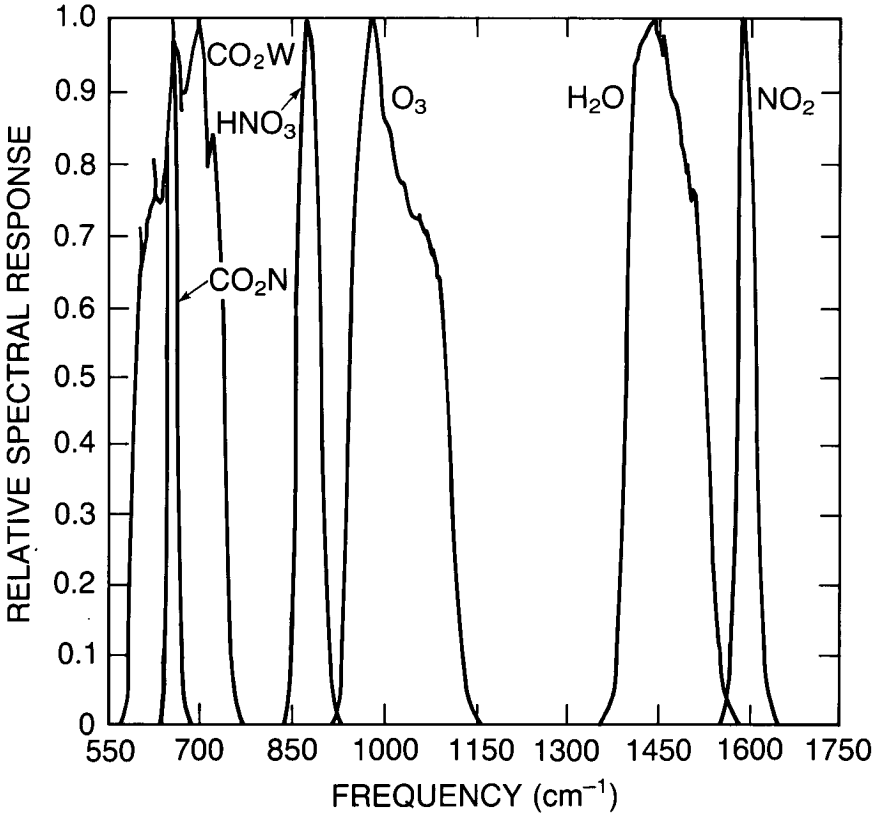

Figure 2.50 Normalized spectral response curves for LIMS channels (from Gille and Russell, 1984).

In addition to the in-band scans, slow scans with lower spectral resolution were performed to look for out-of-spectral-band leaks. The requirement of <0.2 percent of full response in the out-of-band regions was met for all channels from 2 to 20μm, beyond which other optical elements effectively reduced the response to zero.

Finally, the output signal from each channel was measured when every other channel was irradiated with radiance at its center frequency. Responses were $\lesssim$ 1 percent in all cases, with many being zero.

Radiometric Calibrations

This test was carried out in the vacuum chamber while the instrument was being exposed to the range of thermal conditions expected to be encountered in orbit. The radiometer viewed a honeycomb blackbody target (emissivity $\geq$ 0.997) at a series of known, uniform temperatures, so that the radiation reaching the detectors could be calculated accurately and related to the instrument output. The two major functions of this test were to measure any nonlinearity in the radiometer response and to calibrate the IFC so that it could function in orbit as a transfer standard.

The target blackbody radiances (estimated accuracy $\leq$ 0.6 percent) were then convolved with the measured spectral response curves to give the relative signal that each channel was expected to see. Calibrations were performed at three instrument temperatures near 288, 298, and 308 K.

A typical calibration curve at 298 K is shown in Figure 2.51a, which compares the target observation to the IFC, but which does not allow any departures from linearity to be seen easily. Figure 2.51b shows the same results, after the least-squares straight-line fit has been removed. The departures from linearity are consistent, although they are small compared to the requirements, and could be due to problems with the test setup. The radiometer response was taken to be nearly linear, with a slight quadratic component.

The IFC signal does not lie on the same line as the calibration target. This is primarily because the IFC has an emissivity <1 and thus reflects some lower temperature radiation from the surrounding instrument onto the detectors. In addition, there is one more reflection off the primary mirror during calibration than during atmospheric observations (or target calibration). By using the calibration results at all three instrument temperatures, the target and mirror emissivities were determined. These values were used to correct the IFC radiances measured in orbit. The random noise did not depend on target or instrument temperature.

2.7.4 Instrument Calibration and Performance in Orbit

LIMS instrument activation took place on October 24, 1978, during the first few orbits, when pyrotechnic valves were fired, allowing the methane and ammonia to begin subliming to space. The methane temperature, which is very close to the detector temperature, immediately began to drop from the prelaunch value (~70 K) to its expected operating level near 61 K. The subsequent methane temperature history is shown in Figure 2.52. As methane depletion approached, the temperature rose, very slowly at first, then more rapidly. (Small downward spikes indicate the temperature drop when the instrument was turned off.)

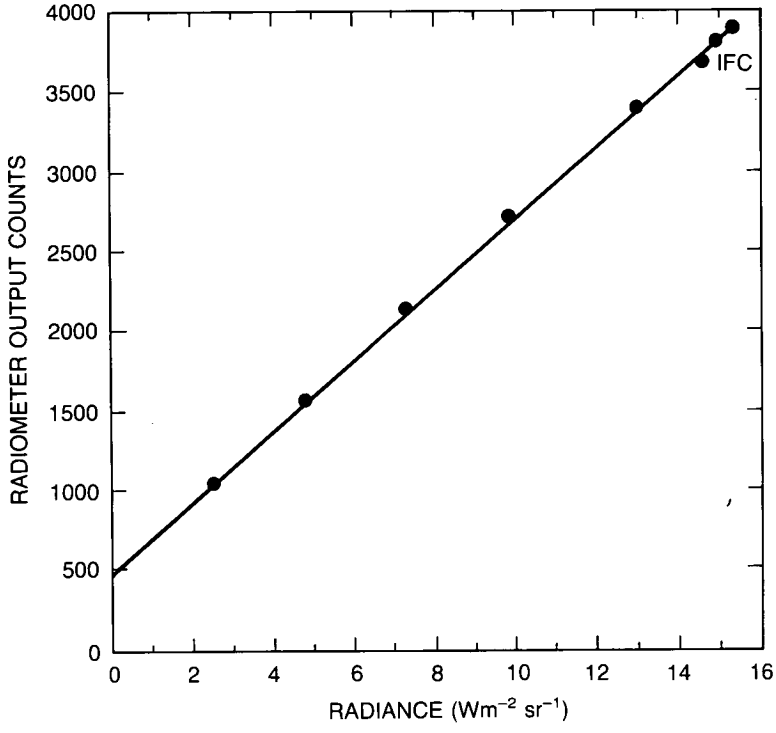

Figure 2.51a LIMS primary calibration curve for ozone channel; • • • indicate measured points; line is least-squares fit.

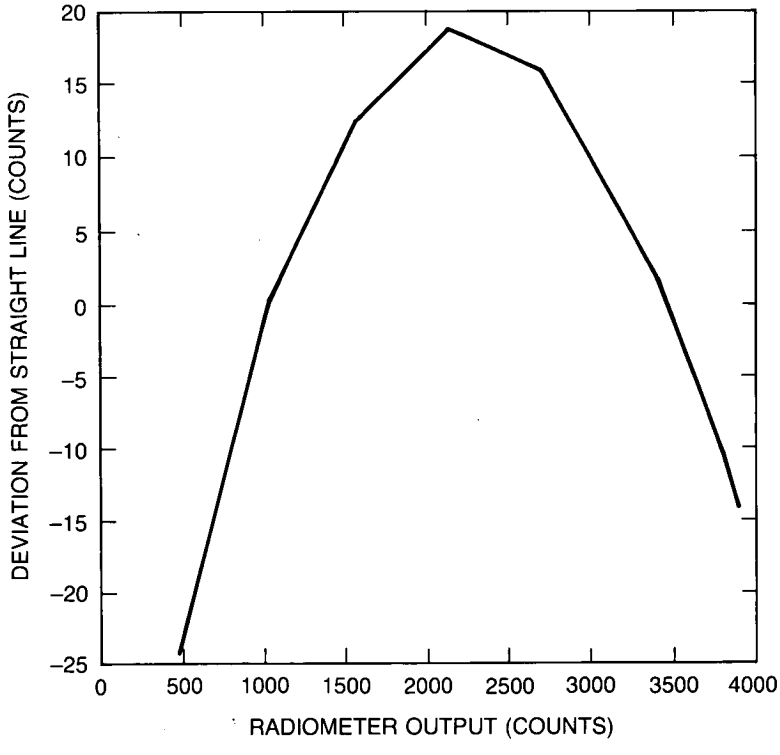

Figure 2.51b Departure of curve in 2.51a from linearity.

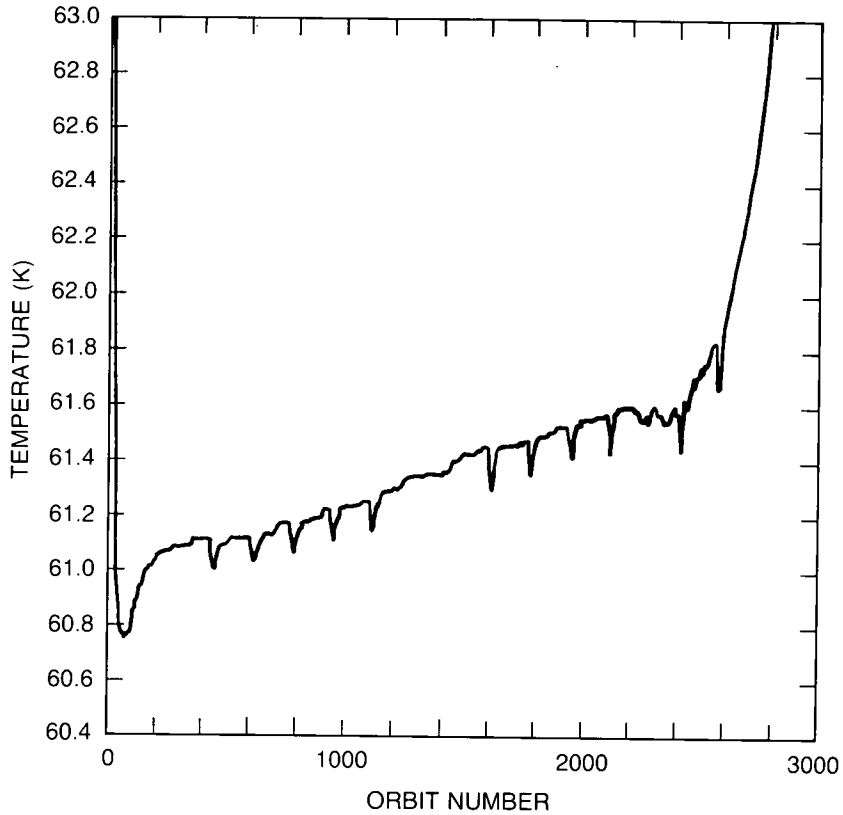

Figure 2.52 LIMS detector temperature vs. time (expressed in orbit number). One week is approximately 100 orbits.

The radiometer performed according to expectations when it was turned on during the first day and whenever it was turned on later. A wide-angle scan located the desired part of the limb, which was tracked by the adaptive scan thereafter.

The operation of the instrument under orbital conditions can be assessed by studying the results of the inflight calibration sequence. The stability of the IFC temperature over the mission is discussed in GR; it was constant to ± 1 bit (0.023°) during an orbit and close to that for the mission. GR also shows the variation of several instrument temperatures around a typical orbit. The temperatures of the outer baffles, primary mirror, and chopper plane drop during the southward (night) part of the orbit, then rise on the northgoing (day) portion. The temperature variation is slightly larger for the outer baffles and the primary mirror than for the focal plane, further inside the instrument. Although the variations are small, their effects must be carefully removed to interpret the small signals in some channels, as well as to take full advantage of the low noise levels of the radiometer.

The IFC and space view signals vary around an orbit, due to radiation reaching the detectors from parts of the radiometer where temperatures vary. The IFC and space signals follow each other closely, although the scale factors between radiance and voltage, which would be constant if the signals varied by the same amount, do show small (~0.5–0.7 percent) variations around the orbit. These are shown for the CO_2 and O_3 channels in Figure 2.53. These variations may be due to a residual and unexplained temperature dependence of the instrument response that had

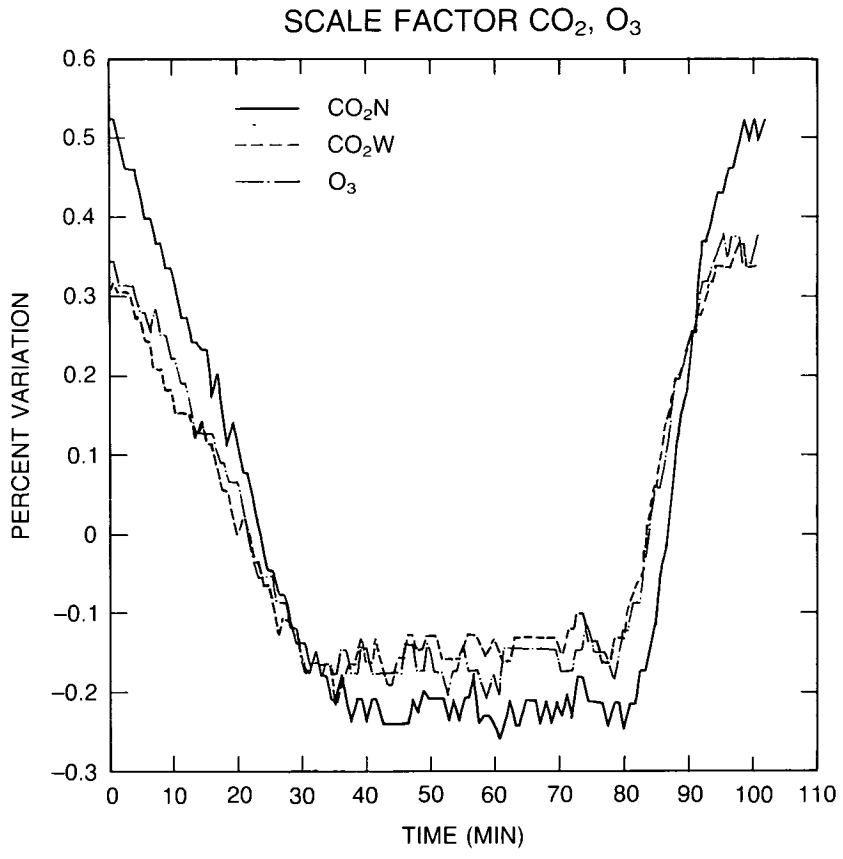

Figure 2.53 Percent variation of indicated scale factor around an orbit for LIMS carbon dioxide (temperature) and ozone channels.

been observed earlier in the laboratory, or may indicate the sizes of residual uncertainties in the inflight calibration.

The long-term stability of the scale factors over the mission is illustrated in Figure 2.54a,b,c, by the performance of the O_3 and CO_2 channels, as well as the similarity to the preflight calibration values. Note that changes in scale factor or offset are not a problem, as they are measured frequently in space.

The noise level may be determined as it was in the laboratory, by calculating the standard deviation of the output radiance when the radiometer is viewing the steady signal from space or the IFC target. These two determinations are quite close, with the IFC giving figures slightly larger, presumably due to tiny variations in temperatures in the IFC cavity or slight movement of the LOS across the target.

The noise behavior determined from the orbital data is illustrated in Figure 2.54d by results from the O_3 channel. There is no change, even at the end of the mission. The noise levels shown in Table 2.11 are based on the more conservative computer calculations.

These figures, taken together, clearly indicate instrument performance that is very close to design levels, stable, and in agreement with values measured on the ground.

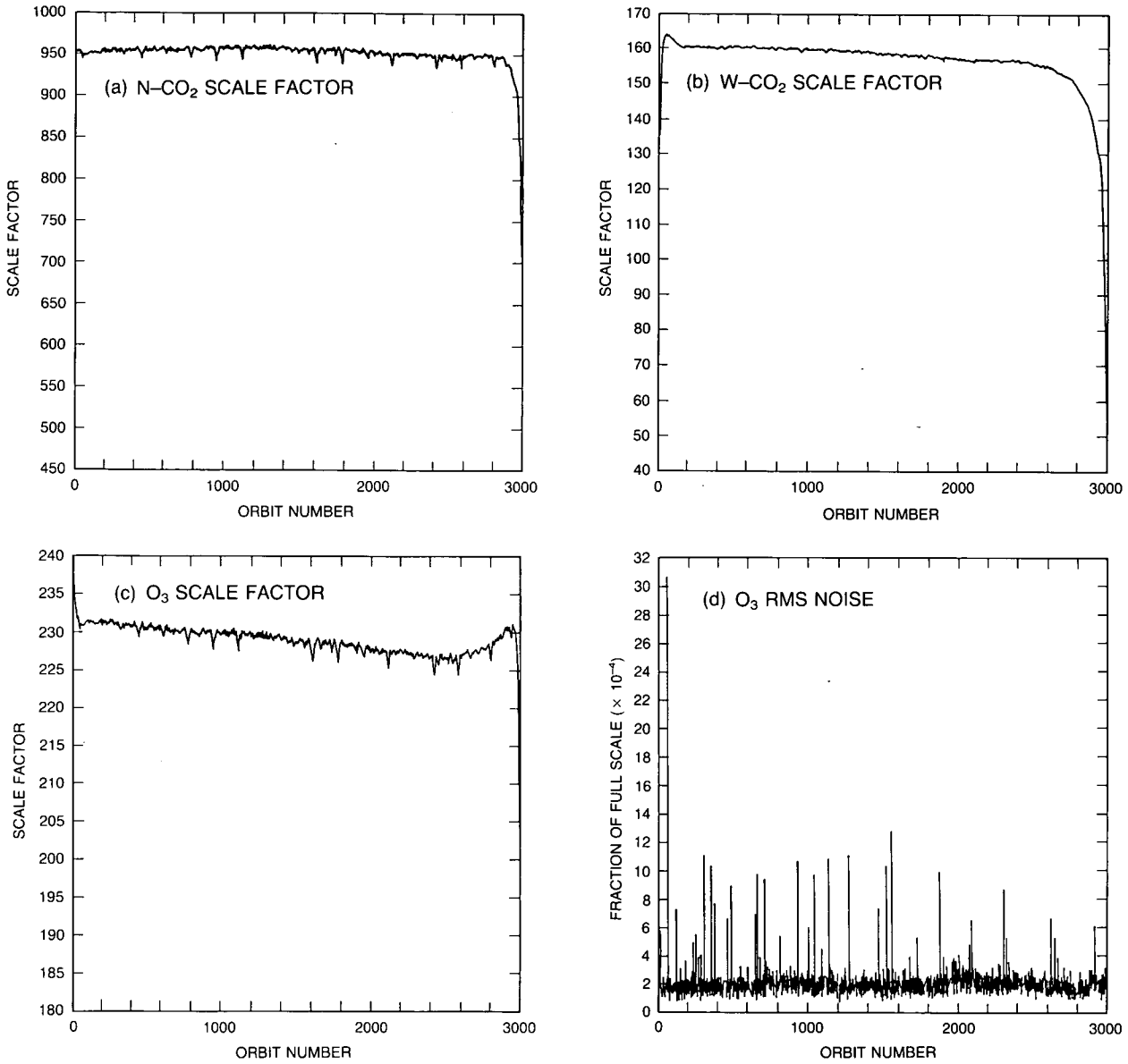

Figure 2.54 (a) Scale factor for narrow CO_2 channel as a function of time during LIMS missions. (b) Scale factor for wide CO_2 channel as a function of time during LIMS missions. (c) Scale factor for wide O_3 channel as a function of time during LIMS missions. (d) RMS noise in O_3 channel as a function of time during LIMS missions.

2.7.5 Instrumental Factors That Could Lead to Measurement Trends

At this point, the instrumental characteristics are discussed in light of possible changes that could take place and result in long-term changes.

Encoder Spacing

The design of the encoder resulted in four series of encoder pulses. These might shift relative to one another, but the spacing in each string should be nearly constant at about 320 arc seconds.

C-2

The spacing of the pulses could be roughly assessed on the assumption that the scan rate was constant, and knowing the time of the pulses to 0.25 ms. This showed no evidence of changes with time over the life of the experiment.

Electronic Filter Response

The chopper frequency was carefully controlled with a feedback loop. The response is determined by the electronics. The low frequency response is determined essentially by the inflight calibration. No evidence of a change in high-frequency response was seen, but it would have been difficult to detect. In the unlikely event that this or a phase shift occurred, it would have affected only the spatial components with higher frequencies and not those on which a long-term mean would have been primarily based.

Field of View

This is determined by a physical mask. It is possible to imagine a mechanical shift of the whole mask, which would have affected all channels. If it were small, it would not matter; if it were large, it would be catastrophic, and impossible to overlook. No evidence for a change was seen.

Spectral Response

It is possible to imagine the filters having a sudden failure, such as a partial delamination, but it seems very unlikely once the filters had been mounted in the detector capsule assembly (which had been evacuated). Similarly, they are not exposed to contaminant buildup from spacecraft outgassing. Outgassing from the interior of the detector capsule assembly (DCA) should be small at those temperatures. In addition, the DCA had been assembled and evacuated for several months when the spectral response measurements were made. Any residual outgassing in the DCA would have been included in the measured spectral response values.

Radiometric Calibration

The radiometric response should depend strongly on detector temperature. As Figure 2.51 shows, the detectors were nearly constant in temperature for both long- and short-term variations. The temperature of the IFC was very constant over the entire life of the mission, as indicated by both readouts. It is possible that the surface emissivity of the material lining the cavity of the IFC changed, but the cavity design requires incident radiation to make several reflections on the average before it reemerges, making the output of the cavity less dependent on the details of the surface state, and more like that of a blackbody.

Because the same optical train is used for calibration and for making atmospheric measurements, the results should be insensitive to changes in instrument response. However, the primary enters into the optical train twice on the calibration, and only once on the measurement. A change in its emissivity would result in some change in response. There is some evidence that something like this might have occurred, as the size of the variation of the calibration around an orbit grew larger with time in orbit. However, the variation was from a peak amplitude of 0.3 percent on orbit 100 to 0.7 percent on orbit 2850. The effect of any such change was clearly quite small, as the regular long-term change of the calibration factor shown in Figure 2.54 indicates. In addition, because of its location well inside the instrument housing, the primary should be relatively protected from the general spacecraft outgassing. This possibility cannot be neglected, however, nor can the effects of outgassing by the instrument baffle material or insulating wraps.

2.7.6 Conclusions

The evidence suggests that the LIMS, because of its design and inflight calibration, operated in a very stable manner from shortly after activation on October 24, 1978, until after May 20, 1979, when its solid cryogen was nearly depleted. The data over this time should not exhibit any spurious trends of more than a few tenths of a percent.

2.8 OTHER INSTRUMENTS

Four other measurement systems that have not been treated in detail are relevant to the present discussion. These are briefly described here.

2.8.1 The Backscatter Ultraviolet (BUV) Experiment

The BUV, which flew on Nimbus–4, was the forerunner of the SBUV. It was launched in April 1970, and operated for 7 years. The experiment is described by Heath et al. (1970, 1973, 1975). Basically it was very similar to the SBUV, but differed in that the input radiance was not chopped and the diffuser was continuously exposed. In addition, power and tape recorder limitations on the spacecraft limited the amount of data collected.

Thus, the data from the BUV are poorer and fewer than those from the SBUV. The BUV diffuser degraded faster than that on SBUV, and the technique to determine degradation constants on SBUV cannot be applied. Some ingenious attempts have been made to correct the instrument drift based on ground-based observations of ozone profiles, and the albedo of the Sahara. All wavelengths show large drifts, but the accuracy and validity are hard to characterize. It appears that effort is better spent trying to understand the SBUV and its degradation. At that point, it may be possible to apply this knowledge to the BUV, but it seems somewhat unlikely at the moment that much additional information on trends can be extracted from BUV.

2.8.2 The SBUV–2 Operational Instrument

The SBUV–2 instrument was designed for flight on the NOAA series of satellites as part of its operational meteorological satellite program. The first instrument was launched in December 1984, and began making operational measurements in April 1985. The design is based largely on that of the Nimbus–7 instrument, and thus only the major differences will be discussed in this section. These are summarized in Table 2.12. A detailed description of the instrument has been given by Ball Aerospace Systems Division (1981).

The largest difference between the two instruments is that the onboard mercury lamp, which was used on Nimbus–7 for wavelength calibration only, can be repositioned on SBUV–2 so that light from the lamp can be either reflected off the diffuser into the instrument, or reflected directly into the instrument. This enables the reflectivity of the diffuser plate to be monitored. A second difference has to do with the photomultiplier output. In SBUV, all three ranges of the electrometer amplifier are taken from the anode; thus, the ratios of the three ranges will be independent of the gain of the photomultiplier. In the SBUV–2 instrument, the least sensitive range of the electrometer (corresponding to the higher photon flux measurements) is taken directly from the cathode of the photomultiplier, while the other two ranges are taken from the anode. The ratio between the anode and the cathode signals is the gain of the photomultiplier. The gain change mechanism has been changed on models after the first one launched. A third

Table 2.12 Comparison of Important Features Between SBUV–2 and SBUV

Features	SBUV–2	SBUV
Monochromator mode	4 (discrete, sweep wavelength, and position)	4 step (continuous wavelength, and cage cam)
Control of monochromator mode	FIX System FLEX System (wavelengths can be changed by command)	One fixed system
Scene mode	4 (Earth, Sun, wavelength calibrate, diffuser check)	2 (Earth and Sun)
Diffuser position	4 (stow, Sun, wavelength calibration or diffuser check, & decontamination	2 (stow and Sun)
Mercury lamp position	2 (stowed and deployed)	1
CCR wavelength	379 nm	343 nm
Shortest wavelength of discrete mode (other 11 wavelengths match)	252 nm (in FIX system)	255.5 nm
Wavelength calibration steps	12	5
Electronic calibration	Every scan in retrace	By command
Scanning discrete mode sweep mode	 32 seconds 192 seconds	 32 seconds 112 seconds
Sampling time discrete sweep	 1.25 seconds 0.1 second	 1 second 0.08 second
Diffuser check	Yes	No
Diffuser decontamination	Yes	No
Gain Range	2 from PMT anode 1 from PMT cathode	3 from PMT 1 from ref. diode
IFOV	11.3° × 11.3°	11.3° × 11.3°
Discrete (step scan) scanning direction	From short to long wavelengths	From long to short wavelengths

difference is that the grating drive on SBUV–2 is direct, through a stepping motor on the grating shaft, and not cam driven as on SBUV.

Although SBUV–2 is an operational instrument, and data collection began 2 years before this study, no data have been available for evaluation of the stability of its calibration, the degradation of its diffuser, or its simultaneous ozone measurements. In addition, it appears that many of the lessons learned by SBUV have not been incorporated by NOAA in the processing of SBUV–2 data. An analysis of the instrument performance of Flight Model 1 during the first 3 months of operation is given in a paper by Frederick et al. (1986), which also contains a fuller overview of the instrument. As is to be expected, the analysis uncovered several aspects of instrument behaviour not expected prior to launch. Recommendations for software changes were made and are now included in the latest engineering algorithm used in the data reduction.

By October 1985, the reflectivity of the diffuser plate, as measured by the onboard mercury lamp, had apparently decreased by 15 percent, yet the solar flux signal at 273.5 nm showed no such degradation. An enhanced deployment of the diffuser plate carried out in August 1986 suggests that the diffuser plate had degraded by no more than 2 percent by that time. Thus, it appeared that the onboard diffuser calibration was in error. The problem was traced to a design error. The lamp is viewed directly when placed in front of the slit, and, as the lamp is in the form of a narrow folded discharge, only a portion of the IFOV is filled. On the other hand, the entire FOV is filled when the lamp is reflected off the diffuser plate. The throughput of the instrument is not constant across the FOV, and, thus, changes in the characteristics of the discharge could manifest themselves as apparent changes in the diffuser reflectivity. In a new design, to be used in all future flight models, the lamp is reflected off a small diffuser before it is used in either mode.

It is interesting to note that the inferred diffuser plate degradation of less than 2 percent by August 1986 is considerably smaller than that for the SBUV instrument for the same period of exposure. This suggests that either the NOAA spacecraft or the SBUV–2 instrument is much cleaner than Nimbus–7 or SBUV. NOAA's failure to process these data for use in this and other aspects of the ozone trend studies has made them much more difficult. NOAA is strongly encouraged to process and understand the SBUV–2 data, which are critical to a continued measurement of ozone trends.

2.8.3 The Solar Maximum Mission (SMM) Ultraviolet Spectrometer Polarimeter (UVSP)

This occultation experiment utilizes the Tanberg–Hanssen ultraviolet spectrometer polarimeter on the SMM spacecraft. Launch occurred in early 1980, but solar pointing was lost in late 1980. In-orbit spacecraft repairs were effected in 1984, and operations have continued since that time. Details of the instrument and its performance have been described elsewhere (Woodgate et al., 1980). Briefly, the instrument consists of a Gregorian telescope having a geometric aperture of 66.4 cm, followed by a 1-m Ebert–Fastie spectrometer and five detectors. The spectrometer is equipped with a 3600-line/mm grating. Rotation of the grating provides wavelength coverage between 1150Å and 1800Å in second order and 1750Å and 3600Å in first order. Areas of the Sun as small as 3 arc seconds can be studied.

The experiment shares with SAGE the advantages and disadvantages of occultation measurements for long-term trend determinations. Because of the wavelengths used, ozone profiles are obtained over the altitude range from 50 to 70 km. Appreciable amounts of data are now

being collected and reduced, but the record with appreciable data is not long, and the profiles barely extend down to levels where they can be compared to other experiments. It could provide data for future studies of trends of mesospheric ozone.

Further details of the experiment may be noted. In conducting the ozone experiment, the entrance slit size is set at 1 × 180 arc seconds and the exit slit width is 0.01Å. Spectral resolution is 0.02Å in second order and 0.04Å in first order. The wavelength drive is fixed at a single wavelength. The experiment is conducted by observing the attenuation of a narrow-wavelength region within the Hartley ozone absorption bands during satellite crossing of the terminator. The resulting intensity during any time of the occultation is given by the Lambert–Beer law relating the observed and unattenuated intensities, respectively, at the tangent height h and the height where no attenuation occurs. The solar intensity is attenuated exponentially by the optical depth. The optical depth is equal to the product of the ozone absorption cross-section and an integral giving the total amount of ozone between the Sun and the satellite. The resulting integral equation is solved for the ozone concentration, making use of the fact that it is a linear Voltera integral equation of the first kind. The atmosphere is divided into a series of concentric shells at altitudes defined by the tangent heights corresponding to averages of the measured points. The integral equation is then represented by a sum over the number of shells so that the equation is now a matrix equation that can be inverted. Complete details are given in a publication by Aikin et al. (1982).

Two observing wavelengths were employed. The first was at 2765Å near the MgII line. In this experiment, the spectrometer wavelength range was 1Å and the maximum intensity in this range was detected. This wavelength was then employed for the occultation. The experiment was performed between November 1984 and March 1985. The remainder of the data from August 1985 until May 1987 were also collected while performing the experiment at a single wavelength. Due to an instrument malfunction caused by a broken wavelength drive, there is some uncertainty in the wavelength utilized in the experiment. This is reflected in the absolute cross-section to be employed in analyzing the ozone data. The final wavelength position was at 1379.528Å in second order. To convert this to first order the wavelength is doubled. In addition, it is necessary to correct for the offset between the different slits employed for experiments in first and second orders. This offset amounts to +4.586Å as determined by prelaunch calibration. The wavelength used for ozone measurements is 2764 with an uncertainty of ±10Å. Using the cross-section data of Molina and Molina (1986), this translates into an uncertainty of +5.25Å percent and -8.33 percent.

In addition to the error introduced by uncertainty in wavelength, there are other sources of error due to pointing uncertainty, photon counting noise, and ephemeris error (Aikin et al., 1982). Pointing introduces ±0.36 km. An ephemeris error in orbital track of 100 to 200 meters will introduce an altitude uncertainty of 0.14 to 0.28 km.

2.8.4 The ROCOZ–A Ozonesonde

The ROCOZ–A ozonesonde (Barnes and Simeth, 1986) is a four-filter, sequential-sampling, ultraviolet radiometer. The instrument is propelled aloft by a Super–Loki booster rocket. At rocket burnout, the instrument and its carrier coast to a nominal apogee of 70 km, where the payload is ejected for deployment on a parachute. The instrument measures the solar irradiance over its filter wavelengths as it descends through the atmosphere. Using the Beer–Lambert law, the amount of ozone in the path between the radiometer and the Sun is calculated from the

attenuation of solar irradiance as the instrument comes down. In addition, radar from the launch site measures the height of the payload throughout its descent. This allows calculation of the fundamental ozone values measured by the radiometer, ozone column amount versus geometric altitude (Barnes et al., 1986). Ozone number density is the derivative of ozone column amount with respect to altitude.

Combined with auxiliary atmospheric soundings for pressure and temperature, ROCOZ–A results can duplicate the fundamental ozone values from all satellite ozone instruments. Details of the performance characteristics of the auxiliary pressure and temperature instruments are given in Barnes et al. (1986, 1987). Auxiliary ozone soundings are made with balloonborne electrochemical concentration cell (ECC) ozonesondes (Komhyr, 1969; Komhyr and Harris, 1971). Analyses of the accuracy and precision of the ECC ozonesonde have been published (Torres and Bandy, 1978; Barnes et al., 1985). ROCOZ–A flights are also accompanied by total ozone measurements with the Dobson spectrophotometer. A preliminary intercomparison with the Dobson, showing no bias at the 1 percent level, has been published (Holland et al., 1985). A complete Dobson intercomparison, again showing no bias between instruments, has been submitted for publication as part of a description of ROCOZ–A measurements at northern midlatitudes.

Measurements of the precision (profile-to-profile repeatability) of ROCOZ–A ozone column amounts and number densities are in the literature (Holland et al., 1985; Barnes et al., 1986). For both column amount and density, the precision of the measurements is 3–4 percent (one sigma). Additionally, the published results of an equatorial ozone measurement campaign (Barnes et al., 1987) showed very low variability in stratospheric ozone, pressure, and temperature. From the results of that campaign, the precision of ROCOZ–A ozone-mixing ratios is estimated to be 3–4 percent. The campaign also produced estimates of the precision of temperature measurements as 1 percent; pressure measurements as 2–2.5 percent; and atmospheric density measurements as 2–3 percent.

The accuracy estimates for ROCOZ–A ozone measurements come from an internal, unpublished error analysis. The analysis is based on errors in the effective ozone absorption coefficients used to convert the radiometer readings into ozone profiles, plus the differences between the ozone values at altitudes where two ROCOZ–A channels give simultaneous readings (Barnes et al., 1986). A laboratory flight simulator, based on long pathlength photometry (DeMore and Patapoff, 1976; Torres and Bandy, 1978), has been constructed to measure the accuracy of ROCOZ–A ozone measurements. Publication of a detailed error analysis will follow the conclusion of experiments with the flight simulator and will complete the primary characterization of the ROCOZ–A ozonesonde. The accuracy of ROCOZ–A ozone column and number density measurements is estimated to be 5–7 percent. For ozone-mixing ratios, the accuracy is estimated as 6–8 percent (Barnes et al., 1986).

Since individual ROCOZ–A radiometers are not recovered after flight, the long-term repeatability of measurements from the instrument is determined by the consistency of the calibrations of the radiometers with time. To ensure this consistency, the calibration facility for ROCOZ–A ozonesondes (Holland et al., 1985) incorporates physical standards that are periodically recertified at NBS. The dominant factor in the response of the four ROCOZ–A radiometer channels is the transmission of the ultraviolet filters. Measurements of the transmission of the optical components within the instrument are made with a Cary model 17–D double-beam spectrophotometer.

The wavelength readings of the spectrophotometer are calibrated in the ultraviolet with a low-pressure mercury discharge lamp. The linearity of the transmittance measurements from the Cary is checked with respect to the high-precision reference spectrophotometer at NBS (Mielenz et al., 1973; Eckerle, 1976). Details of the intercomparison of the spectrophotometers are given in Holland et al. (1985).

The electronic gains for the instrument channels are adjusted to provide output signals that are 80 percent of full scale at the top of the atmosphere. Gains are set with an argon maxi-arc, a somewhat larger version of the previously reported argon mini-arc (Bridges and Ott, 1977). The NBS certification of the maxi-arc is described in Holland et al. (1985). In addition to periodic certification at NBS, the maxi-arc is checked in the laboratory to assess the changes in the arc's output. The NBS certification of the maxi-arc is given as good to within 5 percent. This calibration is typically duplicated in the laboratory at the 3 percent level (Holland et al., 1985).

2.9 CONCLUSIONS

2.9.1 General Comments

It is difficult to design any instrument or system to measure ozone changes to 1 percent or less per year over a period of a few years. This is especially true if one requires that the instrument operate unattended, a condition that severely constrains the amount of recalibration, testing, and adjustment that can be carried out, and usually limits the length of the measurement series to a few years. The difficulties become truly formidable if one further demands that the instrument operate under the harsh conditions in space.

Among the problems in space are the vacuum that allows contaminant molecules to outgas from instruments and spacecraft, and the strong solar ultraviolet radiation. When the contaminants deposit on optical surfaces and are dissociated by the radiation, the optical characteristics change, and the throughput decreases by unpredictable amounts.

Nonetheless, satellite instruments are indispensable for the determination of trends of ozone on a global basis. In spite of the difficulties and the relatively early stages of development of most of the methods and measurement technologies, they have already made enormous contributions to our knowledge of the global distribution of ozone, including its spatial and temporal variations.

Since 1978, seven instruments have collected large amounts of data that have been reduced and are clearly relevant to the problem of ozone trends.

However, none of these instruments was specifically designed for trend measurements. Only two of the experiment descriptions mentioned long-term trends as a goal, but even these instruments did not take measures to ensure that reliable data for trend detection were obtained. Some were designed under cost constraints that precluded planning for extended operations. The operational SBUV–2 instrument was launched for trend measurements in 1984, but data are only now becoming available in sufficient amounts for careful evaluation. Thus, at this time reliance must be placed on instruments for which trend detection is an afterthought. In this situation, it is necessary to make the best use of available data. In most cases, under the impetus of this study, the data were extensively reanalyzed. All available information has been critically evaluated to establish the accuracy and long-term stability of these instruments. In some cases,

the uncertainties in trend-determining capabilities resulting from the present analysis are different from those reported by the experimenters.

It should be pointed out that, to compare the ability of each instrument to determine trends, it is necessary to compare derived ozone amounts. Some of the differences in reported trends may result from effects introduced by the retrieval algorithms.

2.9.2 Instruments and Techniques

This section summarizes some general comments on the measurement characteristics and problems of the different instruments, and reviews the features of their coverage.

The various techniques for measuring ozone are affected to some extent by changes in instrument sensitivity. Some techniques rely to first order on relative measurements or ratios obtained over a short time; from an instrument point of view, these are less susceptible to drift than those that require an absolute radiance measurement. In either case, greater confidence is obtained by monitoring the inflight sensitivity of the instrument, generally through measuring the response of the instrument to a known calibration signal. It is easier to be sure of the output of an inflight calibration source in the infrared than in the visible, where, in turn, more stable sources are available than in the UV. In addition, the effects of instrument degradation are generally more pronounced in the UV than in the visible and infrared.

The SAGE–I and SAGE–II instruments fall into the relative measurement category. They measure infrared solar radiation during the occultation periods at sunrise and sunset; ozone is deduced from the relative attenuation of the solar signal over a period of tens of seconds. For both SAGE instruments, additional information suggests that other instrumental contributions to errors of trend determination are small. The principal limitation in occultation techniques is that only two profiles are obtained per orbit, at two latitudes that depend on spacecraft orbit and astronomical factors, and thus the coverage is sparse compared to other techniques.

A characteristic of these (and other) limb-viewing techniques is that they require very accurate knowledge of the direction of the line of sight or, equivalently, the tangent height of the ray path through the atmosphere. For SAGE–I and SAGE–II, these have now been calculated from the ephemerides of the Sun and the spacecraft. To do this requires accurate spacecraft tracking and accurate timing data, but these problems appear to have been solved satisfactorily for the SAGE instruments.

The SME UVS experiment also makes use of a relative measurement technique. The instrument measures the solar UV radiation scattered by Earth's limb as the IFOV scans across it. The presence of ozone alters the limb radiance profile from that of a purely Rayleigh-scattering atmosphere, and it is the shape of the radiance profile measured by the short-wavelength channel during a single limb scan (fraction of a second) that provides information on the absolute ozone concentration. In this case, measurements are possible anywhere along the orbit on the daylight hemisphere.

However, independent information on SME pointing directions is not available with sufficient accuracy, forcing the use of the UVS itself to determine those directions. In this case, the absolute calibration of the long-wavelength channel enters, making it sensitive to first order to changes in instrument sensitivity and model inaccuracies. This has apparently been several percent; additional information from the visible spectrometer, with some reasonable assump-

tions about the drift of its visible diodes, has been used to establish limits on the drift of the long-wavelength UVS calibration.

Other methods of measuring ozone are directly related to the photometric calibration of the instrument, and trends in ozone can be known only as well as the trends in the instrument response. These can be determined best by using an inflight calibration device. Two such instruments have been included in this study, the SME NIR and LIMS. The NIR measures the 1.27 μm emission from the $^1\Delta_g$ state of molecular oxygen, a product of ozone photodissociation. The instrument has an internal calibration lamp that suggests that the NIR has been quite stable over the 5-year SME mission. Again, the NIR is a limb-viewing instrument, and the pointing direction had to be determined externally from the UVS observations or from the SME horizon sensors. However, the signal is relatively insensitive to altitude at the signal maximum, near 0.75 mb. The technique derives values at the stratopause and in the mesosphere along the orbit over the daylight hemisphere.

LIMS measured the thermal emission of ozone in the 9.6 μm bands in the middle infrared. It carried a small blackbody as an inflight calibration device, so that its output can be calculated from basic physical principles. These have been used with good results in long-lived operational infrared temperature sounders. All inflight calibration data, as well as external comparisons, indicate that LIMS was very stable and well characterized over its short mission. The pointing direction toward the limb was determined from measurements from the LIMS CO_2 channels, and can be done quite accurately. Coverage is possible from any point in the orbit, on the day or night side.

The SBUV and TOMS instruments almost fall in the category of devices making relative measurements. They compare the signals of solar radiation backscattered from Earth's atmosphere to solar radiation directly scattered from an instrument diffuser plate. Unfortunately, the reliability of their ozone determinations is directly related to the knowledge of the scattering efficiency of the diffuser throughout their missions. While there is information on the degradation of the entire optical train, there is no independent information at wavelengths at which ozone absorbs to allow the separation of the degradation in the diffuser reflectivity (which is the only part that affects the determination of the albedo, and thus ozone amounts) from degradation elsewhere in the optical system. While plausible models of the partitioning can be made, they cannot be proven to be correct. These are nadir measurements, and so are insensitive to pointing direction; measurements are possible along the orbit on the daylight hemisphere.

2.9.3 Trend Measurement Capabilities

The findings may be summarized and compared to show the altitude ranges and capabilities of the data now available. Two related quantities are compared: the minimum detectable ozone change over the life of the experiment, and the minimum detectable ozone trend, which is usually the minimum detectable change divided by the life of the experiment.

Measurements of the Vertical Distribution

- SAGE–I and –II—Of the error sources discussed in this chapter, it is apparent that for either instrument the ozone and Rayleigh cross-sections will remain constant. Taking the root sum square of the other error sources leads to the conclusion that SAGE–I can discern an ozone change of 2 percent near 25 km, 4 percent at 20 and 6 percent near 40 km. Similarly, for SAGE–II, the values are 1.3 percent, 4 percent, and 3 percent, respectively. However,

because of the difficulties of sampling the same latitudes at the same seasons and under the same atmospheric conditions, in general it is not possible to detect changes of this size unambiguously. On the other hand, the instrumental uncertainty in the differences between SAGE–I and SAGE–II (for situations carefully matched in latitude and season) is ±1.5–2 percent between 25 and 45 km; this value is plotted in Figure 2.55. This does not include the effects of errors resulting from systematic geophysical variations between the matched pairs of situations that are sampled. At present, these have not been quantified.

To make a rough estimate of the annual rates of ozone decrease that can be determined, it is necessary to consider the time period over which a change might be sought. Although SAGE–I operated for 34 months, only 2 complete years of operation are used because of the sampling problems. A SAGE–II data record of the same length is now available. Dividing the detectable changes mentioned above by their 2 years of operation indicates that, near 40 km, trends of the order of 1.5–3 percent per year are detectable (in principle). Again, the interaction of measurement sampling with natural variability requires that these numbers be regarded as no more than suggestive. It should be pointed out that, as the SAGE–II mission extends to 3 and more years, in principle it will be able to detect correspondingly smaller trends.

There are roughly 5 years between the midpoints of the SAGE–I and SAGE–II data. Dividing this into the ±1.5–2 percent minimum detectable total change based on instrumental factors suggests a minimum detectable trend of ±0.3–0.4 percent per year, which is shown in Figure 2.56.

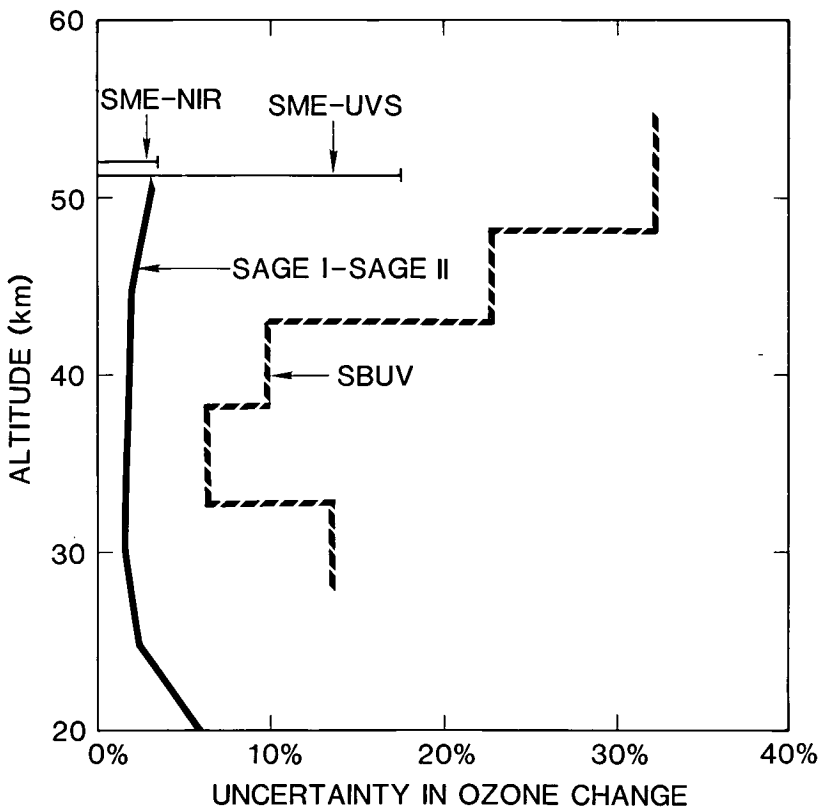

Figure 2.55 Uncertainty in total change determined by the various experiments over their lifetimes, as functions of altitude. For SBUV, the uncertainty is half of the range between models of high and low diffuser degradation.

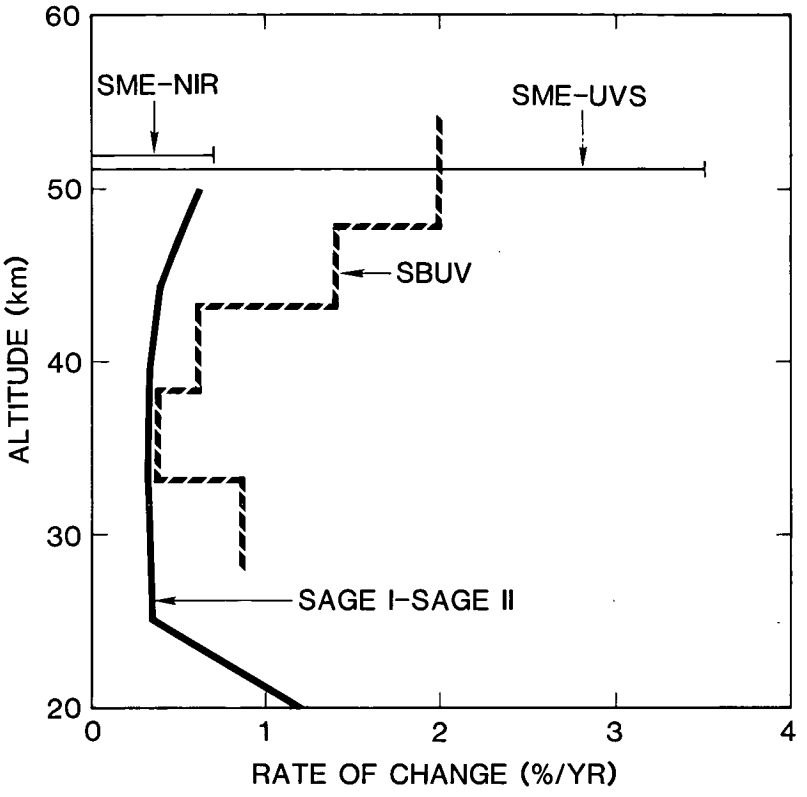

Figure 2.56 Uncertainties of trends determined by various experiments over their lifetimes, as functions of altitude. For SBUV, the uncertainty is half of the range between models of high and low diffuser degradation.

- SBUV—The major instrumental uncertainty in the SBUV results is due to lack of knowledge of the way the diffuser plate has degraded with time. There are no measurements from the instrument that provide this information unambiguously. A family of models was introduced to provide a plausible range of values for the degradation. Based on differences in the model values after 8 years, the range of ozone content was calculated. One half of this range is plotted for Umkehr layers 6–10 in Figure 2.55. Thus, in layer 10, the range is 64 percent, or ±32 percent around the central value. Clearly, the range of ozone content based on these models is very large at all levels. It must be emphasized that the bounding values are rather arbitrary, and the actual values could even be outside this range, although this is felt to be unlikely for reasons mentioned below.

The range of detectable trends is presented in Figure 2.56 in the same way—i.e., in layer 10 the trend range of the models is 4 percent per year, or ±2 percent per year around the midpoint of the model results.

These models assume that the coefficients relating the degradation to the exposure time and the elapsed time are constant over the 8 years, which is not necessarily true, adding another degree of uncertainty.

The change in vertical ozone distribution (in Umkehr layers) from November 1978 to November 1986 is shown in Figure 2.57 for several different diffuser degradation models. The curve labeled OPT is based on the data in the archives in 1987. They show a large decrease near 50

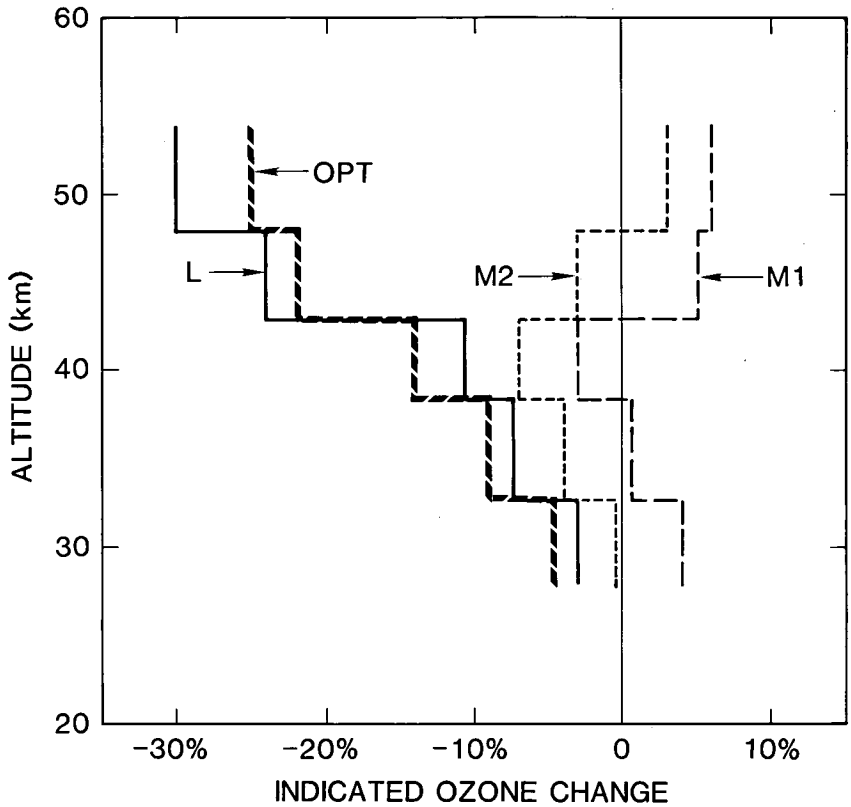

Figure 2.57 Midlatitude vertical distributions of ozone change from 1978–1986 determined from SBUV data, for several models of diffuser degradation. Curve marked OPT used the model employed in producing the data archived as of 1987. Curve L was calculated using a model with less diffuser degradation; M1 and M2 were derived using models with more diffuser degradation than the SBUV archive model.

km, which was reported by the principal investigator (Heath) to the Congress in 1987. The curve labeled L shows the same measurements, interpreted by means of a diffuser model with low degradation, while M1 and M2 indicate results obtained using two models with more degradation than the one used to create the archived data. These illustrate the nonuniqueness of the results, their strong dependence on the diffuser model, and the position of the archived values close to the low extreme of this family of models. M1 and M2 indicate small changes, or a slight increase in ozone near 50 km, with a small decrease near 40 km, similar to that indicated by the SAGE–I/SAGE–II differences. As noted below, total ozone derived using M1 or M2 agrees better with Dobson total ozone than do the archived (OPT) data. The wavelengths that provide information on the vertical distribution at 30–50 km are shorter than those that determine the total ozone, so the shape of the stratospheric profile depends only on the assumptions in the diffuser degradation model. The present results give weak support to the decrease at 40 km. It is possible to construct a reasonable model of the diffuser degradation that causes the vertical distribution of the SBUV rate of ozone decrease to agree with the SAGE–I/SAGE–II rate, and the SBUV change in total ozone to agree with the change in Dobson total ozone, but this provides no additional independent information.

These results indicate that the uncertainties in the diffuser degradation model, and the resulting uncertainties in ozone column amounts and vertical distributions, are much greater than has been stated previously. The weight of evidence also suggests that the diffuser degradation model used in producing the archived data has underestimated the diffuser

degradation, and thereby systematically underestimated the vertical ozone distribution, resulting in a large, but false, decrease.

- SME–UVS—The arguments presented in the report indicate that the SME–UVS instrument can determine an ozone trend at 0.75 mb to ±3.5 percent per year, or detect a ±17.5 percent change over the 5-year lifetime of the SME spacecraft.

- SME–NIR—From the considerations in the report, the trends at 0.75 mb apparently can be determined to be ±0.7 percent per year, or ±3.5 percent over the SME lifetime. However, this technique is very different from those that have been used before, and relies on an involved set of photochemical reactions. Until the underlying chemistry is understood more completely, the possibility exists that additional reactions are involved, or that there are unrecognized sensitivities to other factors. Thus, the instrumental error bars shown here may be unrepresentative of the true variation.

- LIMS—Because of its short lifetime, no attempt has been made to evaluate the LIMS capability to measure long-term trends. In this study, LIMS has served as a useful check and source of comparisons with measurements by other techniques.

As infrared limb scanning uses a stable onboard blackbody for calibration, this technique should be a good candidate for long-term trend measurements. The major difficulty is the requirement that detectors with sufficient sensitivity operate over a period of a few years. This will probably require cooling the detectors well below spacecraft ambient temperatures.

Comparison of Trend Detection Capabilities for the Vertical Distribution

Figure 2.55 shows that, at present, the SAGE–I/SAGE–II difference sets the most sensitive limits on the detection of a change in the stratosphere, followed by the SME–NIR (in the lower mesosphere). Similarly, Figure 2.56 compares trend detection capabilities. The SAGE–I/SAGE–II difference is capable of detecting trends of less than 0.5 percent per year in the stratosphere above 25 km. As noted above, as the SAGE–II record becomes longer, it should be able to detect smaller trends, but this must be evaluated in light of its sparse coverage and of the problems of obtaining comparisons under similar seasonal, latitudinal, and atmospheric conditions.

In the future, if the SBUV–2 results can be proven to be highly accurate, it should be possible to use them with the SBUV measurements to determine long-term changes to better than 1 percent per year. Determining the time history of the changes will be a more difficult task.

Total Ozone Determinations from SBUV and TOMS

Because SBUV and TOMS employ the same wavelengths and share the same diffuser plate, they show the same trends and have the same sensitivity to diffuser degradation. The uncertainties in total ozone were calculated, using a range of diffuser degradation models for wavelengths of 312.5 nm and longer. This leads to a range of about 4 percent in total ozone change over 8 years, and a consequent range of total ozone trends of 0.3–0.5 percent per year.

In this case, the diffuser model used to obtain the archived data results in ozone amounts near the minimum of the range. The true total ozone values could be 4 percent higher than those suggested by the archived TOMS data, and the downward trend could be smaller than that of the

archived data by ≈ 0.4 percent per year. Diffuser models M1 and M2 thus give total ozone changes that are in good agreement with the changes observed by the Dobson network.

A Final Observation on SBUV and TOMS Results

The evidence indicates that the uncertainties in the total ozone changes and in the changes in the vertical distributions are considerably larger than has been stated previously. The preponderance of evidence suggests that the model adopted in producing the archived data has underestimated the diffuser degradation, and thereby underestimated total column ozone and ozone profile amounts in recent years. Within the uncertainties, the total amounts could have changed by the amounts indicated by the Dobson network, while the vertical profiles could have remained nearly unchanged, or had a small decrease near 40 km with a small increase near 50 km.

2.9.4 Ongoing Work

Many studies were carried out as part of this investigation. Two in particular that were not completed at the time of this writing should be brought to completion:

- A comparison of SBUV and SBUV–2 results during the period of overlap.
- A comparison of the SBUV, SME, and other solar measurements.

2.9.5 Future Satellite Measurements of Ozone Trends

The analyses discussed here have shown that the measurement of long-term ozone trends from satellites is a difficult but viable task. Results to date, with data that, for the most part, were not taken for this purpose, have proven to be very instructive, and such a measurement program should continue. The measurement system should be based on a careful scientific analysis of the capabilities of the techniques with a view to optimizing them. Of necessity, this will need to be tightly linked with studies on the best methods of implementation to define the instruments employed by such a system. The methods for demonstrating the stability of the systems results will also need to be addressed. This study suggests that a measurement program should include the following features:

- The instruments should be designed for long life and stable operation. All instruments should include provisions for monitoring their operations and characteristics in space, preferably by including a stable inflight calibration source.
- Attempts should be made to reduce the amount of contamination to which the instruments are subject. This applies most strongly to instruments making measurements in the UV, but is relevant for all instruments. It should begin with concerted efforts to reduce the amount of outgassing from the spacecraft. Additional attention should be paid to the cleanliness of the individual instruments. Testing should not be carried out in vacuum systems that are oil pumped, since this often results in traces of the pump oil being adsorbed by the spacecraft materials. As noted above, degradation effects are most noticeable on surfaces that are exposed to solar UV radiation. Such surfaces and the amount of exposure should be minimized. Strategies of heating such surfaces before solar exposure, to drive off adsorbed contaminants before they are fixed on the surface, should also be investigated.

- Ideally, the program should consist of more than one satellite instrument, employing different experimental techniques. If a sequence of instruments is used over time, then adequate overlap between instruments must be made, such that differences in trends (or lack thereof) can be firmly established. Thus, for the present SBUV–2 series of instruments on the NOAA operational spacecraft, the ideal arrangement would be to collect data from each instrument for its life, without being governed by the operational need for the instrument, which would have an instrument turned off as soon as its successor is put in operation. While the SBUV–2 system is in operation, the shuttle SBUV is an extremely desirable component of the overall program.

- The system should also consist of a continuous long-term set of ground-based measurements, carefully maintained at a high level of accuracy. Such systems are the proposed Global Network for the Early Detection of Stratospheric Change, for the vertical distribution of ozone, and the Dobson network for total ozone. It is important for the stations to be accurate and very stable. Only a limited number of such stations is needed, but they should be capable of obtaining data on a nearly daily basis, preferably under all weather conditions.